MICROCOPY RESOLUTION TEST CHART
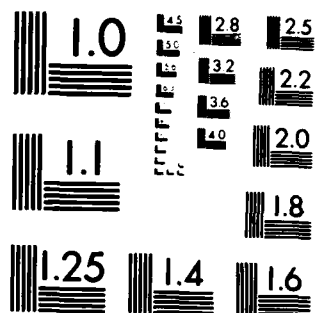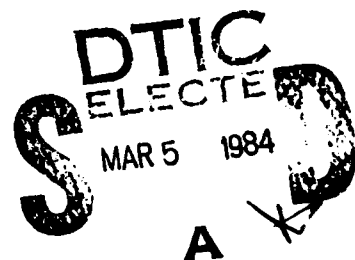
NATIONAL BUREAU OF STANDARDS-1963-A

FOCAL REGION CHARACTERISTICS

OF

FOCUSED MICROWAVE ARRAY ANTENNAS

Report No. TR-753-2

Prepared For

MR. J. W. WILLIS
NAVAL AIR SYSTEMS COMMAND
WASHINGTON, D. C.

9 September 1983

DTIC
ELECTE
MAR 5 1984

S A

Final Report on

Contract N00019-82-C-0157

R. C. HANSEN, INC.

Box 215

Tarzana, CA 91356

REPORT DOCUMENTATION PAGE

1. REPORT NUMBER	2. GOVT ACCESSION NO.	3. RECIPIENT'S CATALOG NUMBER
TR-753-2	AD-A138557	

4. TITLE (and Subtitle)	5. TYPE OF REPORT & PERIOD COVERED
FOCAL REGION CHARACTERISTICS OF FOCUSED MICROWAVE ARRAY ANTENNAS	Final Report
	6. PERFORMING ORG. REPORT NUMBER
	TR-753-2

7. AUTHOR(s)	8. CONTRACT OR GRANT NUMBER(s)
Robert C. Hansen	N00019-82-C-0157

9. PERFORMING ORGANIZATION NAME AND ADDRESS	10. PROGRAM ELEMENT, PROJECT, TASK AREA & WORK UNIT NUMBERS
R. C. Hansen, Inc. Box 215 TARZANA CA 91356	

11. CONTROLLING OFFICE NAME AND ADDRESS	12. REPORT DATE
Naval Air Systems Command Code AIR-033, Attn: Mr. J. W. Willis Washington, D. C. 20361	9 Sept 1983
	13. NUMBER OF PAGES
	103

14. MONITORING AGENCY NAME & ADDRESS(if different from Controlling Office)	15. SECURITY CLASS. (of this report)
DCASMA Van Nuys 6230 Van Nuys Blvd. Van Nuys, CA 91408	UNCLASSIFIED
	15a. DECLASSIFICATION/DOWNGRADING SCHEDULE

16. DISTRIBUTION STATEMENT (of this Report)

Distribution list provided by Naval Air Systems Command

APPROVED FOR PUBLIC RELEASE:
DISTRIBUTION UNLIMITED

17. DISTRIBUTION STATEMENT (of the abstract entered in Block 20, if different from Report)

18. SUPPLEMENTARY NOTES

19. KEY WORDS (Continue on reverse side if necessary and identify by block number)

Antenna Arrays, Focused Antennas, High Power Microwave, Near Fields, Near Field Power Density, Antenna Near Fields

20. ABSTRACT (Continue on reverse side if necessary and identify by block number)

Fields in the focal region of a focused microwave aperture or array antenna are examined thru detailed calculations. Transverse near field patterns are well behaved with only slightly higher closest sidelobes, and with a rapid sidelobe falloff. Peak axial power density available from an aperture is a function only of distance, but the relationship is non-linear. This relationship and simple formulas allow system tradeoffs of aperture size,-

DD FORM 1473   EDITION OF 1 NOV 65 IS OBSOLETE
1 JAN 73

unclassified

frequency, focal distance and peak power density to be made. Effects of aperture amplitude taper are investigated:uniform excitation gives comparable axial and transverse subsidiary lobes, and is probably the best choice. Taylor tapers give low sidelobes but high forelobes and aftlobes, plus a modest gain degradation. Inverse tapers give low forelobes and aftlobes but very high sidelobes and large gain degradation. A brief comparison of Gaussian, Romberg, and summation calculation methods is given.

FOCAL REGION CHARACTERISTICS

OF

FOCUSED MICROWAVE ARRAY ANTENNAS

Report No. TR-753-2

Prepared For

MR. J. W. WILLIS
NAVAL AIR SYSTEMS COMMAND
WASHINGTON, D. C.

9 September 1983

R. C. HANSEN, INC.
BOX 215
TARZANA, CA   91356-0215

TABLE OF CONTENTS

1.0   INTRODUCTION

1.1   History and Nature of Focused Fields

Focused antennas are of interest for microwave power transmission (solar power satellite) and for applications requiring high power density at moderate ranges. Probably the earliest work on focused antennas was that of Wehner, reported in a 1949 RAND report. Subsequently, Cheng (1955, 1957) calculated defocus regions, while Bickmore (1957) calculated depth of field and measured a far field pattern in the near field of a focused antenna. This antenna was an 8 ft. long linear slot array at 34 Ghz. The normal 2200 ft. half far field distance was reduced to 65 ft. by bending the array into a circular arc, with excellent results. In 1962 Sherman published several calculated patterns of focused antennas. (See also ECI, 1962). Wheeler (1962) discussed the effects of focusing on difference (monopulse) patterns. Partially coherent excitation was treated by D'Auria and Solimini (1967). Measurements of focused linear arrays have also been made by Fahey et al (1972). In a related work Fresnel zone plates for focusing are evaluated by Van Buskirk and Hendrix (1961), and, as expected, the gain is very low. Although focused antennas are simple, the record is indeed meager.

A simplified picture of power flow from an aperture antenna is sketched in Figure 1; the power is contained in a corrugated tube whose mean diameter is that of the aperture. The surface undulations increase in size and period as distance increases, finally spreading out to form the far field beam. This tube extends to roughly twice the hyperfocal distance $R = L^2/2\lambda$ where L is the aperture width or diameter. To allow accurate pattern measurements, the far field distance is usually taken as $2L^2/\lambda$. Beyond L^2/λ, the beam flares out into the 3 db beamwidth of $\theta_3 \simeq \lambda/L$. To focus the antenna, a rotationally symmetric quadratic phase is added to the aperture excitation,
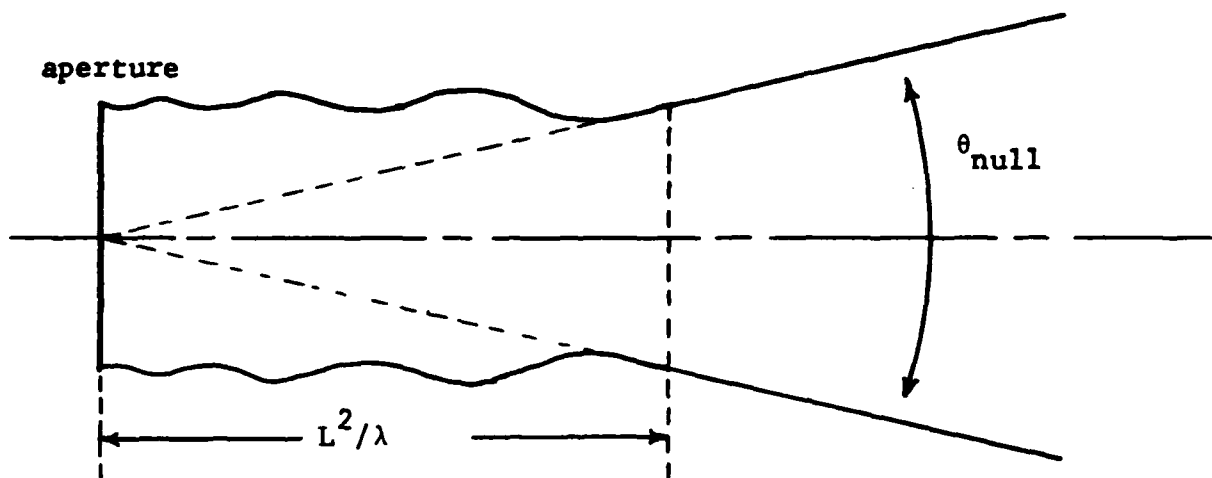
Figure 1
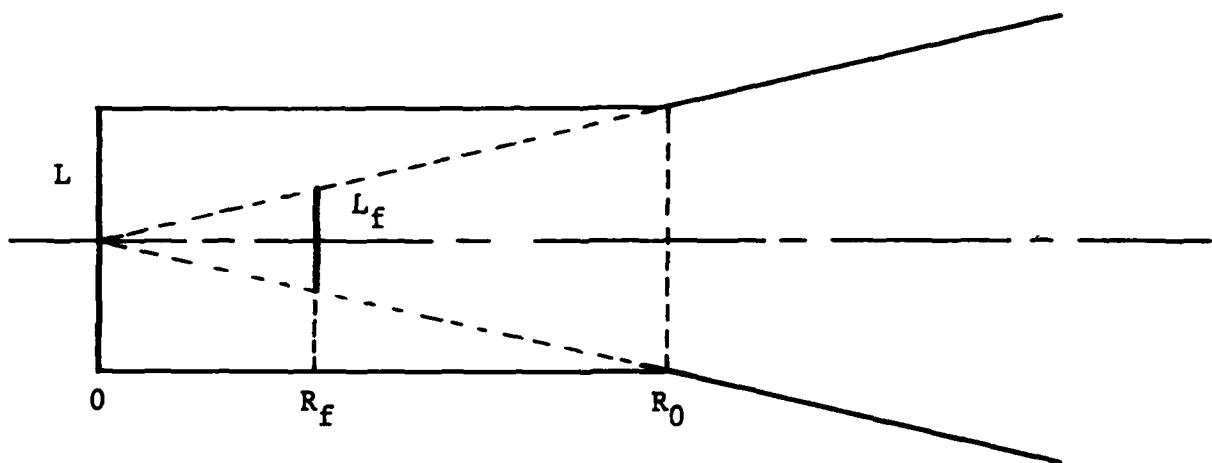Sketch of Main Beam Power Surface

Figure 2
Sketch of Focused Spot

allowing all parts of the aperture to contribute in phase at the focal point at distance r_0. This gives a far field type pattern in the focal region, with near field type patterns at closer distances, and in the far field. Because of this and other complexities, the terms 'Fraunhofer' and 'Fresnel' regions are deprecated. Rather the IEEE (1969) field definitions of far field, radiating near-field and reactive near-field are preferred. For antenna focused at infinity or at the hyperfocal distance, the spot size is roughly L. When the antenna is focused at a shorter distance, the spot size is reduced as sketched in Figure 2. The spot width W is approximately proportional to focal distance:

$$\frac{W}{L} = \frac{r_0}{L^2/\lambda} \qquad \text{or} \qquad WL = r_0\lambda$$

Thus high power densities require small spots, which are produced by large antennas at short wavelengths. Power density is, for any focused antenna (Hansen, 1959):

$$PD = \frac{PG}{4\pi r_0^2}$$

where P is the radiated power and G is the antenna gain. Note that G is the focused antenna gain at the observation point which will not be the same as the unfocused gain. In terms of aperture size, the far field power density is roughly:

$$PD = \frac{PL^2}{r_0^2\lambda^2}$$

Figure 2 and the equations above imply a zero width spot at zero distance, but the spot width actually levels off at a

minimum value of roughly $\lambda/3$ as shown by direct calculations, by an uncertainty argument, and by microscope theory (Hansen, 1965).

1.2 Near Field Calculations

The calculation of accurate fields close to an aperture has always been and still is a difficult problem. This problem is eased when long distances are involved so that phase and amplitude approximations allow such techniques as Fast Fourier Transform to be applied or when the observation angles of interest are close to the axis and at the same time the distance is not too short. All of these ameliorating circumstances approximate the two dimensional field (or diffraction) integral by a simpler form. Narrow angle Fresnel theory is from the 19th century; see Hansen (1964) for historical references. More recent work in utilizing narrow angle Fresnel approximations is by Woonton (1950), Lechtreck (1955), Bates and Elliott (1956), and Melpar (1964). Calculations involving directivity as well have been made by Yang (1955), Polk (1956), Kay (1960), Jacobs (1962), Soejima (1962), and Lind (1966). Other approximate methods include the inverse distance series of Barrar and Wilcox (1958) and simplification of the integrand by Shinn (1956). Measurements in the near field have been made by Bickmore, as previously mentioned, and by Jull (1962) and Scharfman and August (1970). Unfortunately, all of these analytical techniques are simplistic and severely limited. As a result, they have not received attention in recent years. There is an extensive body of experience and literature in the extrapolation of measurements made in the near field close to the surface of an antenna to the far field, the 'near field pattern range'. This work will not be discussed here as it is not relevant or useful but only interesting. Surveys of this work are given by Johnson et al (1973) and Wacker (1982).

There are three techniques for reducing the labor of calculating accurate fields from large apertures, and these techniques need to be evaluated for focused near field usage. Two of these have connections to the work in the 19th century. The first is the Zernike-Jacobi polynomial approach. In this

technique, originated by Zernike (1934), a set of orthogonal polynomials is established in the unit circle. These are sometimes called circle polynomials and are members of the Jacobi family. When used for the diffraction field of an optical device, the result is a double series which converges rapidly for small angles. The Zernike-Jacobi polynomials were applied to electromagnetic problems by Cornbleet (1963) and subsequently utilized by Galindo and Mittra (1977), Galindo and Rahmat-Samii (1981), and by Rahmat-Samii et al (1981). The last reference is a review of this technique and a discussion of its application to near fields. A closely related approach is that of Hu (1960, 1961) who obtained an improvement on the small angle Fresnel formulation, with the resulting field expressed as a sum of Lommel functions of two variables. See also Hansen (1964). Lommel's work dates from 1884. When the Lommel function of two variables is expanded in a series of Bessel functions, a connection can be made with the Zernike polynomials. The Zernike-Jacobi method is, however, basically a small to moderate angle approach in that for large angles the series diverge very slowly. Thus, it cannot be considered here, because wide angle pattern behavior of high power micro-wave antennas is important due to personnel hazards, gain loss, equipment interference, etc.

The second technique with ancient roots is that of field interpolation using a sampling function. Instead of sampling the aperture distribution at a discrete number of suitably closely-spaced points to compute the far field (this, of course, is what an array does), the far field is calculated by interpolating between a discrete number of far field sample points. The number of far field sample points is comparable to the number of aperture sample points so it might appear that no saving would occur. However, the sampling technique is advantageous when the far field points can readily and easily be obtained, e.g. by FFT, and when the angular region over which the field is needed is considerably smaller than the complete

-6-

range of angles. For linear or rectangular apertures in the
far field, the interpolation function is typically the sinc
function, $\sin x/x$. For circular apertures, it is $2J_1 \, x/x$,
again for the far field. Interpolation functions for near
field regions are discussed later. This technique was applied
to antennas by Ruze (1964), with applications for paraboloidal
reflectors in which the surface curvature must be taken into
account made by Bucci and Franschetti (1980, 1981 a & b). In
applying this technique to calculations in the near field,
there are some important questions that must be answered, such
as how close must the samples be spaced and how difficult is
it to calculate the starting near field values. These questions
are answered in Appendix A with the results that the sampling
interpolation technique is not at all attractive for near field
calculations, and, in fact, is slower than direct numerical
integration.

The third method is somewhat more recent and was
developed by Hansen and Bailin in 1959. Here the Hertzian
dipole kernel is expressed as a triad of spherical Bessel
functions; these are then expanded by the Bessel function ad-
dition theorem which allows the original double integral to
be expressed as a sum of radial integrals which involve only
Bessel functions and the aperture distribution (but not the
observation angles) and angular integrals which involve only
associated Legendre functions and elevation angle (but not the
aperture size). The azimuth angle appears simply in the series
coefficients. This method is exact and gives accurate results
and is believed to be comparable in efficiency to the method
used in this report as long as more than several patterns are
to be calculated. However, the mathematics of the program
are complex, while the selected method has the virtue of
simplicity.

The method that is used in the remainder of the
report is direct double numerical integration. There are
three widely used, highly efficient methods for this task, and

each of these is evaluated quantitavely in Appendix B. The
methods are Romberg, which is an adaptive trapezoidal inte-
grator; Gaussian, wherein the coefficients are related to
improved convergence series ala Shanks, and replacement of the
aperture by a discrete array with summation thereof. In all
cases, the number of points must be two per wavelength in each
aperture coordinate for accurate results near broadside and
four per aperture wavelength for accurate results near endfire.
Thus, a 15 wavelength source requires roughly either a seventh
order Romberg, a 32-step Gaussian, or 60 array points. From
Appendix B the conclusion is that the Gaussian has the best
combination of accuracy and speed. In this report two Gaussian
integrators are used, with steps of 32 and 128. The latter
allows wide angle results from apertures as large as 60 wave-
lengths in one dimension. Axial fields are calculated with
the smaller integrator as they do not experience the rapid phase
changes that large apertures have near endfire.

1.3   Outline of the Report

Section 2 of the report is concerned with calculated results of focal region fields. Axial power density, including designs for low transverse sidelobes and designs for low forelobes and aftlobes, are included in Section 2.1. Transverse fields are presented in Section 2.2. References are contained in 2.3. Conclusions and system tradeoffs are given in Section 3. Appendices cover an evaluation of the sampling interpolation technique, an evaluation of numerical integration methods, and listing of computer codes.

2.0   CALCULATION OF FOCAL REGION FIELDS

An excellent picture of the behavior of focal region
fields can be obtained from various transverse pattern cuts
along with a plot of axial power density. The axial case is
treated first as it is somewhat easier, and this section is
followed by the transverse case. The aperture investigated is
square as this is expected to be representative of typical high
power microwave antennas. Such an antenna must be an array to
allow variable focus; and depending on the type of elements,
the array shape may be square, hexagonal, octogonal, circular,
etc. The focal field results will vary in a small way with the
array shape so that the results herein are expected to be
typical of all focal region fields. Since a tapered aperture
distribution may be used, the one-dimensional Taylor one-parameter
distribution is applied to the x and to the y axes of the array.
This is a low Q, robust, highly efficient distribution which
has a far-out sidelobe envelope decreasing as $1/u$, where $u =$
$(L/\lambda) \sin \theta \cos \phi$. The pattern is a modified sin x/x through
the Taylor parameter B. This pattern is described in Appendix
A, and the corresponding aperture distribution is

$$g(x) = I_0 \left(\pi B \sqrt{1-x^2} \right)$$

The sidelobe ratio (inverse of sidelobe level) is given by

$$SLR = 20 \log \frac{\sinh \pi B}{\pi B} + 13.26 \text{ db}$$

Table 1 gives the parameter B for various sidelobe ratios along
with normalized beamwidth, aperture efficiency, and excitation
edge taper. For additional information, consult Hansen (1983).

Table 1—*Taylor one-parameter line source characteristics*

SLR dB	B	u_3 rad	η	ηu_3	edge taper dB
13.26	0	0.4429	1	0.443	0
15	0.3558	0.4615	0.993	0.457	2.5
20	0.7386	0.5119	0.933	0.478	9.2
25	1.0229	0.5580	0.863	0.481	15.3
30	1.2762	0.6002	0.801	0.481	21.1
35	1.5136	0.6391	0.751	0.480	26.8
40	1.7415	0.6752	0.709	0.479	32.4
45	1.9628	0.7091	0.674	0.478	37.9
50	2.1793	0.7411	0.645	0.478	43.3

Other distributions such as the Taylor $\bar{n}$ are slightly more efficient, but the Taylor one-parameter distribution is representative of all cases likely to be of interest.

2.1   Axial Power Density

The discussion of power density along the axis in the focal region is divided into two parts. The first part is concerned with axial power density for uniform and Taylor distributions; these give low sidelobes in the transverse planes. The second section is concerned with low forelobes and aftlobes along the axis, and follows a method developed by Graham (1983).

2.1.1   Taylor Patterns

The square aperture of concern is shown in Figure 3 where the focal distance is r_0 and the point along the axis is specified by R_0. The field on the axis is given by

$$F(0,0) = \frac{2L^2}{R\lambda} \int_0^1 \int_0^1 g(x)g(y) \exp jk(R-r) \, dx \, dy$$

where

$$R^2 = R_0^2 + \frac{L^2}{4} (x^2 + y^2)$$

and

$$r^2 = r_0^2 + \frac{L^2}{4} (x^2 + y^2)$$

The exponential form is needed as x, y enter only as squares, and thus cannot make a cosine form. The aperture distribution in each coordinate is given by $g(\zeta)$. It is convenient to normalize the focal distance in terms of the far field distance $2L^2/\lambda$ and also to normalize the distance along the axis to the focal distance. These are

$$\beta = \frac{R_0}{r_0} \qquad , \qquad \gamma = \frac{r_0}{2L^2/\lambda}$$

Note that normalized observation distance is: $\dfrac{R}{2L^2/\lambda} = \beta\gamma$
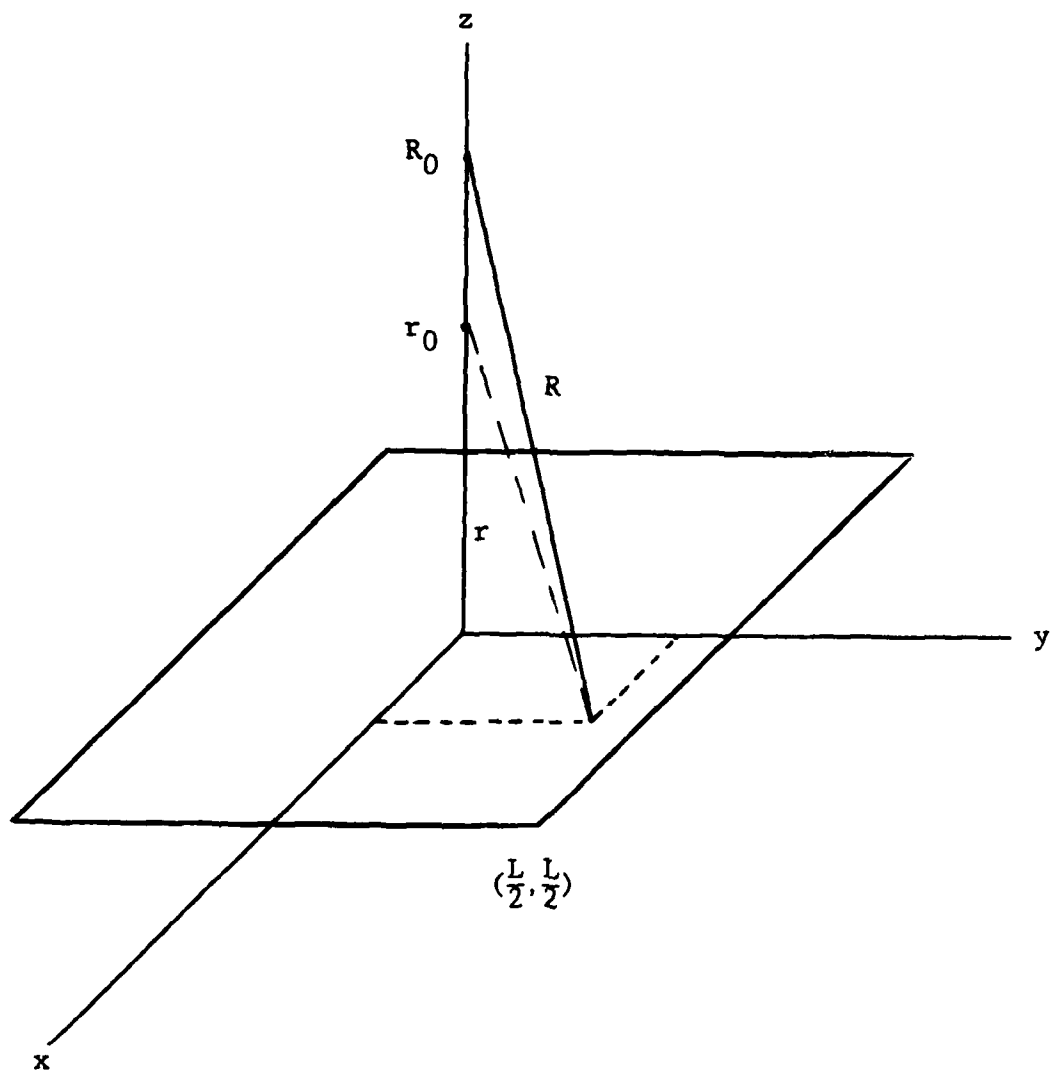
-13-

Figure 3

On-Axis Geometry

When these are inserted, the equation for R becomes

$$R = L \left[4\beta^2 \gamma^2 \left(\frac{L}{\lambda}\right)^2 + \frac{x^2 + y^2}{4} \right]^{1/2}$$

Focused antennas for high power applications will most likely
be arrays, whether of resonant elements such as slots or dipoles
or of larger elements such as horns or dishes. Since all of
these have an element pattern, the most representative results
are obtained by including a suitable element pattern in the
calculations. This pattern is the ideal active element pat-
tern for a half-wave spaced array, and is a power pattern of
$\cos \theta$ in all planes. Since the integration involves 32 steps,
a 32-step approximation to the active element pattern is used
by virtue of incorporating the element pattern into the inte-
gration subroutine. The active element pattern is simply
given by

$$AEP = \sqrt{R_0/R}$$

For uniform excitation the integral can be approximately writ-
ten in terms of Fresnel integrals; this approximation is good
for large γ and D/λ. However, for small apertures and for ta-
pered apertures, it is necessary to use other techniques for
evaluating the double integral. An extensive discussion of
this problem is given in Section 2.2, but here the method
recommended in that section will be used. This is double Gaus-
sian integration. For large L/λ, the phase term may be approx-
imated by separating it into x and y factors; each factor is
kept in the square root form:

$$F(0,0) \simeq \frac{2L^2}{R\lambda} \int_0^1 g(x) \exp jk(R_x - r) \, dx \int_0^1 g(y) \exp jk(R_y - r) \, dy$$

-15-

where $\qquad R_x = L \left[(2\beta\gamma L/\lambda)^2 + (x/2)^2 \right]^{1/2}$

To evaluate this approximation, calculations have been made for $L = 20\lambda$ with this formula and with the exact result. A further simplification has been evaluated, where each separated phase square root expression is replaced by a simple quadratic phase term. For uniform excitation this quadratic phase term leads to the Fresnel integral form

$$F(0,0) = \frac{4L}{R\lambda(1-\beta)} \left[C^2(arg) + S^2(arg) \right]$$

$$arg = \sqrt{(1-\beta)/4\beta\gamma}$$

Figures 4, 5, and 6 show the results for $\gamma = .025$ and for uniform excitation. Figure 4 is the result of the exact calculation, Figure 5 is the result of using the separated quadratic phase terms while Figure 6 is the Fresnel approximation. It can be noted that the separated quadratic phase approximation yields results that are very close for the first forelobe, main lobe, and back lobe with close in forelobes having lower peaks and less deep nulls. Thus, the forelobe envelope in the approximate form decays somewhat faster than the exact result. The Fresnel approximation gives a main lobe broader than actual with an aftlobe several db too low. The forelobes are displaced in position and have an envelope that decays much faster than the actual. For small values of β the results are due to computer errors. Similar results were obtained for the 25 db Taylor case. In general, the separated phase calculation agrees more closely with exact calculation for larger γ and for larger L/λ. Since practical high power microwave apertures are likely to be much larger than 20λ, the separated phase results are quite adequate and are used for more extensive calculations.
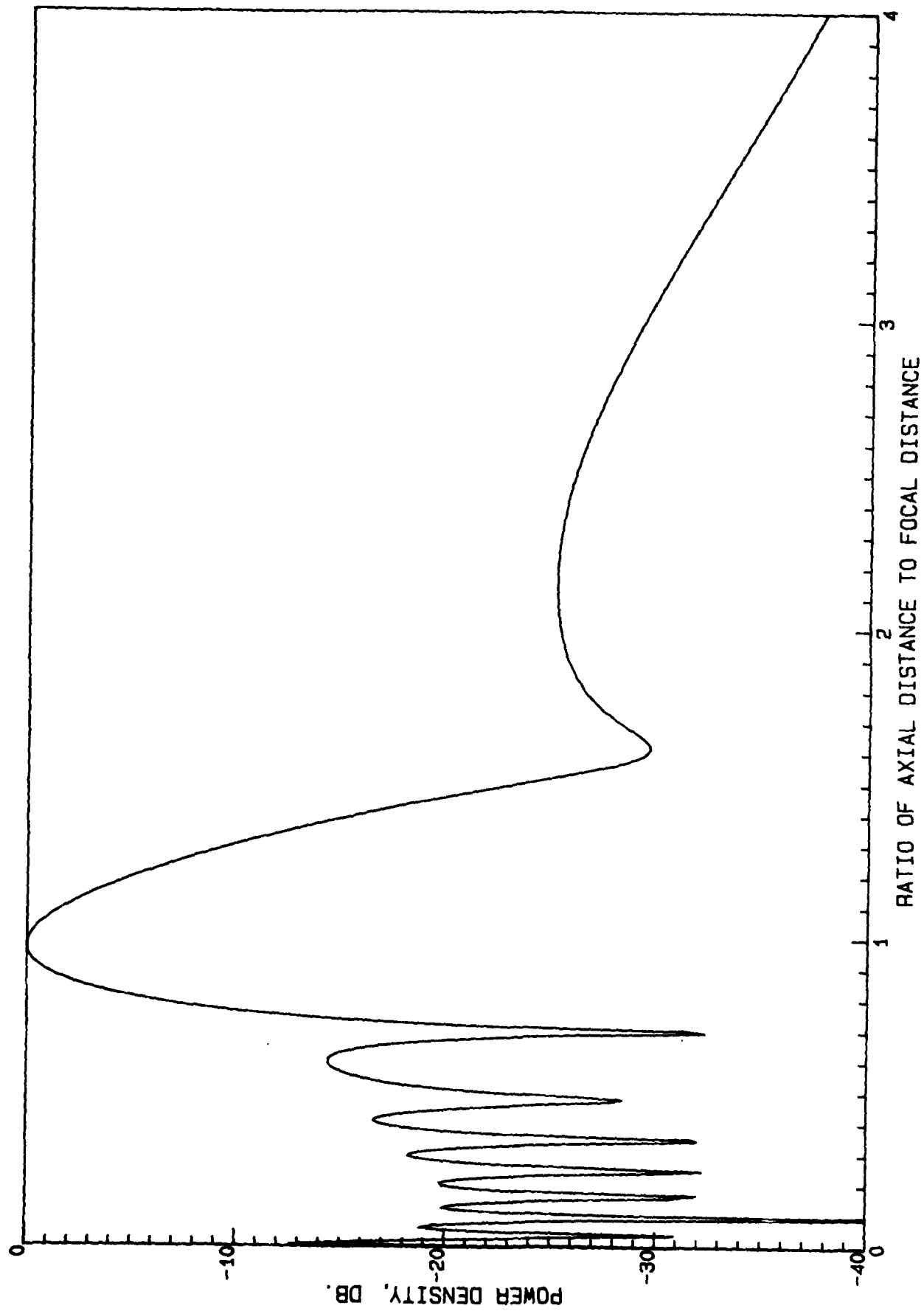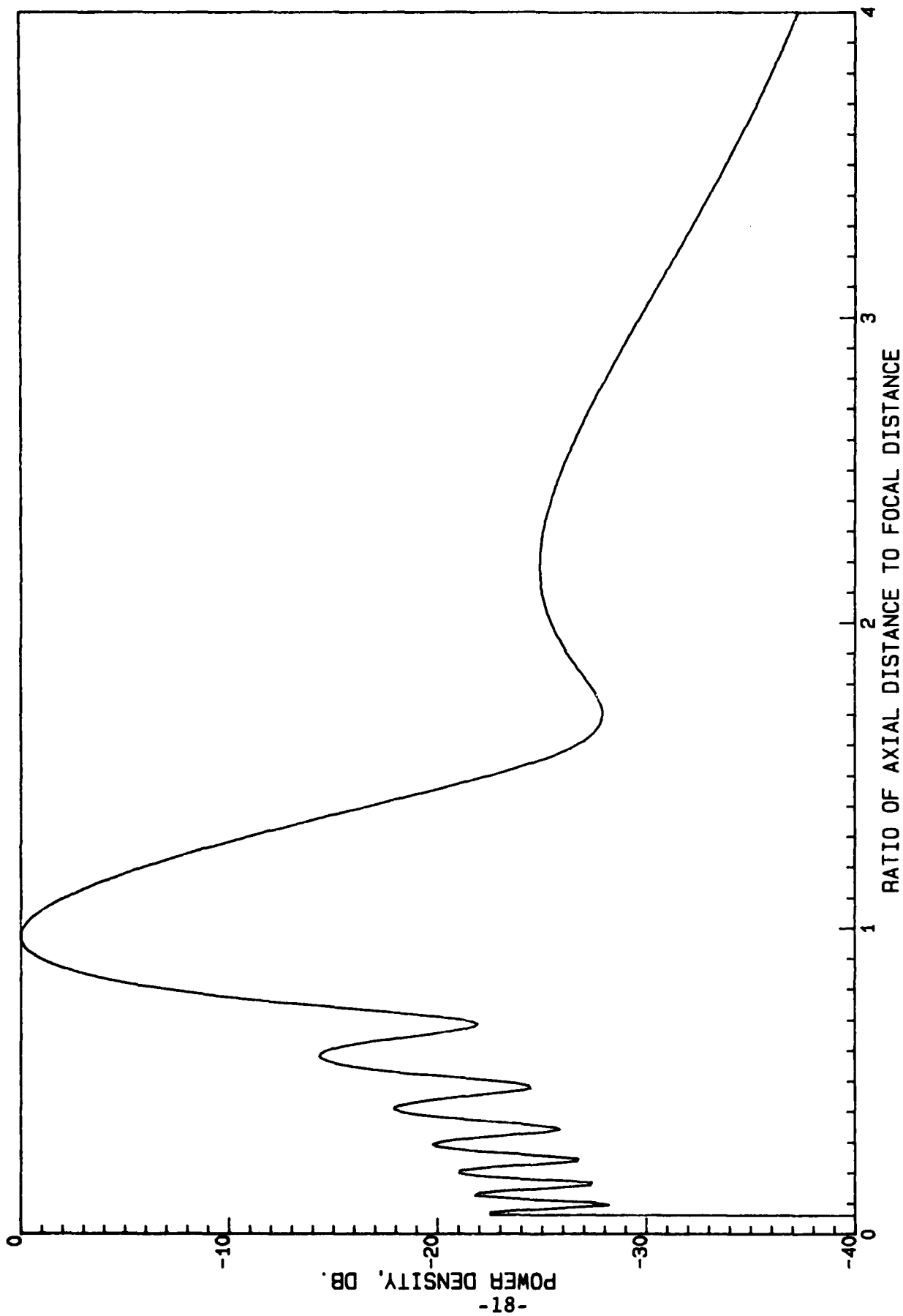
RATIO OF AXIAL DISTANCE TO FOCAL DISTANCE

AXIAL P D OF UNIFORM 20 WV SQUARE APERTURE, GAMA=.025

Figure 4

-17-

RATIO OF AXIAL DISTANCE TO FOCAL DISTANCE

AXIAL P D OF UNIFORM 20 WV SQUARE APERTURE, GAMA=.025

Figure 5

POWER DENSITY, DB.

RATIO OF AXIAL DISTANCE TO FOCAL DISTANCE

AXIAL P D OF UNIFORM 20 WV SQUARE APERTURE, GAMA=.025
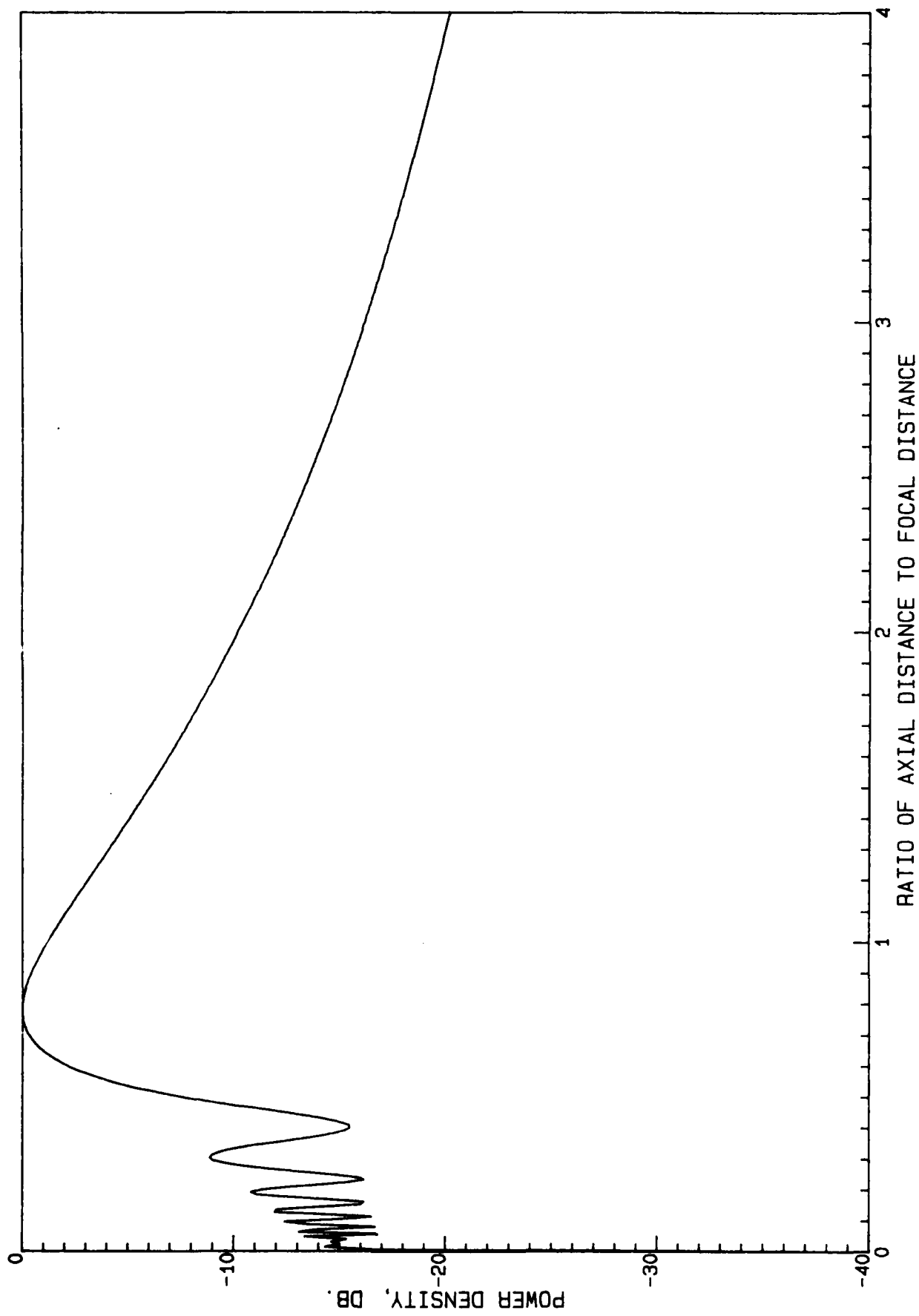
Figure 6

POWER DENSITY, DB.

-61-
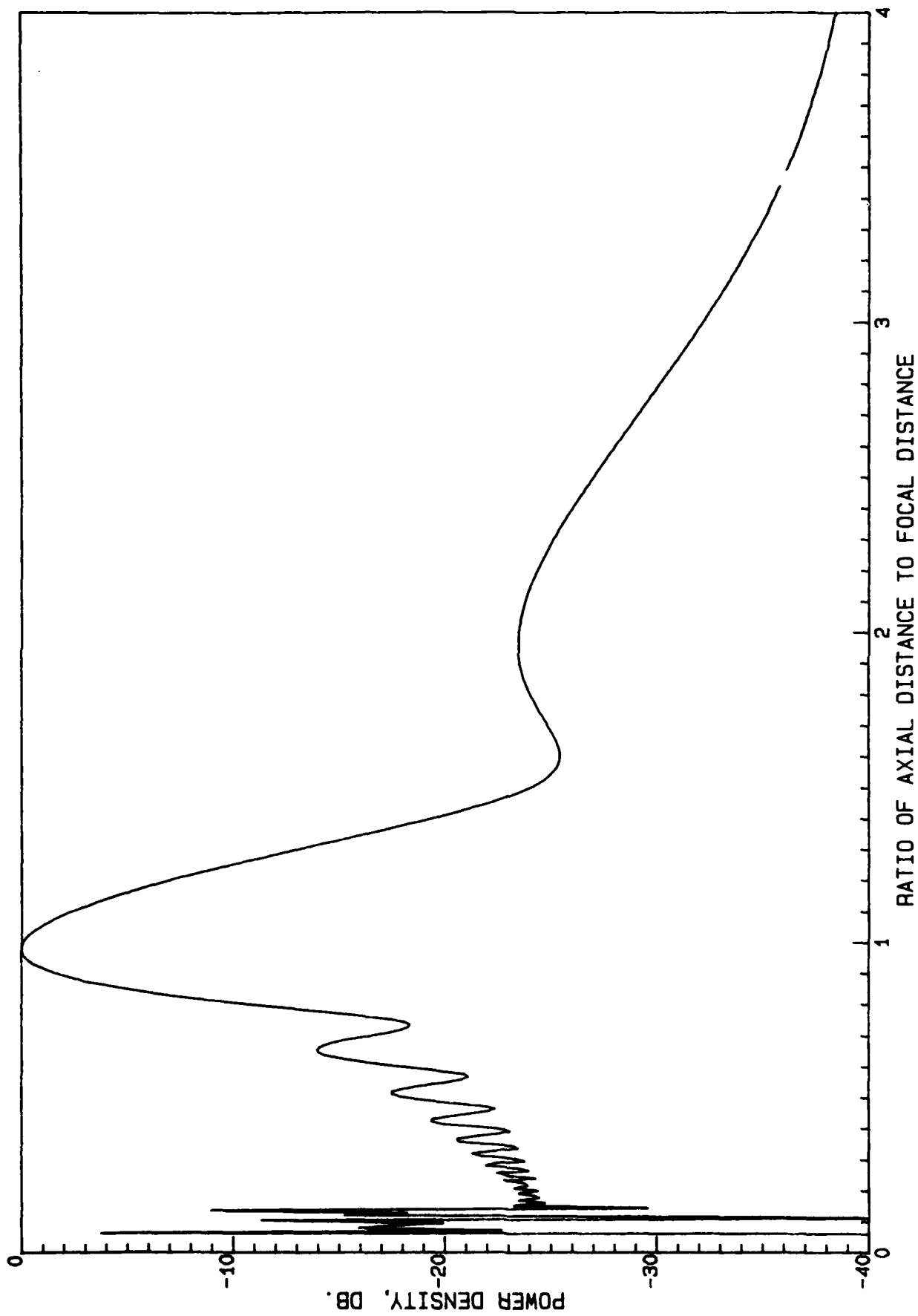
Figures 7, 8, 9, and 10 show the axial distribution
of uniformly excited square apertures for larger values of γ.
It may be noticed that at distances approaching L^2/λ the pat-
terns peak occurs significantly closer to the aperture due to
the $1/R^2$ effect. As γ becomes smaller, the peak moves closer
to the focal point, at $\beta = 1$. Also, as γ increases, the fore-
lobe level increases. This level is roughly -12 db at $\gamma = .05$
and increases to -4 db at $\gamma = .5$. Note that there are no
aftlobes at all. Figures 11 through 14 show the axial distri-
bution for a square aperture with a 25 db Taylor distribution
along each axis. Not surprisingly, the forelobe oscillations
are considerably reduced, but the forelobe envelope is increased.
For example, for $\gamma = .05$ the forelobe is not quite -8 db and
for $\gamma = .2$ it has increased to less than -3 db. Figures 15
through 18 show uniform and 25 db results for a 100λ square
aperture. The 100λ results are very close to those of 20λ,
except for low forelobes at small values of β. It appears that
the axial field distribution is essentially independent of L/λ,
as long as $L \gg \lambda$. Thus these axial results are expected to
be representative of all large square apertures.

From the sequence of Figure 5, and 7 through 10, the
effect of the $1/R^2$ can be observed. As mentioned above, for
small γ the peak occurs close to $\beta = 1$, i.e. near the focal
point. As the focal point moves away from the aperture, the
peak moves away also but at a progressively slower rate so
that as the focal point approaches infinity, the peak merges
into the $1/R^2$ contour. The behavior can be understood quan-
titatively by utilizing the approximate Fresnel integral form
which, although inaccurate for forelobes and aftlobes, gives
good results for the lobe peak. When the aperture power den-
sity is normalized to unity at a distance of $2L^2/\lambda$, the power
at the beam peak is as shown in Figure 19. Power is plotted
here against $\beta\gamma$ as this is distance in terms of far field dis-
tance. It can be seen that for large distance the focal spot
is merging into the $1/R^2$ contour at a point which gives a
power density of roughly 11 db. This curve can be used in the
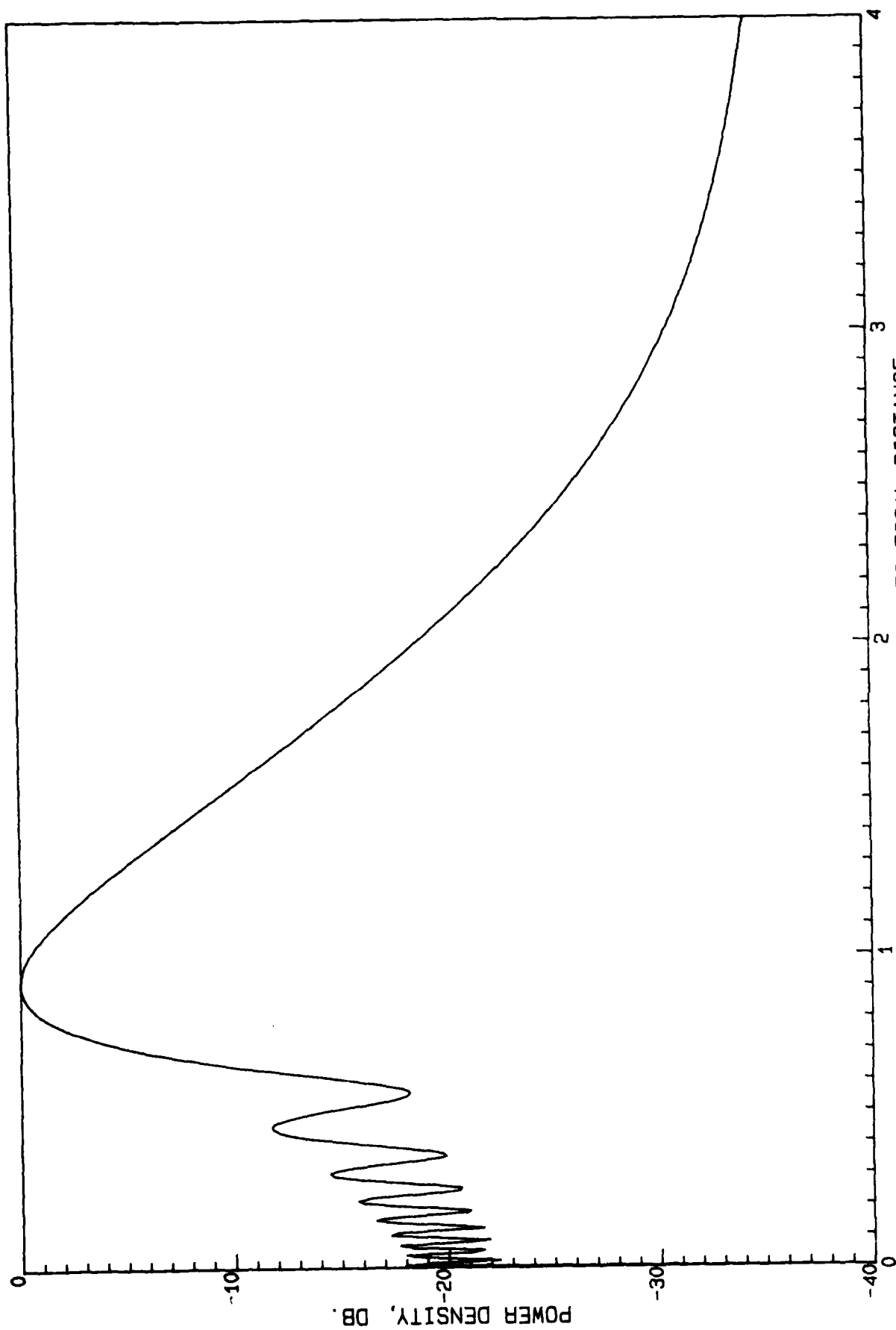
RATIO OF AXIAL DISTANCE TO FOCAL DISTANCE

AXIAL P D OF UNIFORM 20 WV SQUARE APERTURE, GAMA=.05

Figure 7

RATIO OF AXIAL DISTANCE TO FOCAL DISTANCE

AXIAL P D OF UNIFORM 20 WV SQUARE APERTURE, GAMA=.1

Figure 8

-22-

RATIO OF AXIAL DISTANCE TO FOCAL DISTANCE

AXIAL P D OF UNIFORM 20 WV SQUARE APERTURE, GAMA=.2

Figure 9

POWER DENSITY, DB.

-23-

RATIO OF AXIAL DISTANCE TO FOCAL DISTANCE

AXIAL P D OF UNIFORM 20 WV SQUARE APERTURE, GAMA=.5

Figure 10

POWER DENSITY, DB.

-24-

RATIO OF AXIAL DISTANCE TO FOCAL DISTANCE

AXIAL P D OF 25 DB TAYLOR 20 WV SQUARE APERTURE, GAMA=.025

Figure 11

RATIO OF AXIAL DISTANCE TO FOCAL DISTANCE
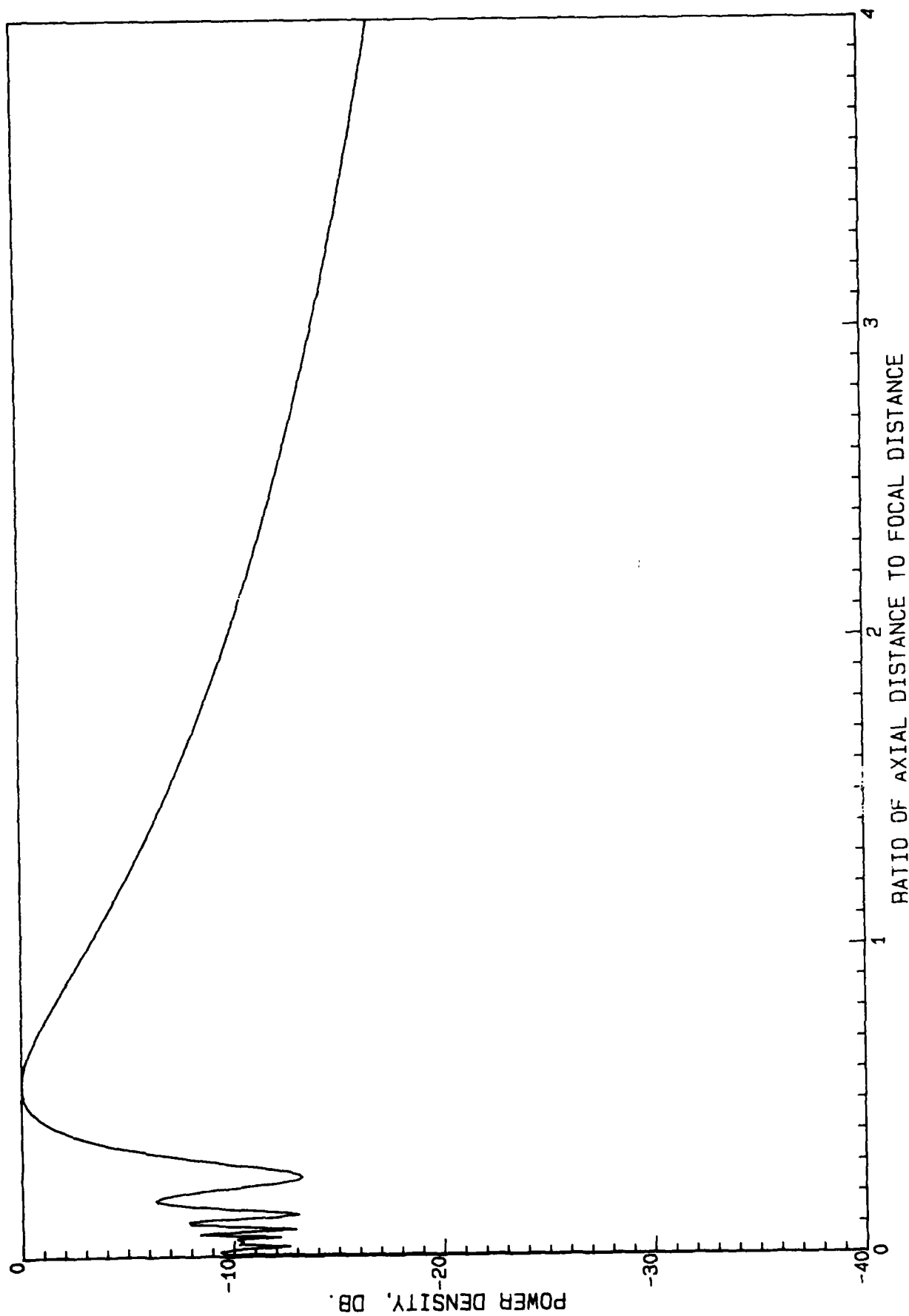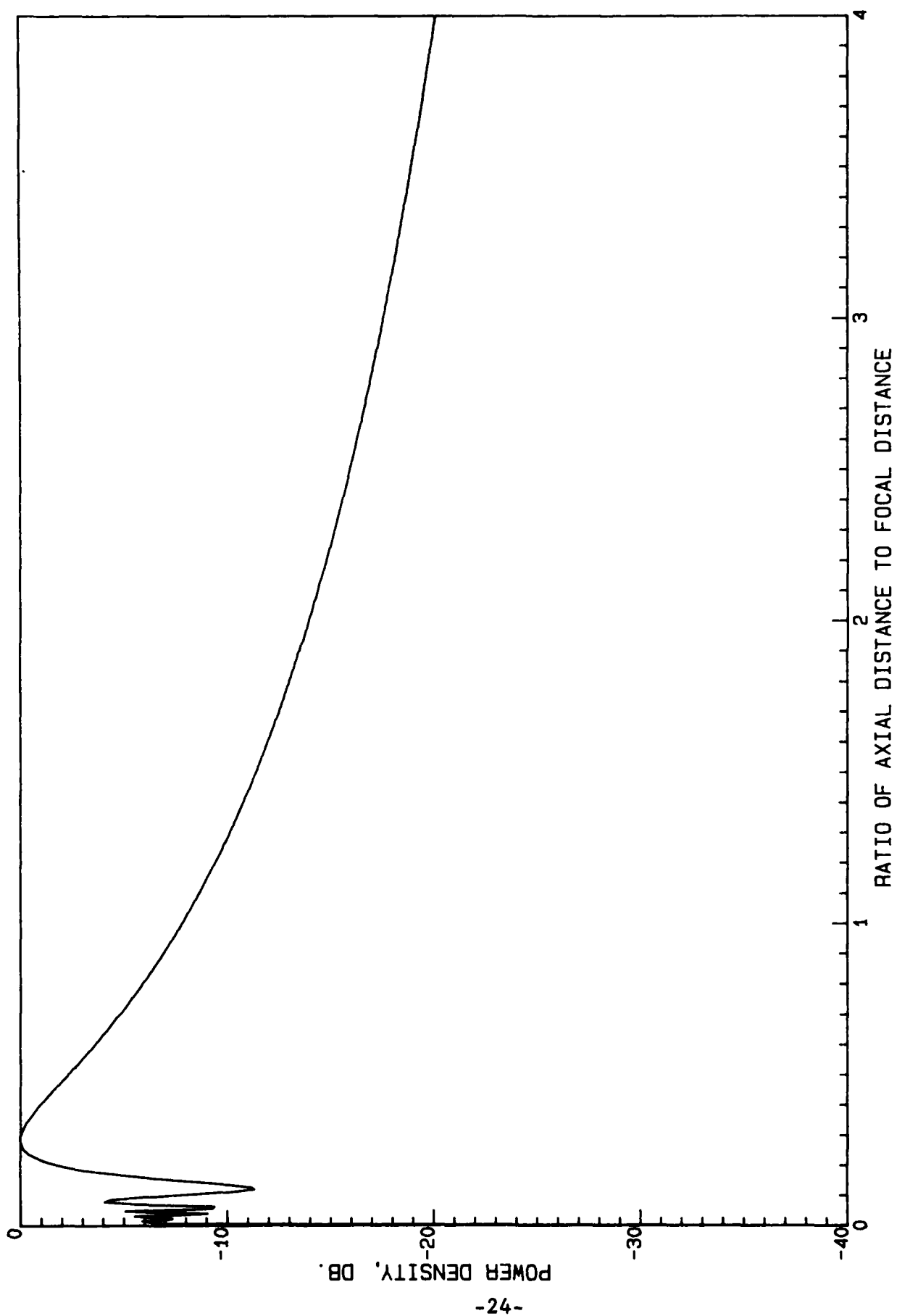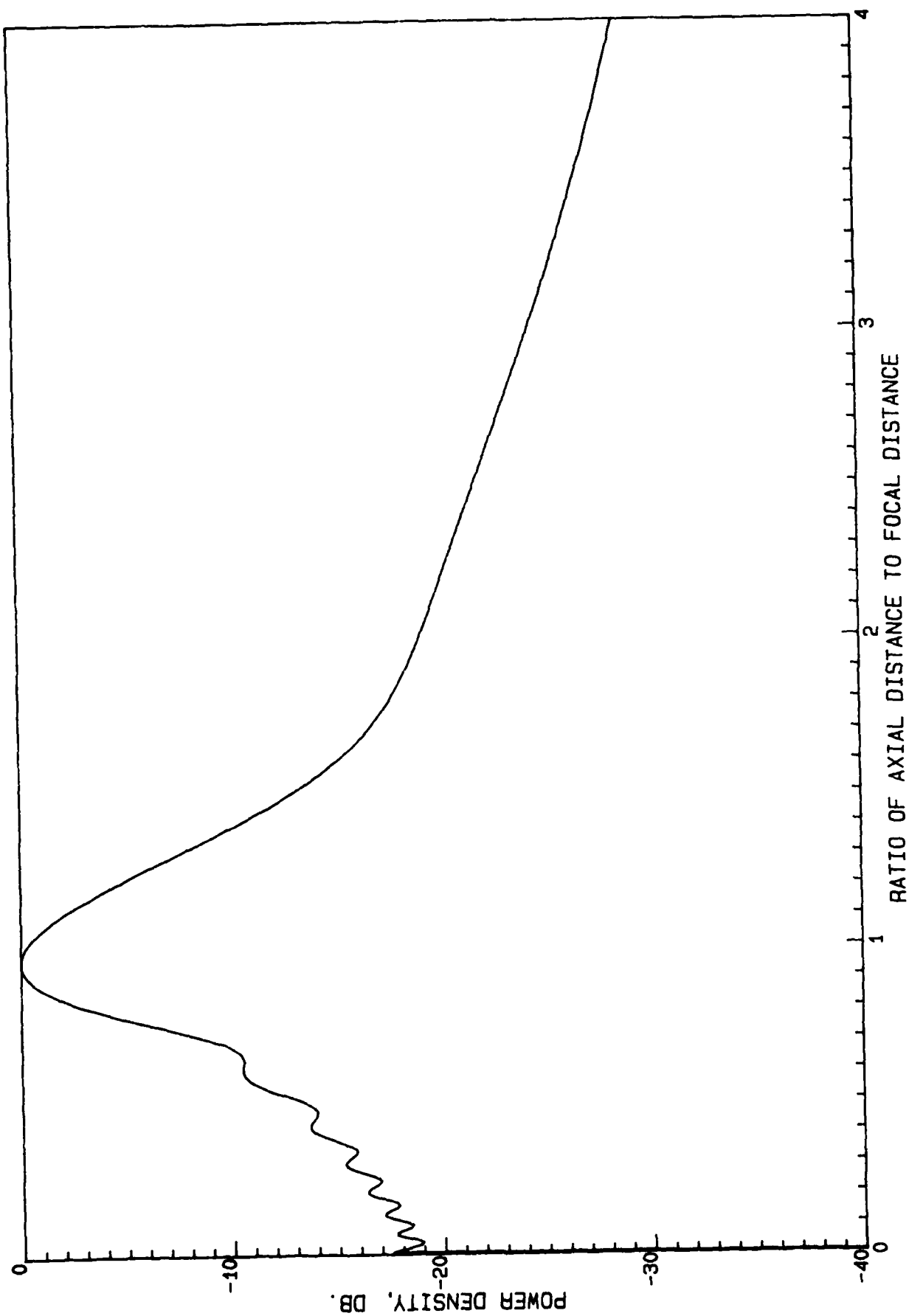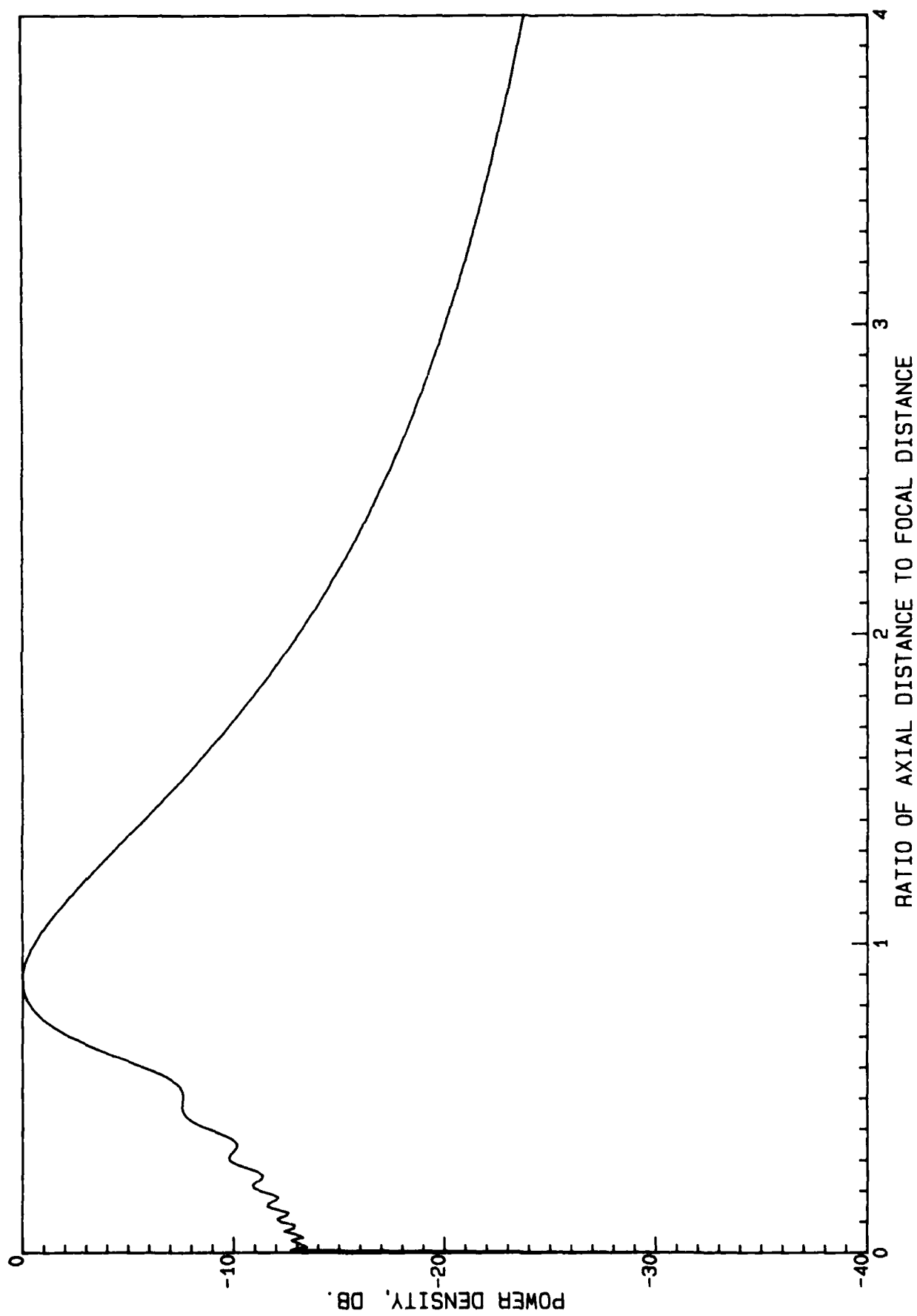
AXIAL P D OF 25 DB TAYLOR SQUARE APERTURE, GAMA=.05

Figure 12
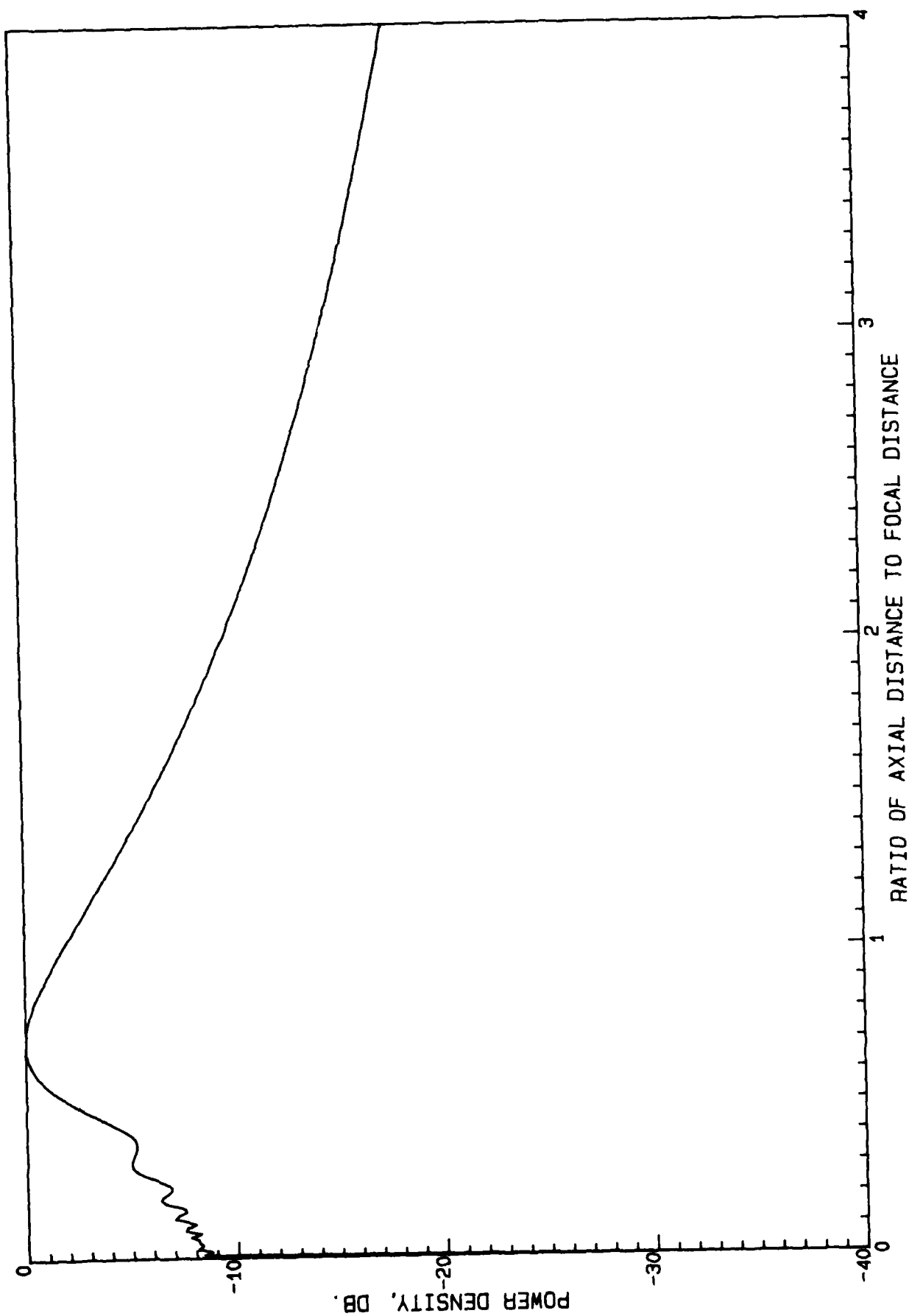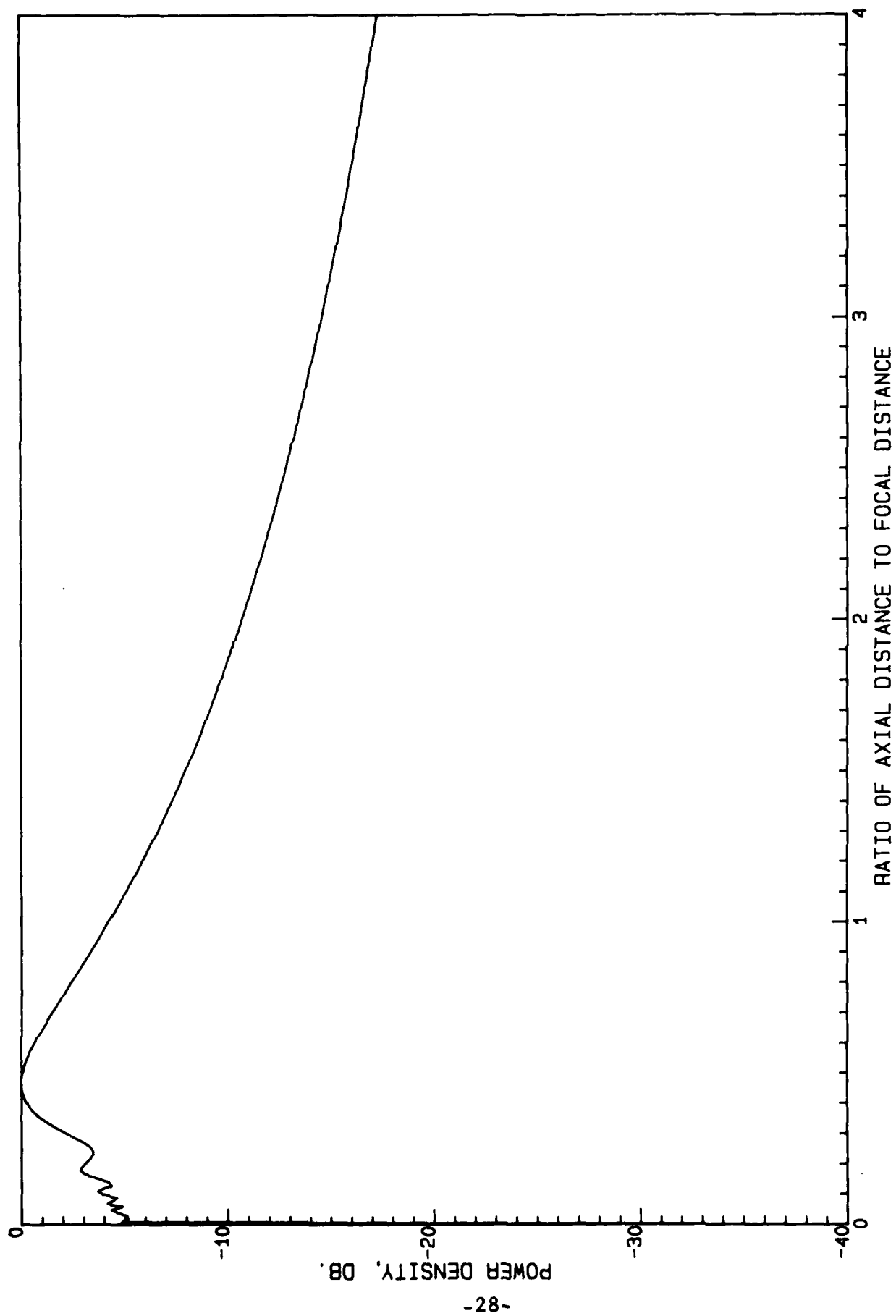
RATIO OF AXIAL DISTANCE TO FOCAL DISTANCE

AXIAL P D OF 25 DB TAYLOR 20 WV SQUARE APERTURE, GAMA=.1

Figure 13

RATIO OF AXIAL DISTANCE TO FOCAL DISTANCE

AXIAL P D OF 25 DB TAYLOR 20 WV SQUARE APERTURE, GAMA=.2

Figure 14

RATIO OF AXIAL DISTANCE TO FOCAL DISTANCE

AXIAL P D OF UNIFORM 100 WV SQUARE APERTURE, GAMA=.05

Figure 15

POWER DENSITY, DB.

RATIO OF AXIAL DISTANCE TO FOCAL DISTANCE

AXIAL P D OF UNIFORM 100 WV SQUARE APERTURE, GAMA=.1

Figure 16

RATIO OF AXIAL DISTANCE TO FOCAL DISTANCE

AXIAL P D OF 25 DB TAYLOR 100 WV SQUARE APERTURE, GAMA=.05

Figure 17

POWER DENSITY, DB.

RATIO OF AXIAL DISTANCE TO FOCAL DISTANCE
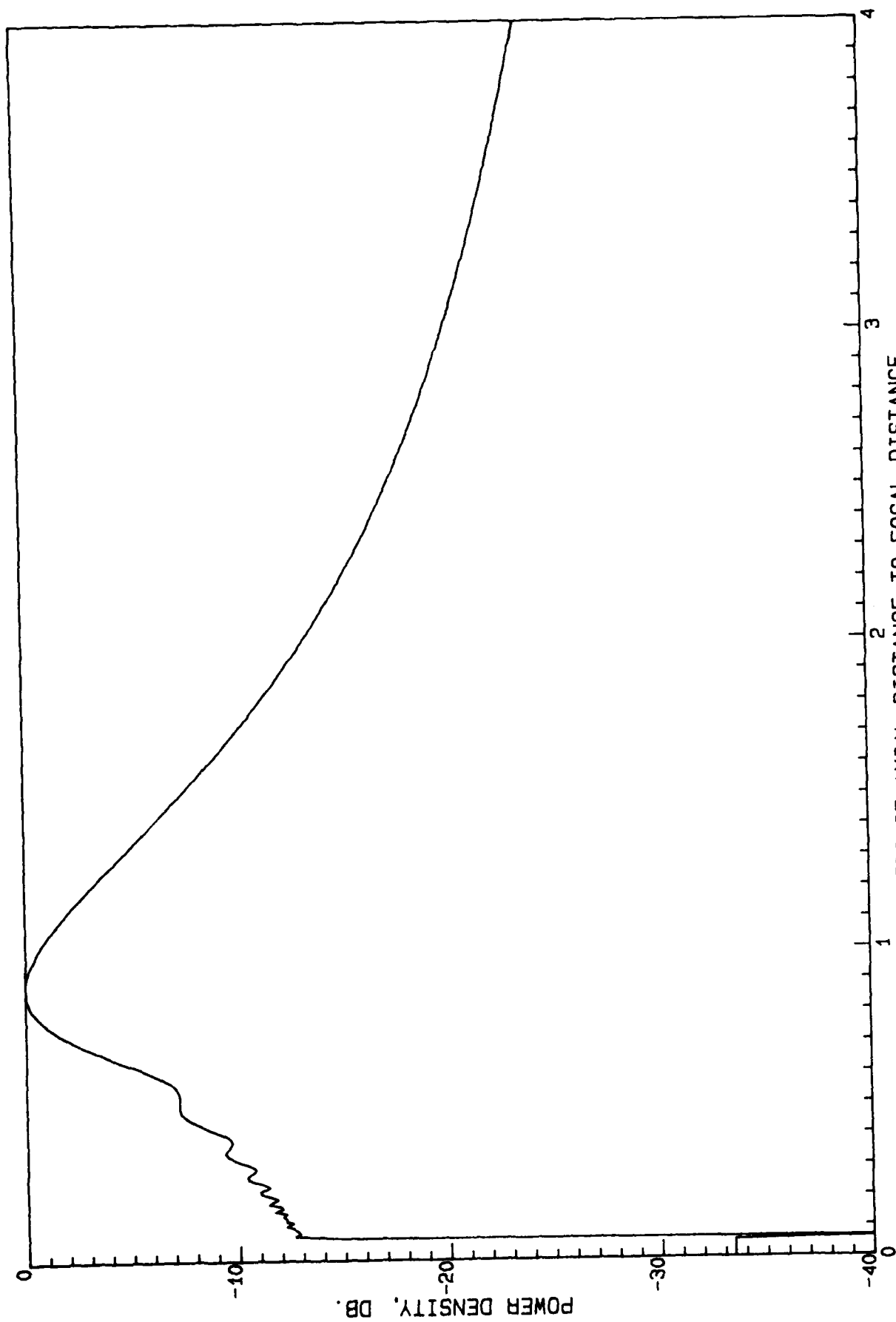
AXIAL P D OF 25 DB TAYLOR 100 WV SQUARE APERTURE, GAMA=.1
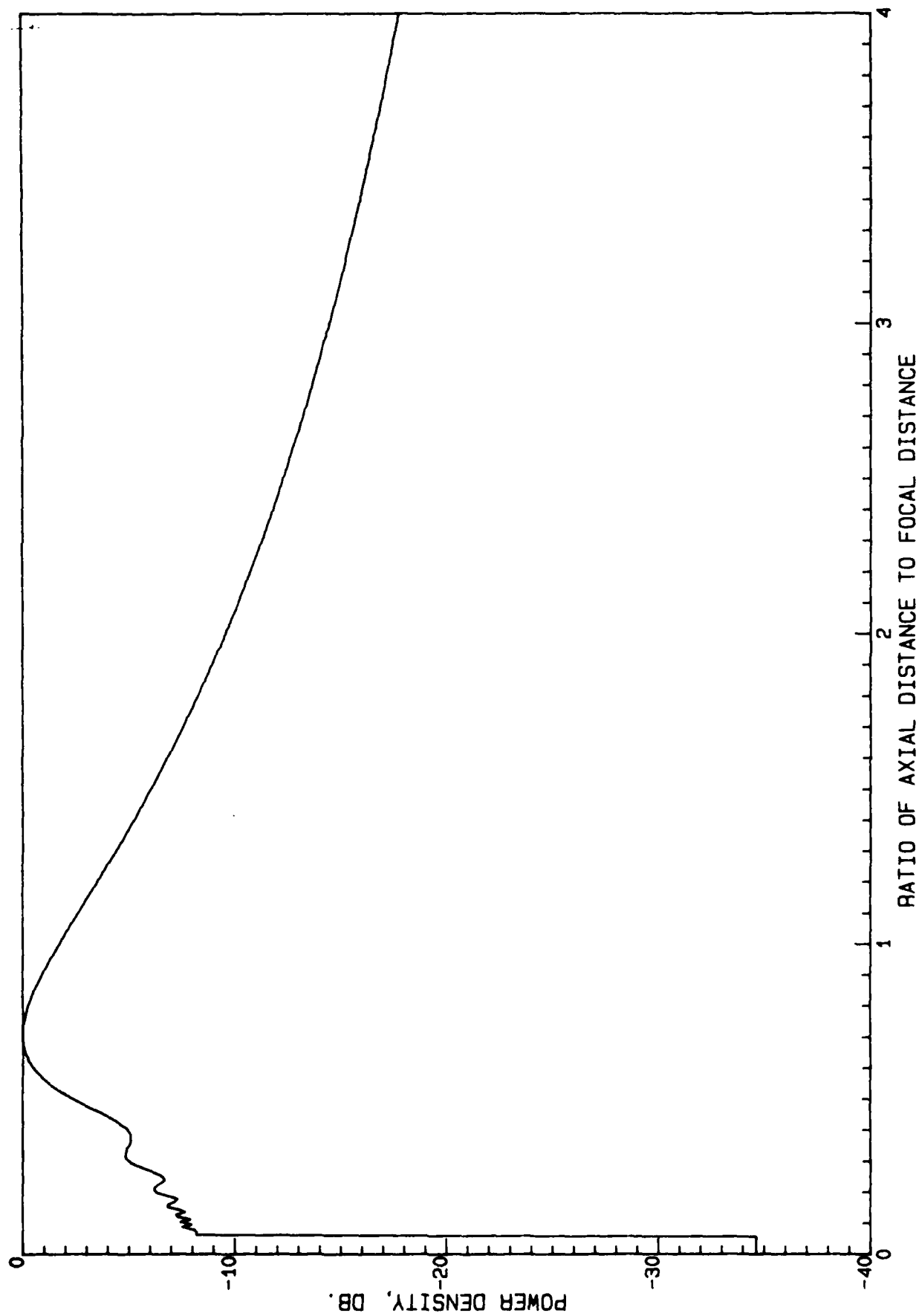
Figure 18

Figure 19

Focal Spot Power Density
(normalized to 0 db
at $2L^2/\lambda$)
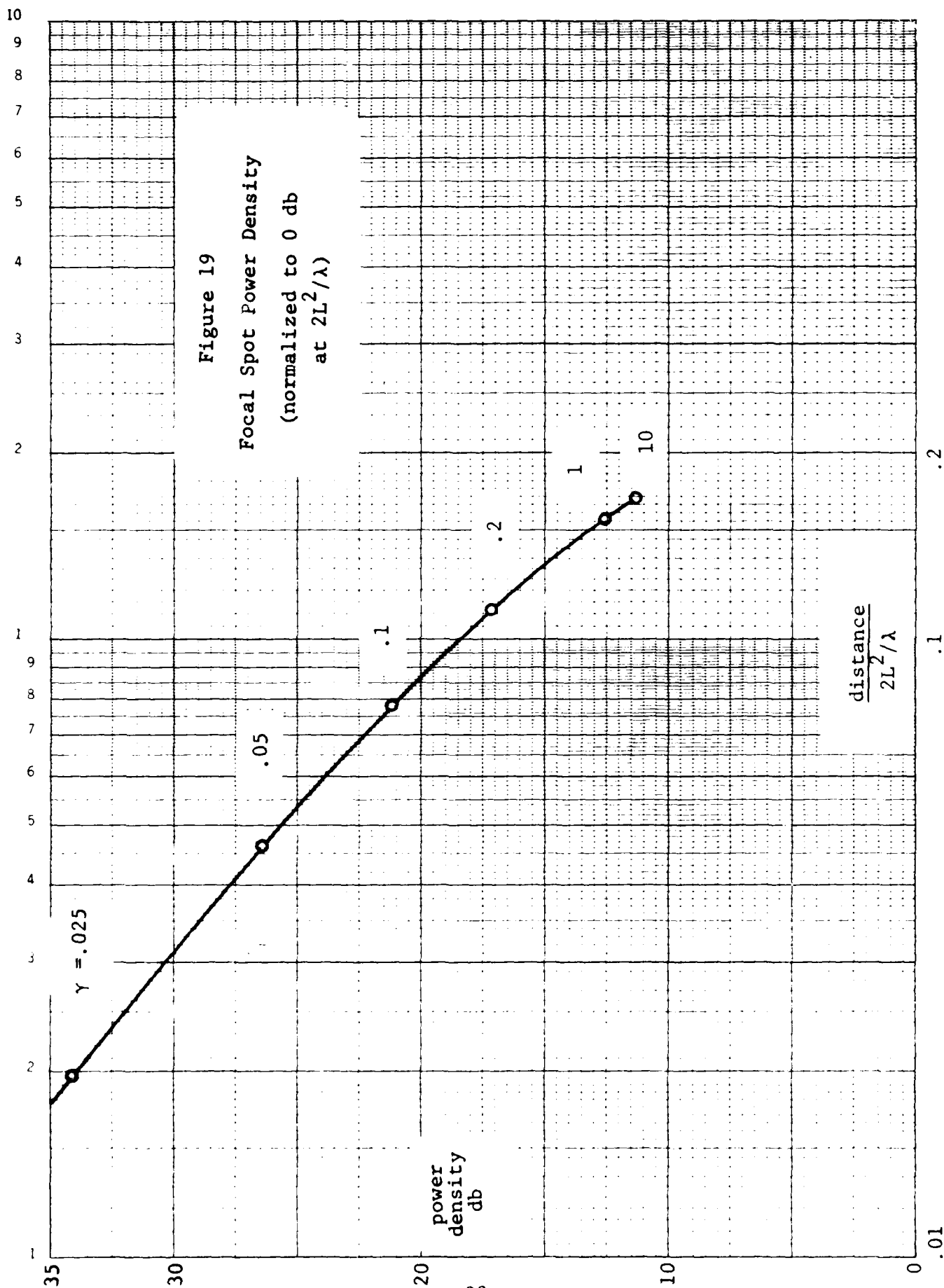
tradeoff of aperture size, wavelength, focal distance, and power density. For example, selection of $\beta\gamma = .02$, which is for a spot maximum at $R = .04L^2/\lambda$, gives a power density increase of 34 db (2500) over the unfocused value at $2L^2/\lambda$, from Figure 19. That unfocused value is:

$$PD = \frac{PG}{4\pi R^2} = \frac{PL^2\eta}{R^2\lambda^2} = \frac{P\eta}{4L^2}$$

where η is the array efficiency (wrt lossless uniform excitation). The spot maximum power density is then $P\eta/4L^2$ times 2500. The focal distance is found from Figure 19 where $\alpha = .025$.

2.1.2   Low Forelobe and Aftlobe Axial Patterns

From the previous work, it was observed that a
tapered distribution which gave lower transverse pattern side-
lobes yielded higher for forelobes and aftlobes along the axis.
One might expect that an inverse aperture taper, i.e. one
higher at the edges than at the center, would reduce the axial
lobes. This type of distribution is not to be confused with
a monopulse distribution, where the two halves of the aperture
are out of phase. Graham (1983) has discovered a clever way
of exhibiting this property for line sources. Note that line
sources are intrinsically different as shown by Ricardi and
Hansen (1973). In a two-dimensional aperture the near field
phase smear degrades the pattern directivity in both planes,
thereby negating the $1/R^2$ field increase with decreasing dis-
tance. The result is that between the aperture and the focal
peak the power density for an unfocused planar aperture is
roughly constant, i.e. the oscillations are about a constant
level. For a line source, the pattern can be degraded in only
one plane and thus only $1/R$ effects are cancelled, leaving a
$1/R$ envelope. Thus, the field oscillations for an unfocused
line source are about a $1/R$ line as shown by Ricardi and Hansen.
And so the power density behavior for a focused line source can
be expected to be different also.

The quadratic phase approximation of the previous
section can be used for the line source with the result that

$$F = \int_0^1 g(x) \exp j\pi\zeta^2 x^2 \, dx \quad ,$$

where
$$\zeta^2 = \frac{1-\beta}{8\beta\gamma}$$

By making a substitution of y for x^2, the formula becomes

$$F = \frac{1}{2} \int_0^1 \frac{g(\sqrt{y})}{\sqrt{y}} \exp j\pi\zeta^2 y \, dy$$

This is now similar to the formula for pattern of a uniform line source which is

$$F(u) = \int_0^1 \cos \pi u y \, dy = \frac{\sin \pi u}{\pi u}$$

Graham noticed the similarity between these results, although the uniform line source pattern only matches the real part of the axial field expression. However, an approximate correspondence can be made between the angular variable u and the axial variable ζ^2 providing that the weighting factor which is $g(\sqrt{y})/\sqrt{y}$ can be made unity. The result is that an amplitude excitation of $|x|$ gives approximately a sinc ζ^2 axial distribution except that the 1/R factor is not incorporated. Even lower axial forelobes and aftlobes can be produced by using a $|x| \, g(x^2)$ distribution. For example, low axial lobes can be produced by the Taylor distribution

$$g(x) = |x| \, I_0 \, (\pi B \sqrt{1-x^4})$$

Note, however, that the parameter ζ is not convenient, and the lobe behavior in terms of β, or $\beta\gamma$, will exhibit lobes that are squeezed together for small β and stretched out for large β.

These ideas have been used to determine behavior of the square aperture with inverse tapers, using the more accurate separated quadratic phase expression. Figures 20

-36-

through 22 show the axial power density for γ = .025, .05, and .1 and it may be seen, as expected, that the forelobes are higher than the aftlobes because of the $1/R^2$ effect. The forelobe level is considerably below the roughly -13 db obtained by Graham for line sources, because the square sources here have elemental aperture areas in two dimensions that are contributing to the out of phase interference that produces the forelobes. For this reason, the forelobe level vari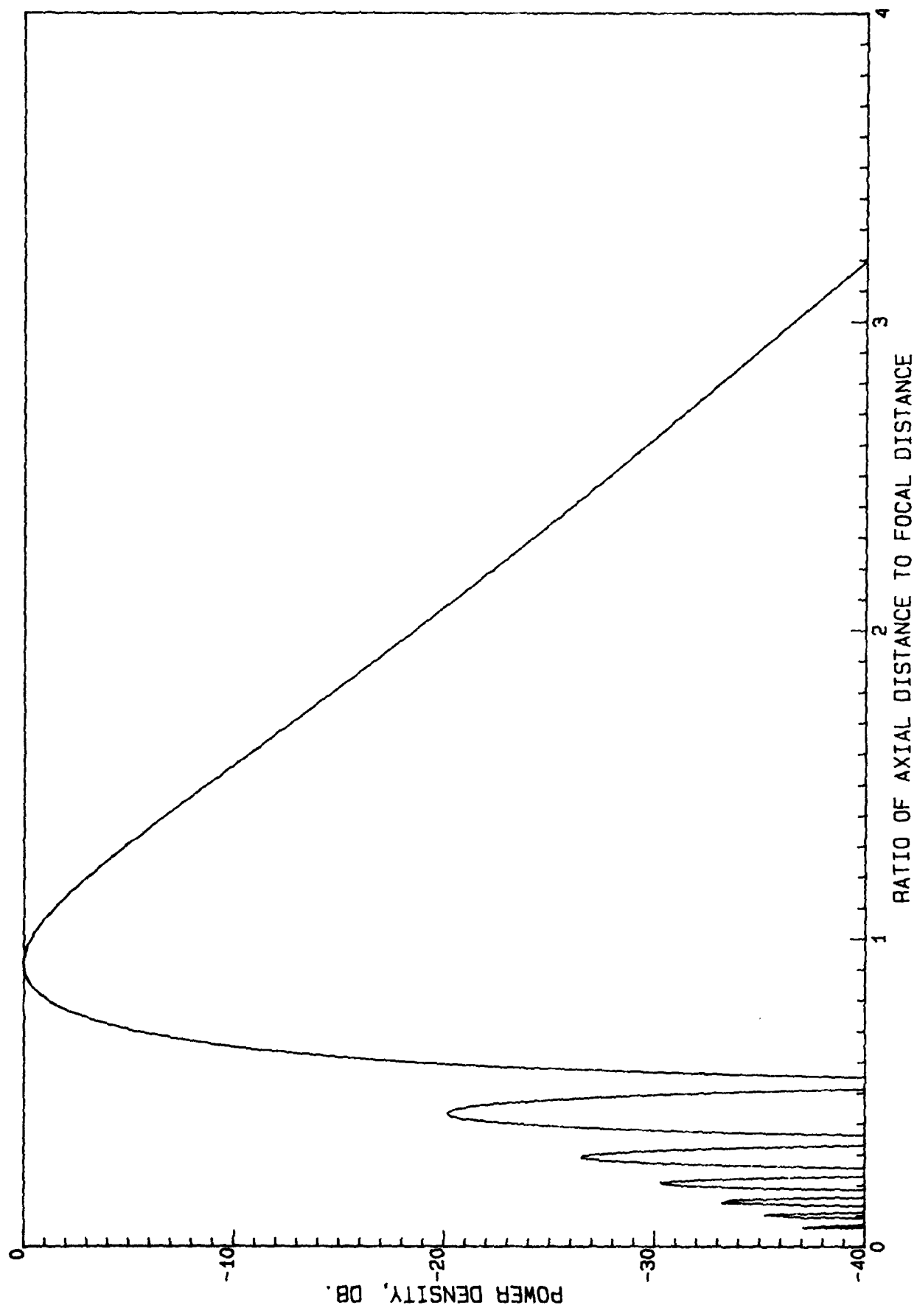es more with γ than for the line source case. In fact, it varies from -22 db to -18 db for the three cases shown. A narrower main lobe and higher fore and aftlobes can be obtained by putting a pedestal on the inverse distribution, just as in conventional transverse pattern synthesis. For example, a pedestal of .5 added to x gives a forelobe level of -18 db for the γ = .025 case. Lower distributions are obtained by using the inverse Taylor distribution, as shown in Figures 23, 24, and 25. Note that in these figures and the previous triad, the figure captions for simplicity show 'uniform axial' and '25 db Taylor axial', although the patterns only roughly fit these. Thus, the inverse distribution plus pedestal allows any reasonable forelobe level to be reached between those of the pure inverse and the uniform distributions. And the inverse Taylor allows even lower distributions to be realized. For a given aperture, an axial sidelobe level and envelope can be optimally synthesized, although the results are not expected to be significantly different from those here. There is an appreciable gain loss in any inverse distribution, and this is related to the increase in sidelobes in transverse patterns. Both of these effects will be addressed in Section 2.2. Note that for the inverse distribution the excitation is zero at the center of the aperture and +1 at the aperture edges.

RATIO OF AXIAL DISTANCE TO FOCAL DISTANCE
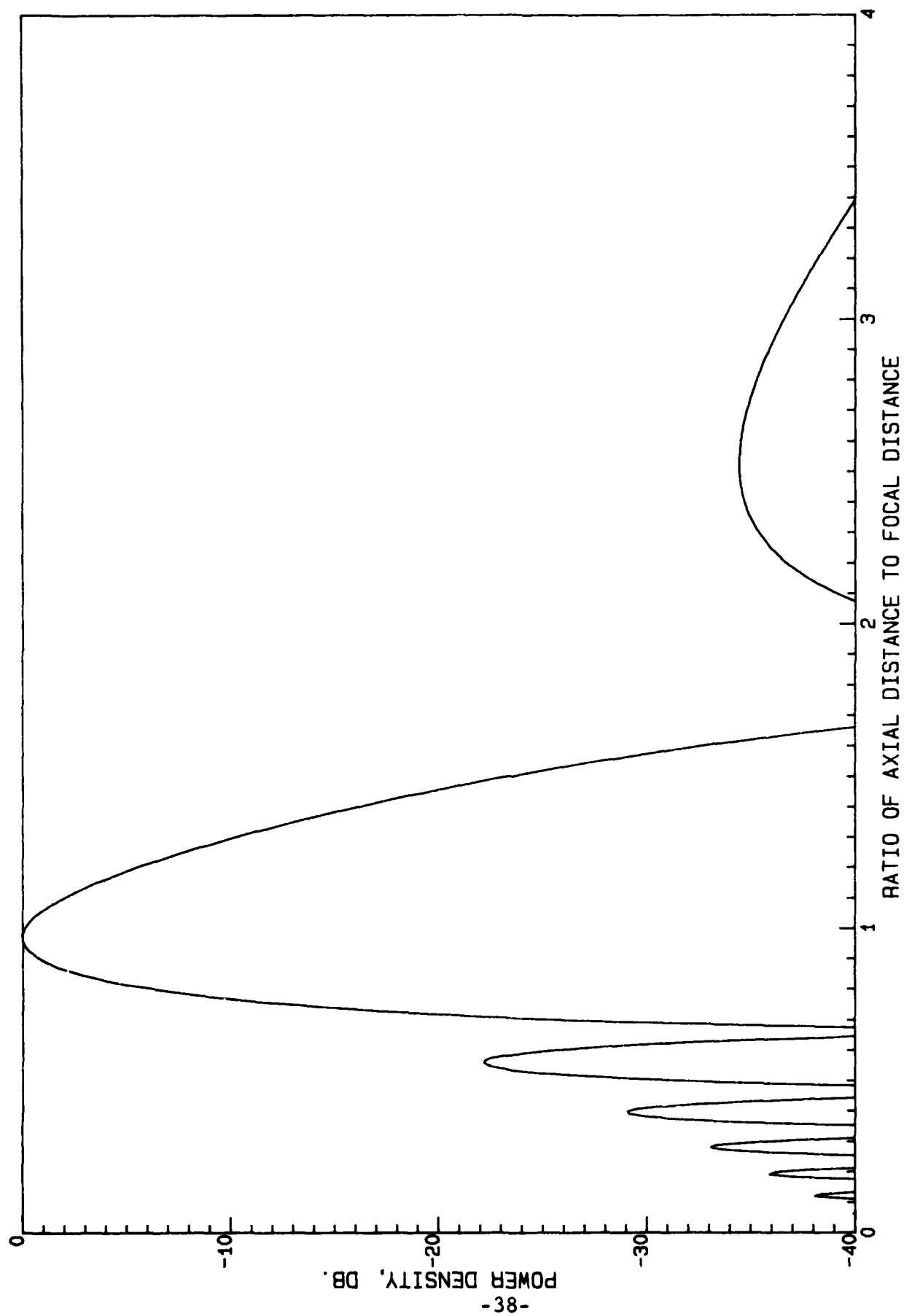
AXIAL P D OF 20 WV SQUARE APERTURE WITH UNIFORM AXIAL PATTERN, GAMA=.025

Figure 20

AXIAL P D OF 20 WV SQUARE APERTURE WITH UNIFORM AXIAL PATTERN, GAMA=.05
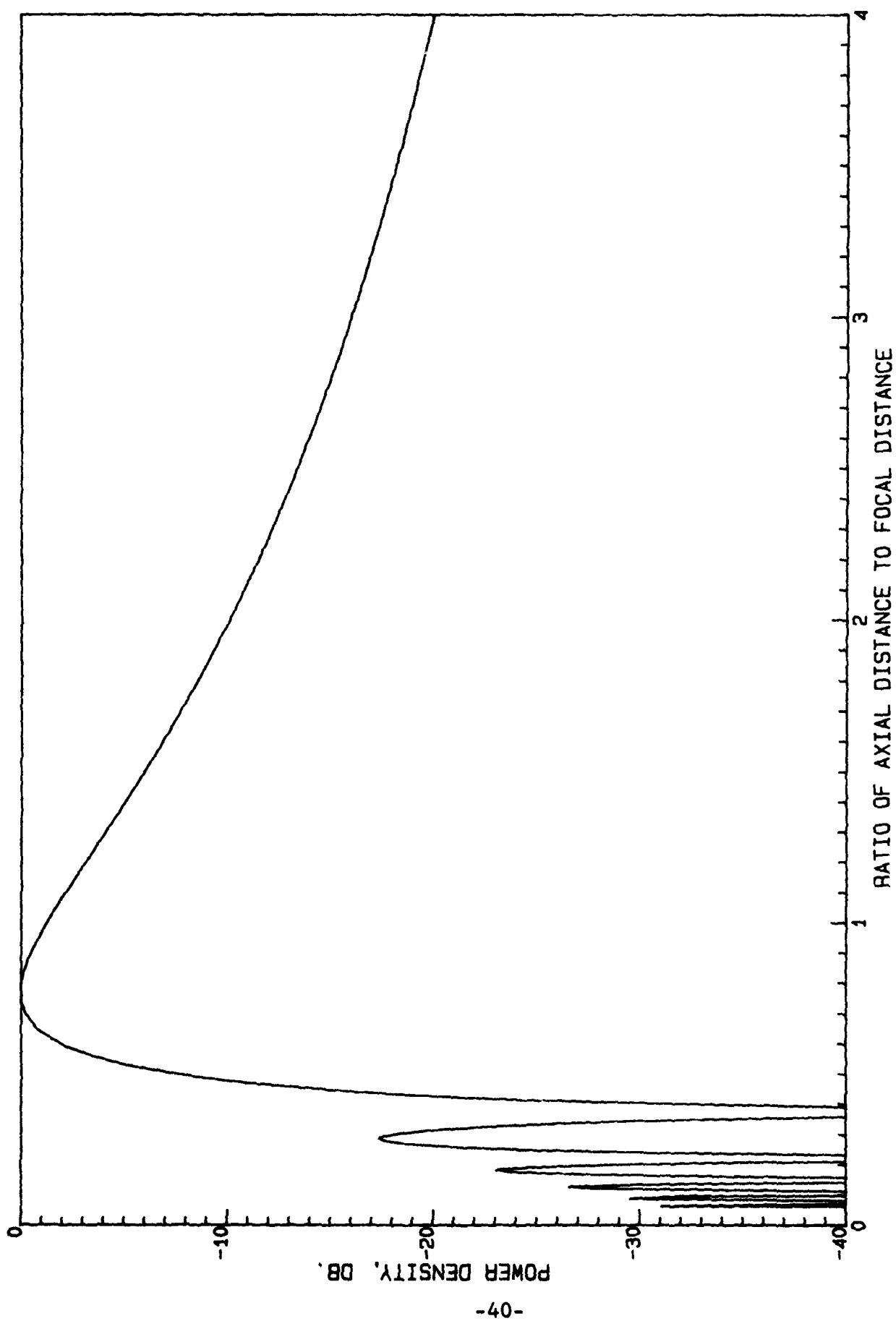
Figure 21

RATIO OF AXIAL DISTANCE TO FOCAL DISTANCE

AXIAL P D OF 20 WV SQUARE APERTURE WITH UNIFORM AXIAL PATTERN, GAMA= .1

Figure 22

RATIO OF AXIAL DISTANCE TO FOCAL DISTANCE

AXIAL P D OF 20 WV SQUARE APERTURE WITH 25 DB TAYLOR AXIAL PATTERN. GAMA=.025

Figure 23

POWER DENSITY, DB.

-41-

RATIO OF AXIAL DISTANCE TO FOCAL DISTANCE

AXIAL P D OF 20 WV SQUARE APERTURE WITH 25 DB TAYLOR AXIAL PATTERN, GAMA= .05

Figure 24

RATIO OF AXIAL DISTANCE TO FOCAL DISTANCE
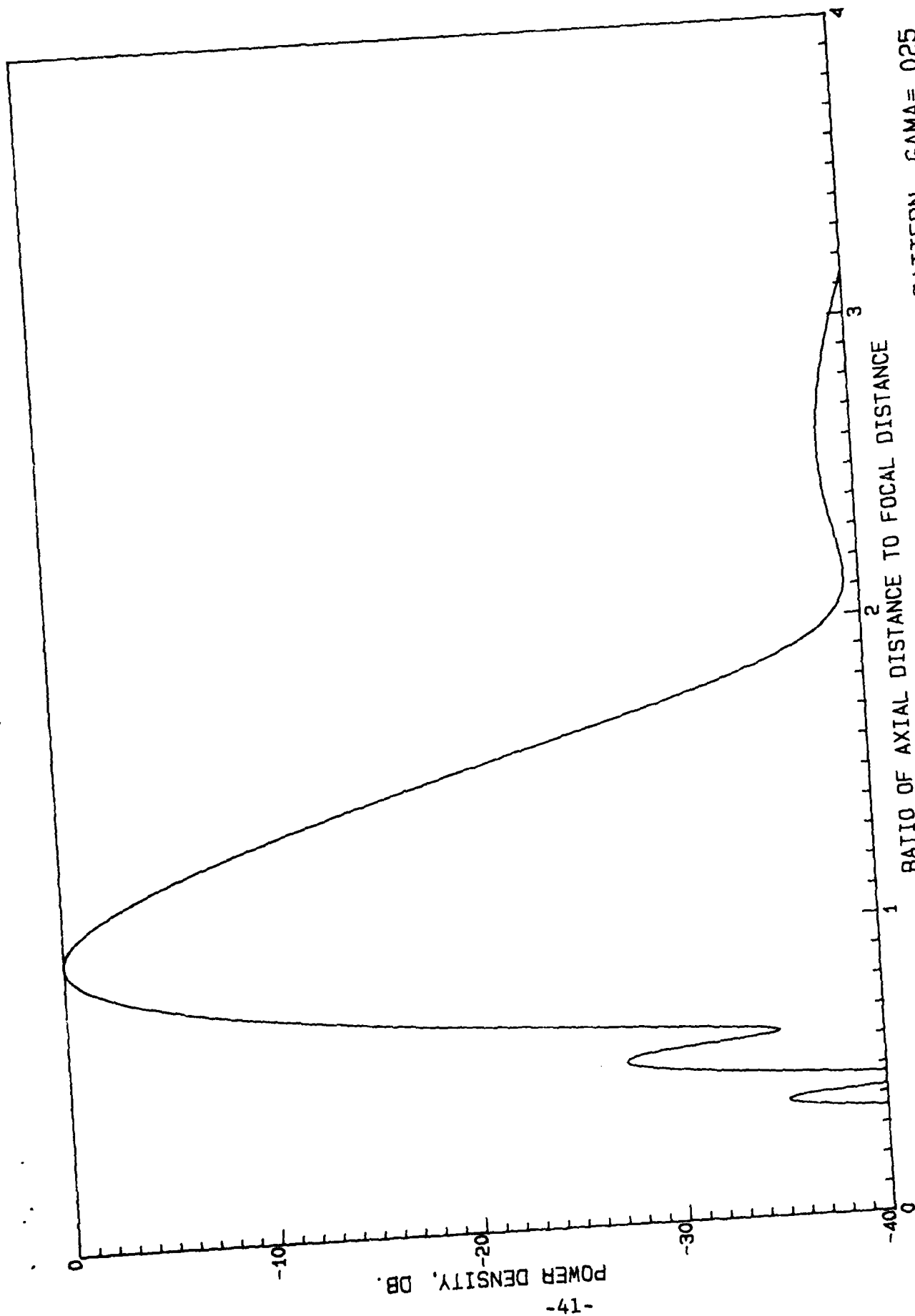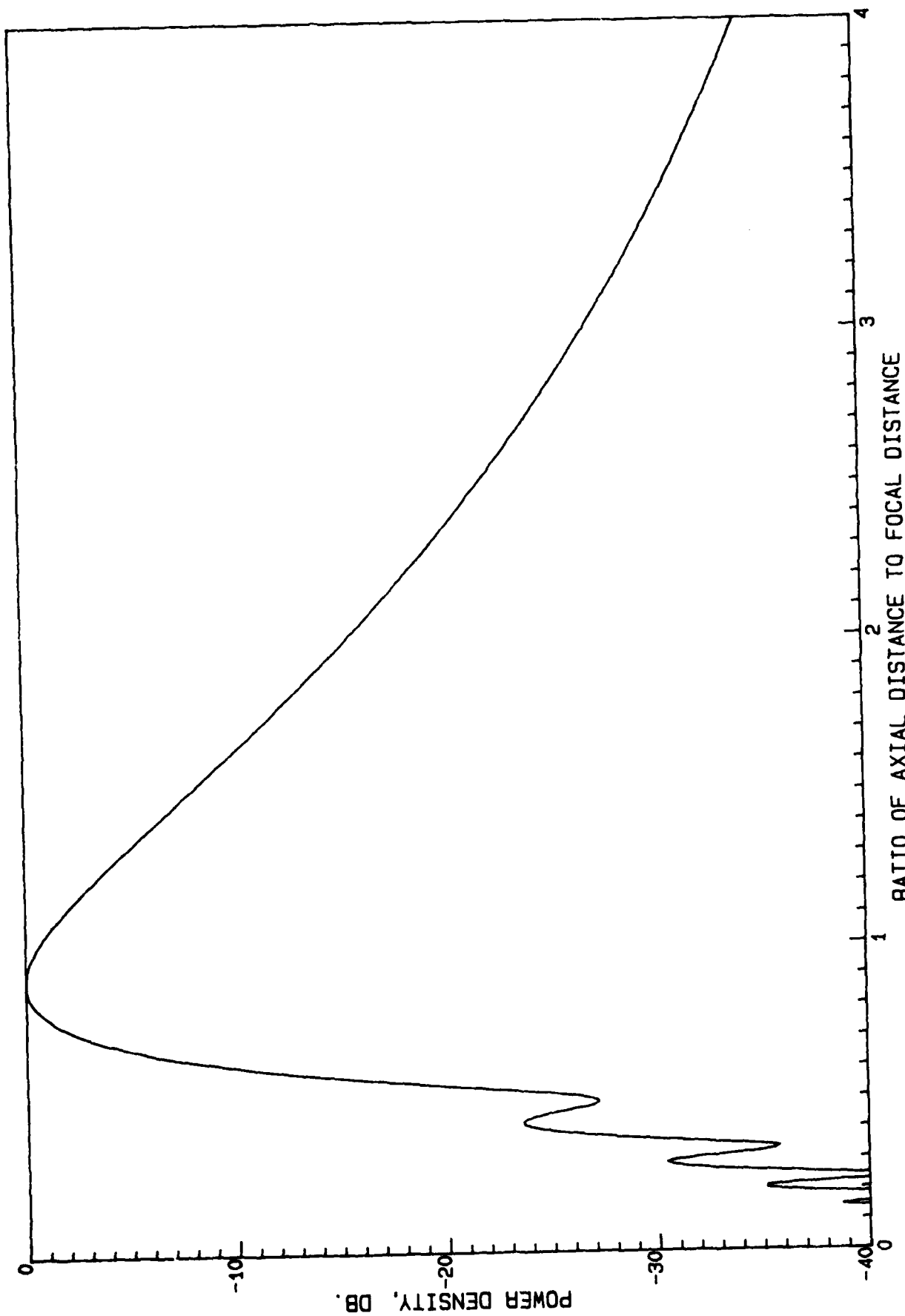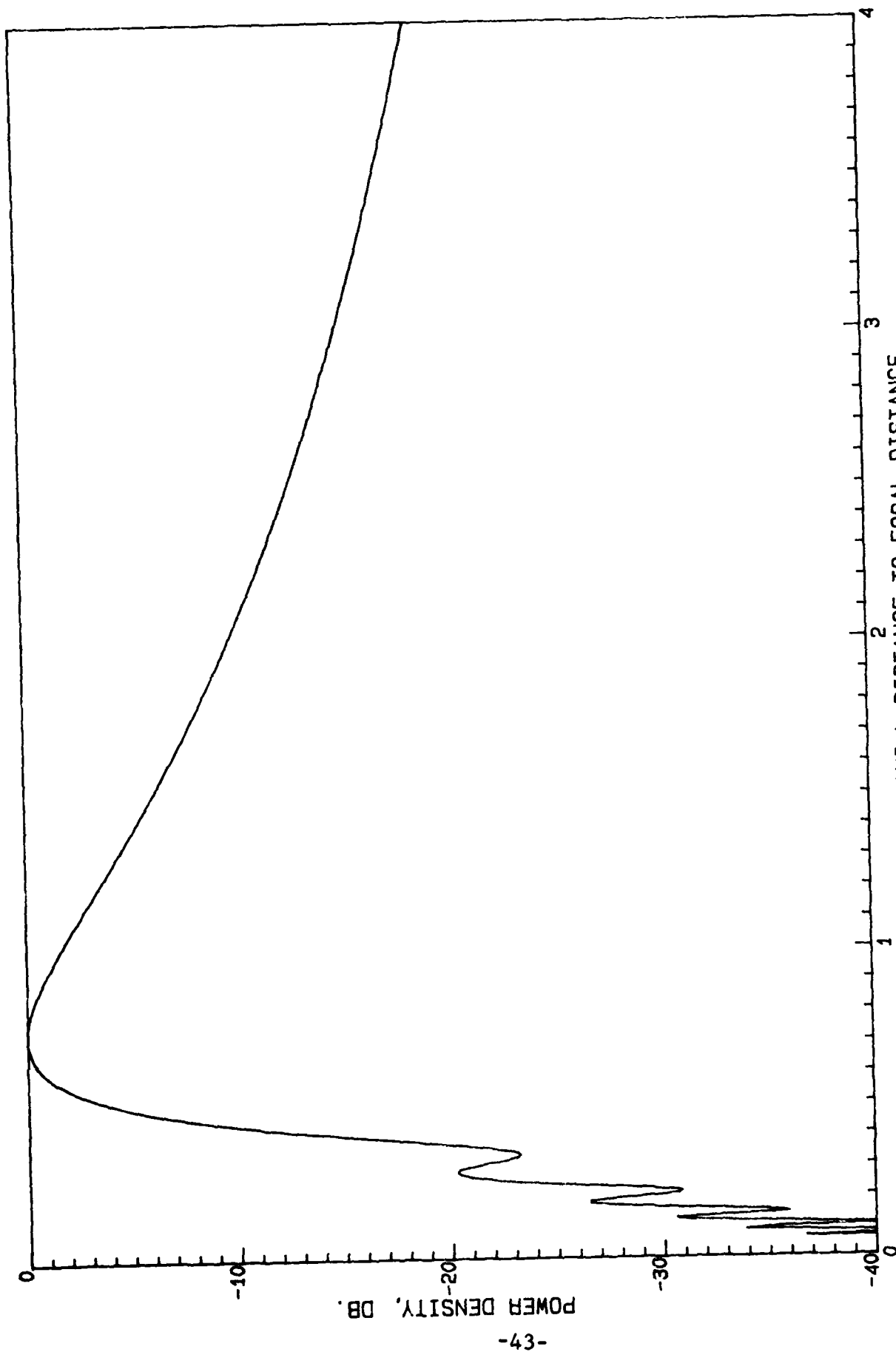
AXIAL P D OF 20 WV SQUARE APERTURE WITH 25 DB TAYLOR AXIAL PATTERN, GAMA=.1

Figure 25

2.2   Transverse Power Density

Based on the evaluation of interpolation and integration methods in the Appendices, and due to errors at wide angles and short distances in the Zernike-Jacobi and Fresnel approaches alluded to in the Introduction, the transverse field calculations are made using Gaussian integration. Again, two calculations have been made, with one utilizing the exact phase square root term, while the other separates the phase into x and y square root factors. The approximation in the latter is evaluated by comparing results with the former for $L = 10\lambda$. Figure 26 shows the geometry, with a square aperture L by L used. The focal distance is r_0 while the observation distance from the center is R_0. Conventional spherical coordinates are used. The field is given by:

$$F(u,v) = \frac{1}{4} \int_{-1}^{1} \int_{-1}^{1} g(x)g(y) \exp -jk(R-r)\, dx\, dy$$

where $g(x)$ is the Taylor linear one-parameter distribution used in Section 2.1. Distances are:

$$R^2 = (R_0 u - Lx/2)^2 + (R_0 u - Ly/2)^2 + R_0^2 \cos^2 \theta$$

$$r^2 = r_0^2 + (Lx/2)^2 + (Ly/2)^2$$

and $u = \sin \theta \cos \phi$, $v = \sin \theta \sin \phi$. In all of these calculations, the ideal active element pattern (obliquity factor) is utilized. Again, it is convenient to normalize focal distance in terms of far field distance, and observation distance in terms of focal distance:
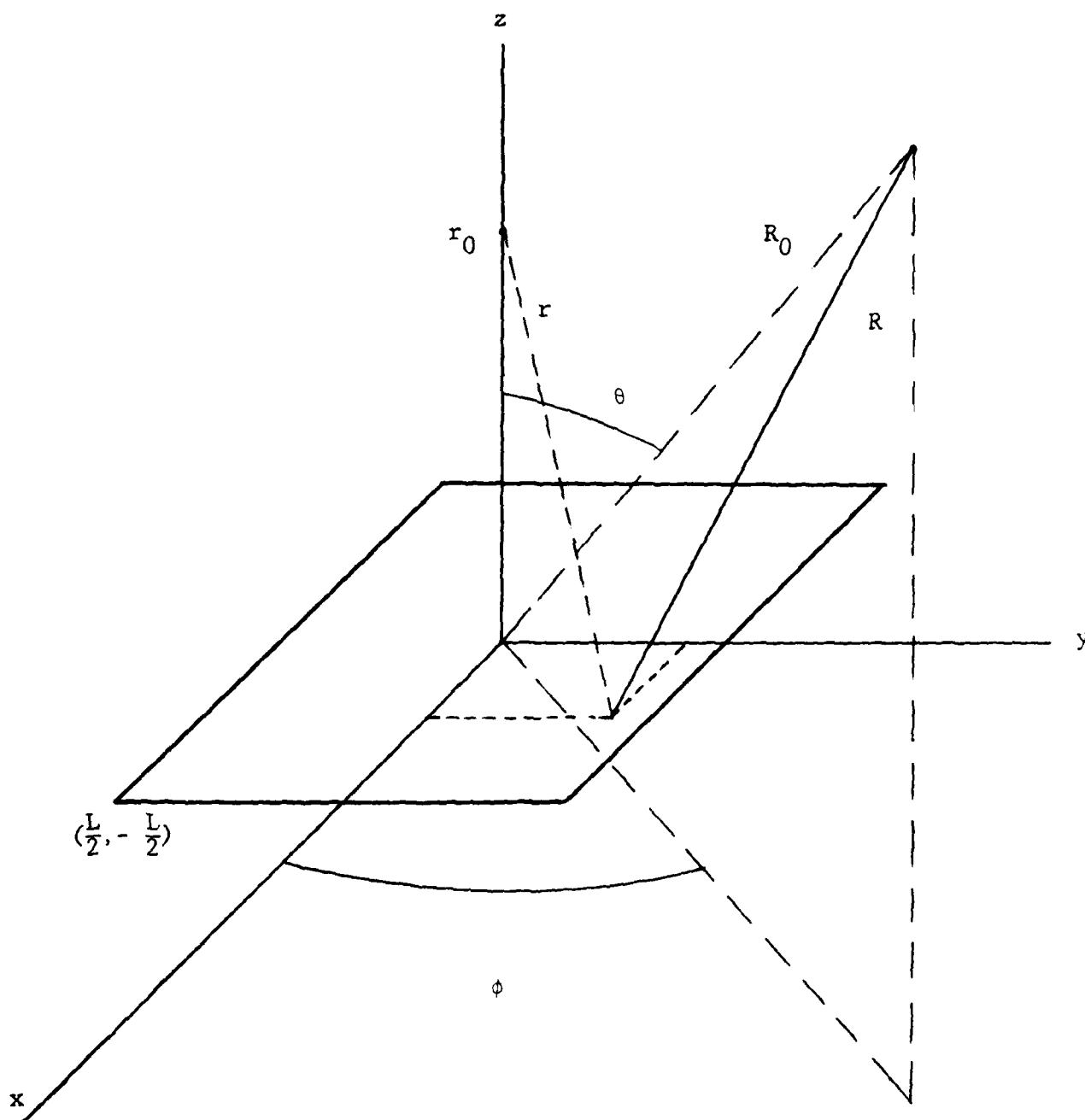
Figure 26

Transverse Geometry

$$\beta = \frac{R_0}{r_0} \qquad , \qquad \gamma = \frac{r_0}{2L^2/\lambda}$$

Then the phase terms become:

$$R^2 = L^2 \left[(2\beta\gamma L/\lambda)^2 - 2\beta\gamma(ux+vy)L/\lambda + (x^2+y^2)/4 \right]$$

$$r^2 = L^2 \left[(2\gamma L/\lambda)^2 + (x^2+y^2)/4 \right]$$

For the approximate form the double integral is separated:

$$F(u,v) \simeq \frac{1}{4} \int_{-1}^{1} g(x) \, \exp -jk(R_x - r_x) \, dx \int_{-1}^{1} g(y) \, \exp -jk(R_y - r_y) \, dy$$

where

$$R_x^{\,2} = L^2 \left[(2\beta\gamma L/\lambda)^2 - 2\beta\gamma uxL/\lambda + x^2/4 \right]$$

$$r_x^{\,2} = L^2 \left[(2\gamma L/\lambda)^2 + x^2/4 \right]$$

The 32-step Gaussian integrator is accurate for D/λ up to 15, while the 128-step Gaussian allows D/λ up to 60. Figure 27 shows the far field pattern of a uniformly excited square aperture 15 wavelengths each side. Figures 28 and 29 show the pattern in the focal plane for a normalized focal distance of $\gamma = .025$, with Figure 28 from the exact calculation and Figure 29 from the separated phase approximation. Note that even at this very close distance (focus less than one diameter away) the exact transverse field sidelobe envelope drops off rapidly whereas the separated phase approximation has a side-lobe envelope decay very close to that of the far field pattern.
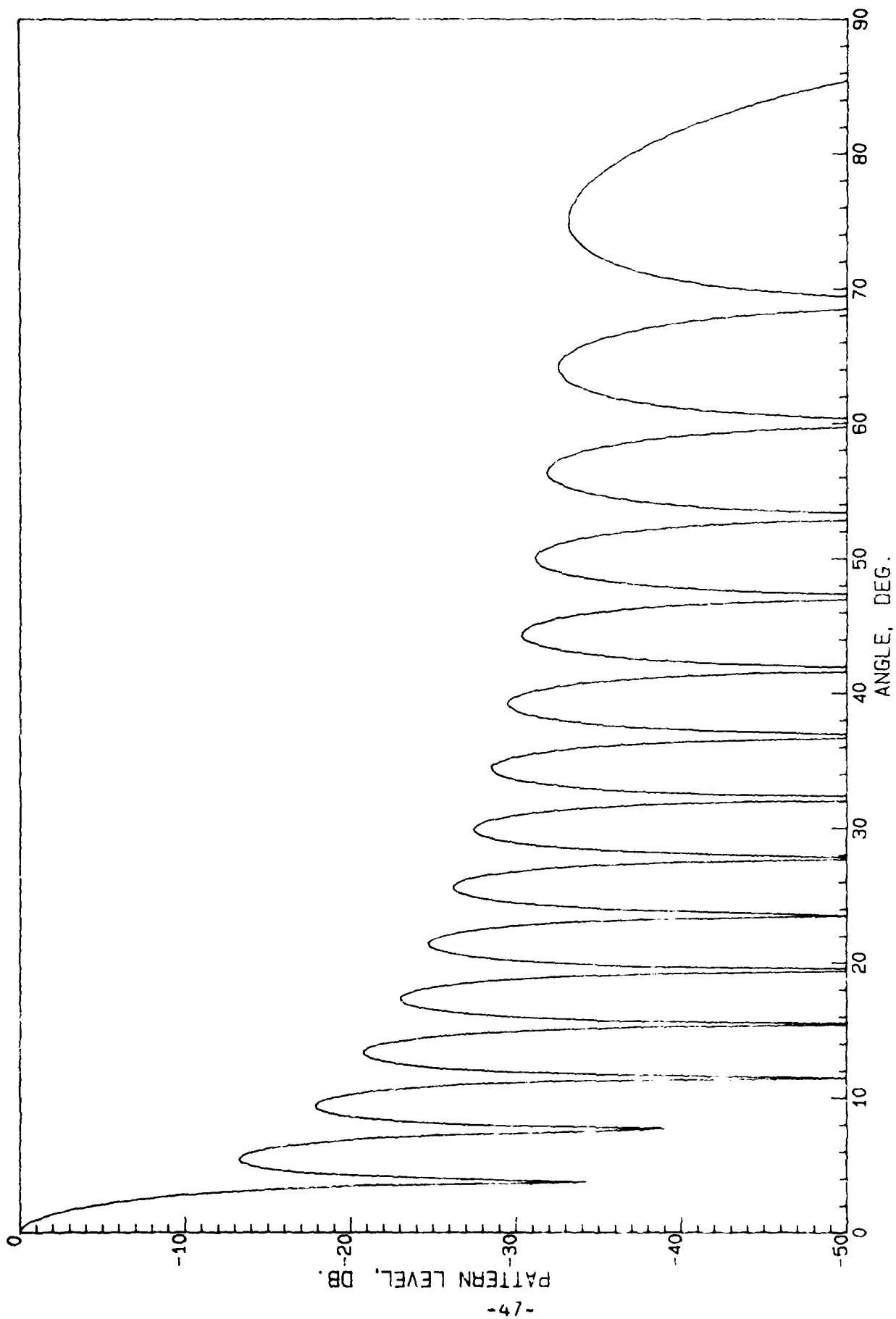
PATTERN OF UNIFORM 15 WV SQUARE APERTURE

Figure 27
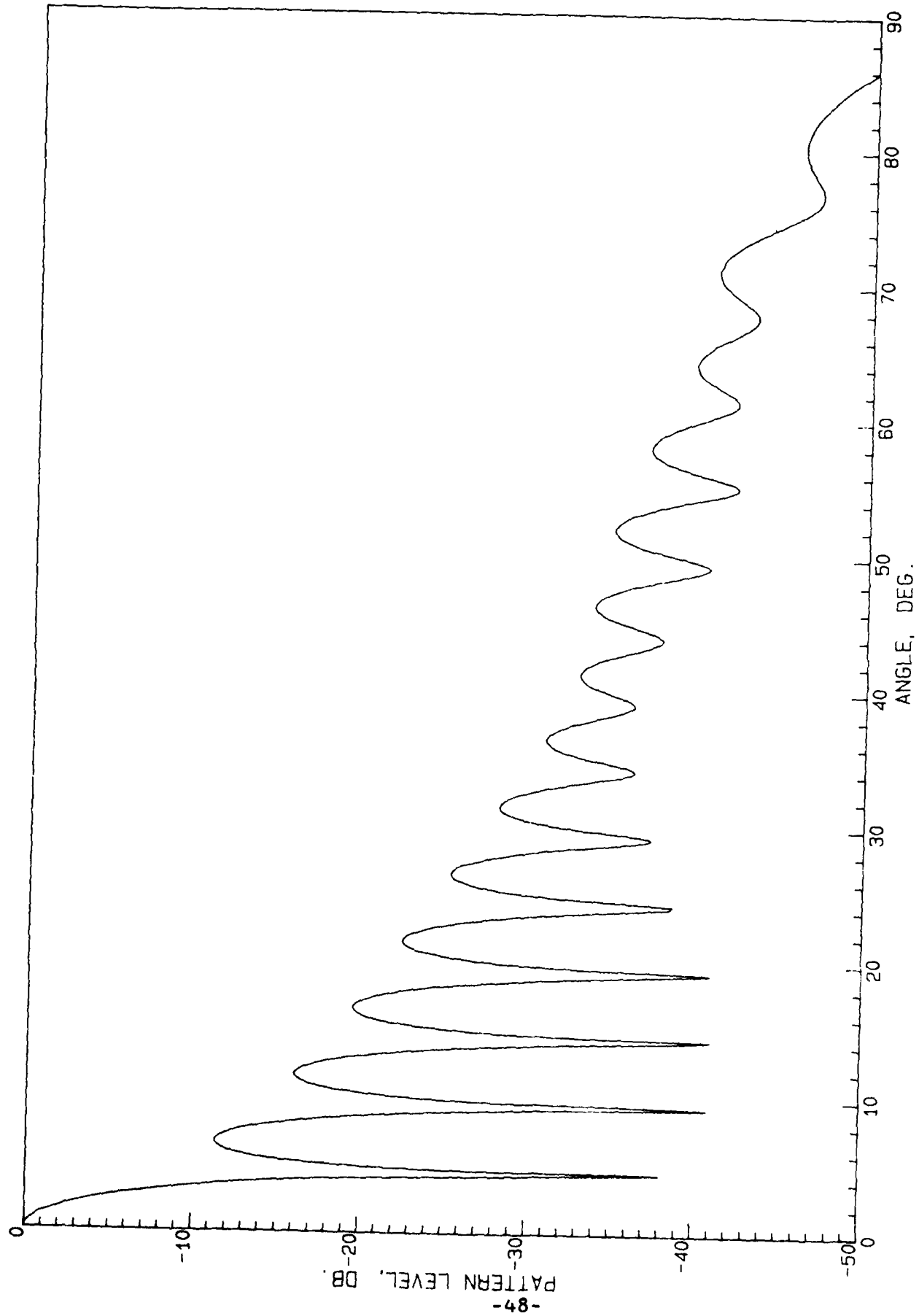
PATTERN OF UNIFORM 15 WV SQUARE APERTURE, BETA=1, GAMA=.025

Figure 28
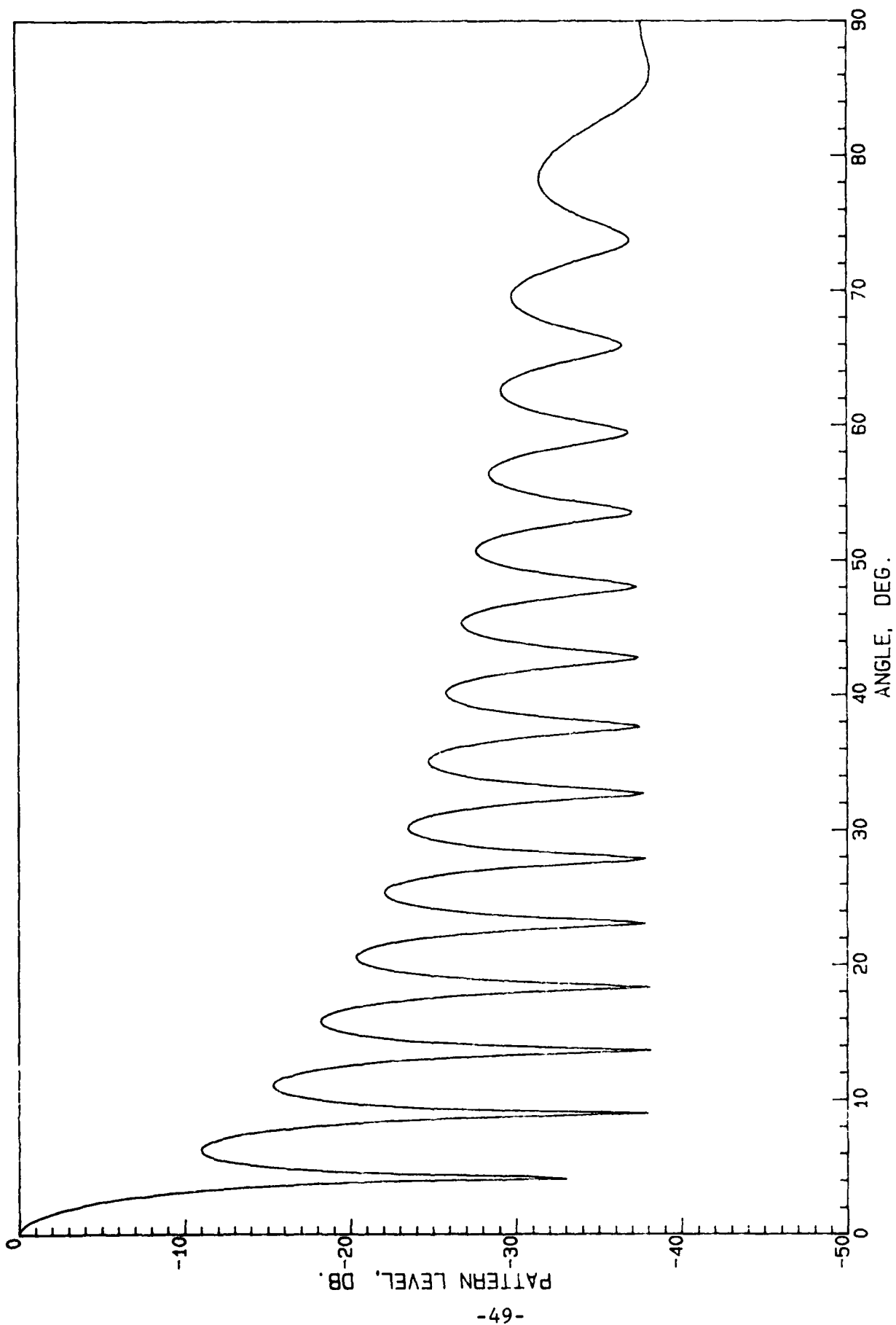
PATTERN OF UNIFORM 15 WV SQUARE APERTURE, BETA=1, GAMA=.025

Figure 29

However, for the main lobe and first several sidelobes, the approximate and exact results are very close, with the side-lobe level being about 2 db higher. Figures 30 (exact) and 31 (approx.) show the pattern of the same aperture in the focal plane at a focal distance of γ = .05. Now the near field sidelobe inter-ference process is least destructive with a resulting higher sidelobe envelope. The sidelobe level is now only about 1 db below that of the far field. Figure 32 shows the pattern for γ = .1, and it is approaching the far field pattern. For the 60 wavelength aperture there is much less difference between the exact and approximate patterns, and these are very close to the far field pattern. Figure 33 shows the focal plane pat-tern for pattern = .025 (at a distance of 3 diameters).

Turning now to the aperture with 25 db Taylor dis-tribution along x and along y, Figure 34 shows the far field pattern while Figures 35 and 36 show the exact and approximate patterns. It is interesting to note that the main beam and first couple of sidelobes are very close between exact and approximate results, and that the sidelobe level is roughly 6 db higher than the nominal -25 db. Again, the exact pattern sidelobe envelope falls off rapidly due to the phase inter-ference. At twice the distance, γ = .05, the sidelobe level degradation is only 3 db and the exact sidelobe envelope taper is not as strong. For a γ of .1, the sidelobe level degrada-tion is less than 1 db and the envelope is closely that of the far field pattern. For the 60 wavelength aperture the side-lobe envelope is almost exactly that of the far field and the sidelobe level is raised less than 1 db, for γ = .025 (a dis-tance of 3 widths). See Figure 37. For γ = .05 the pattern is almost exactly the far field pattern.

In Section 2.1.2 inverse aperture distributions which produced lower axial forelobes and aftlobes were investigated. It was anticipated that the transverse sidelobes would be adversely affected. Figures 38, 39, and 40 show the focal plane
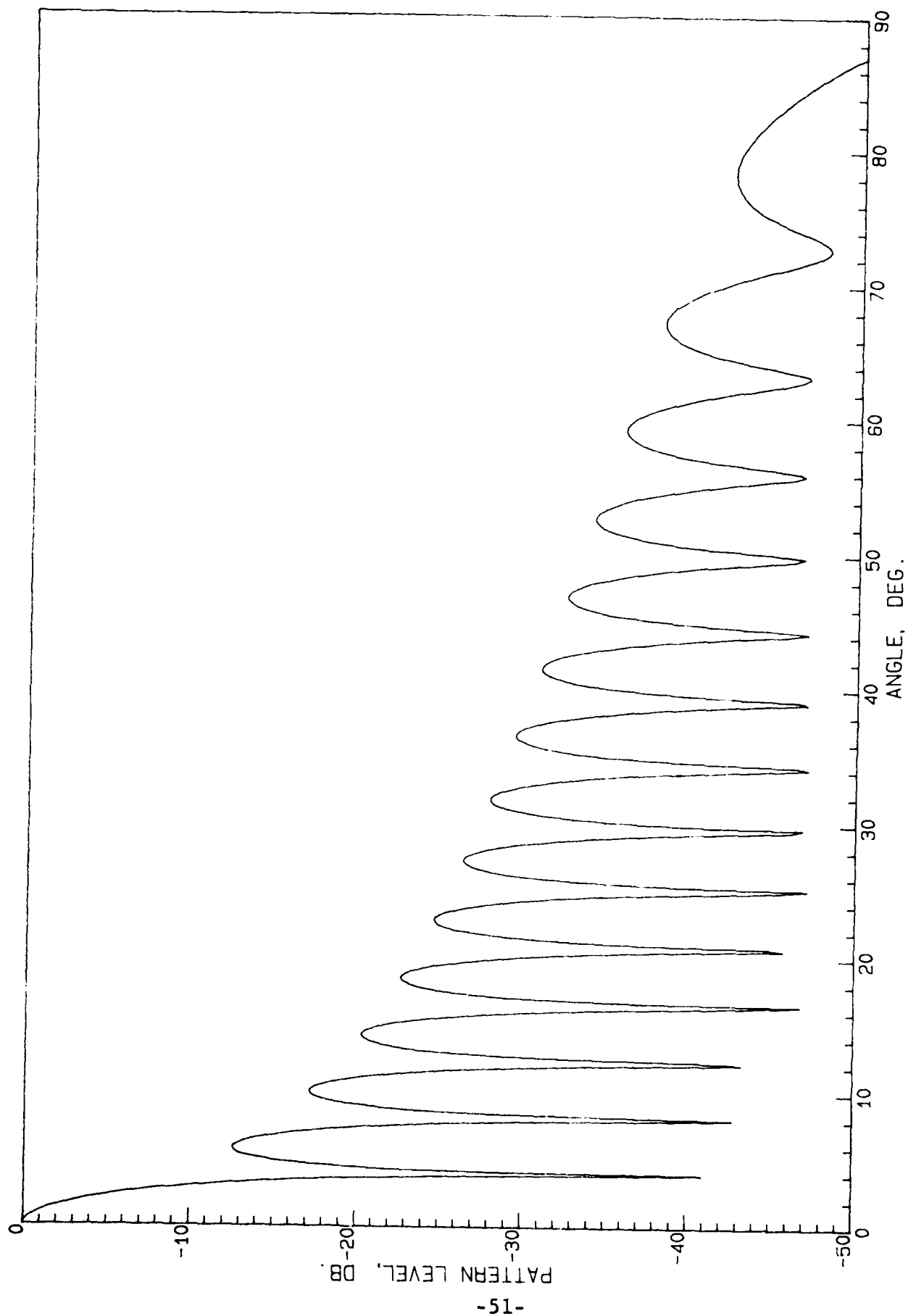
PATTERN OF UNIFORM 15 WV SQUARE APERTURE, BETA=1, GAMA=.05

Figure 30
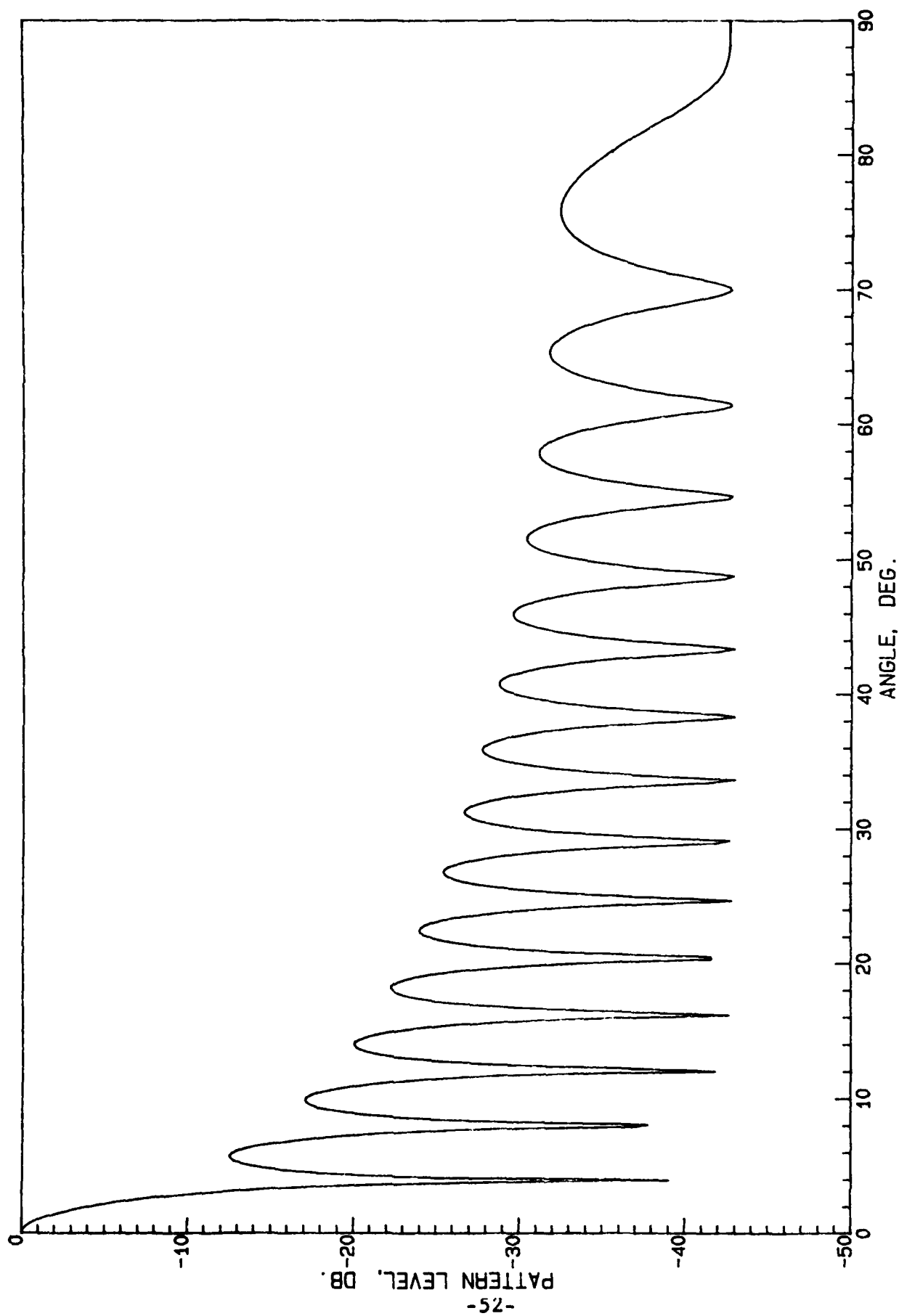
PATTERN OF UNIFORM 15 WV SQUARE SOURCE, BETA=1, GAMA=.05

ANGLE, DEG.

Figure 31

PATTERN OF UNIFORM 15 WV SQUARE APERTURE, BETA=1, GAMA=.1

Figure 32

PATTERN OF UNIFORM 60 WV SQUARE APERTURE, BETA=1, GAMA=.025

Figure 33

PATTERN OF 25 DB TAYLOR 15 WV SQUARE APERTURE

ANGLE, DEG.

PATTERN LEVEL, DB.

Figure 34

PATTERN OF 25 DB TAYLOR 15 WV SQUARE APERTURE, BETA=1, GAMA=.025

Figure 35

PATTERN OF 25 DB TAYLOR 15 WV SQUARE APERTURE, BETA=1, GAMA=.025

Figure 36

PATTERN OF 25 DB TAYLOR 60 WV SQUARE APERTURE, BETA=1, GAMA=.025

ANGLE, DEG.

PATTERN LEVEL, DB.

Figure 37

PATTERN OF INVERSE TAPER 15 WV SQUARE APERTURE, BETA=1, GAMA=.025

Figure 38

PATTERN OF INVERSE TAPER 15 WV SQUARE APERTURE, BETA=1, GAMA=.05

Figure 39

PATTERN OF INVERSE TAPER 15 WV SQUARE APERTURE, BETA 1, GAMA 1

Figure 40

patterns of the inverse taper aperture for γ = .025, .05, and .1. It can be seen that the sidelobe level is high, roughly -4 to -5 db. Further, the first sidelobe is a salient in that it is considerably above the projected sidelobe envelope. The second sidelobe, however, is above -10 db for γ = .025 and only approaches -13 db for γ = .1. These results are not expected to change significantly for larger apertures. In addition, there is a significant gain loss associated with this distribution; for the 15 wavelength aperture it is 12 db. Because of the high transverse sidelobes and sizeable loss of gain, the inverse distribution is not a serious candidate.

The preceeding pattern plots were all at a constant radius in the principal plane through the focus. It is important to know what the behavior of the transverse field is for other distances. Calculations cf the transverse pattern at the peak of the first forelobe and first aftlobe have been made. Figure 41 shows the transverse cut through the first forelobe of the 15 wavelength square aperture, where the peak in this figure corresponds to the forelobe height which is 14.4 db below the axial peak value. Similarly, Figure 42 is a transverse pattern through the aftlobe where the peak in Figure 42 is 25.7 db below the axial peak. Similarly, Figures 43 and 44 are transverse patterns through the highest forelobe and aftlobe of the uniform 60 wavelength aperture. Note the rapid falloff for this larger aperture. The scales on these two graphs are respectively 14.1 db and 24 db below the axial peak. The apertures with Taylor distribution do not exhibit aftlobes for γ as small as .025; the transverse patterns through the highest forelobe are presented in Figures 45 and 46 for 15 and 60 wavelength apertures. Again, note the rapid falloff for the larger aperture. The peaks in these figures are 11.4 db and 9.5 db respectively below the axial peaks. Thus the transverse patterns outside the axial main beam regions are well behaved, especially so for larger apertures.
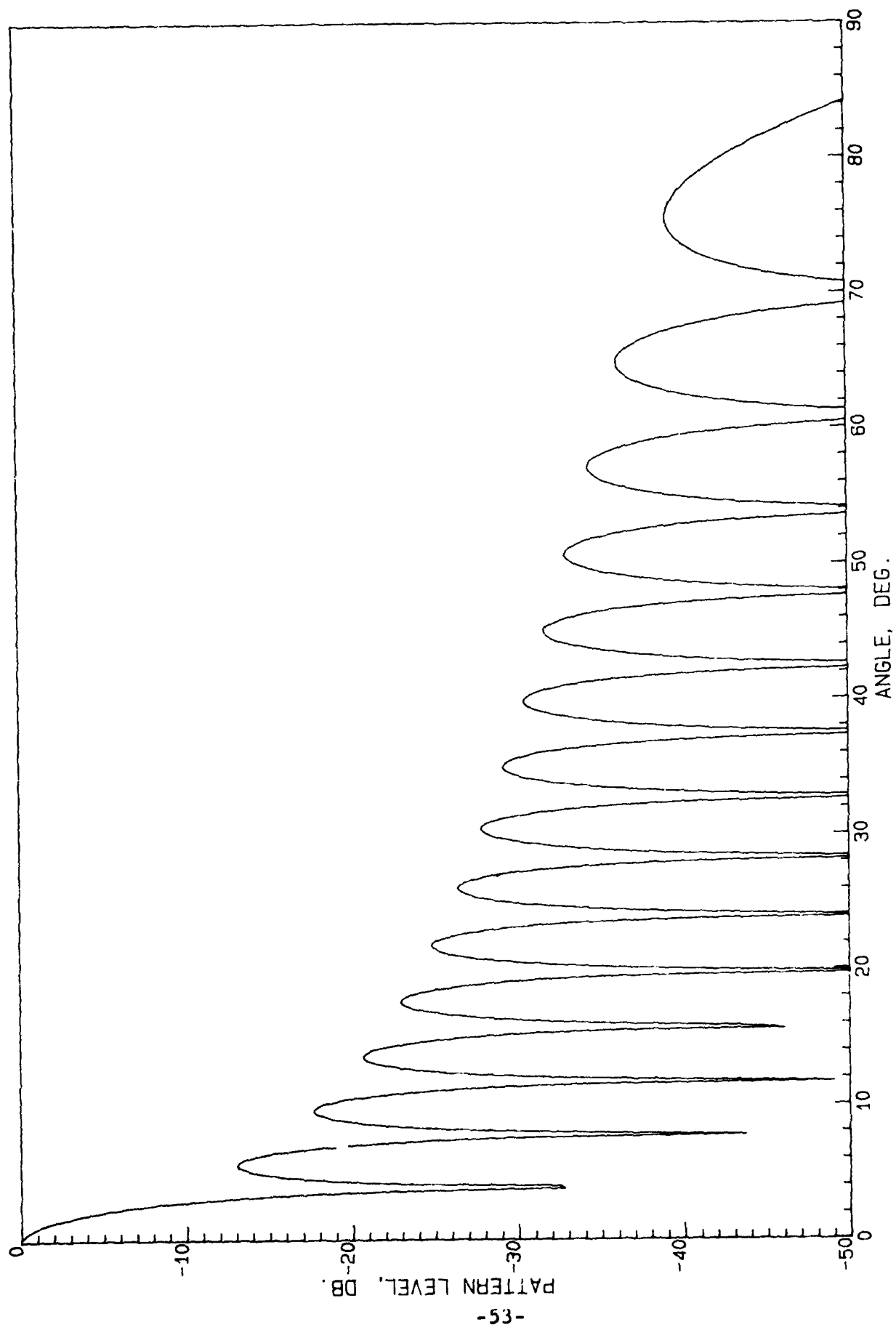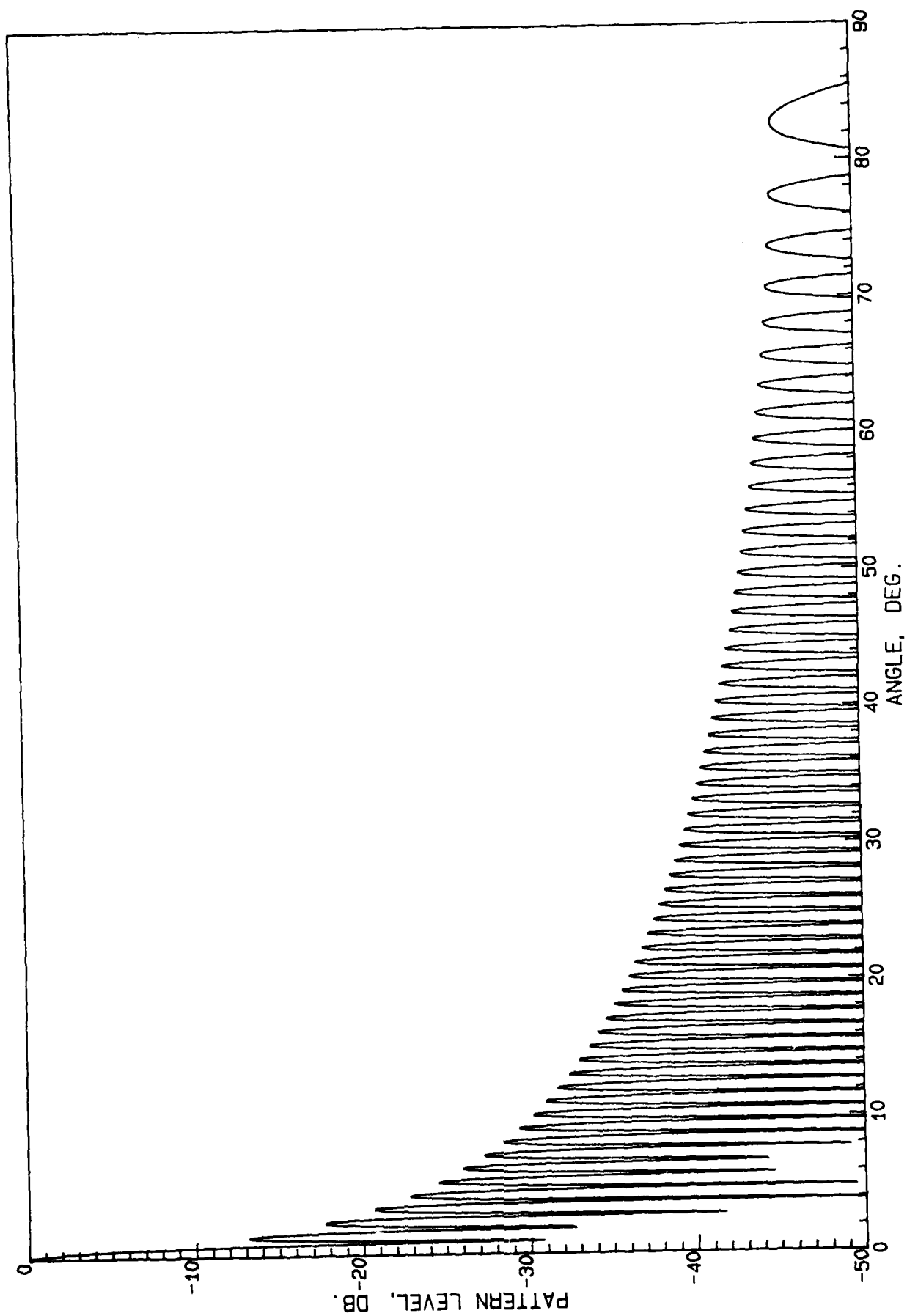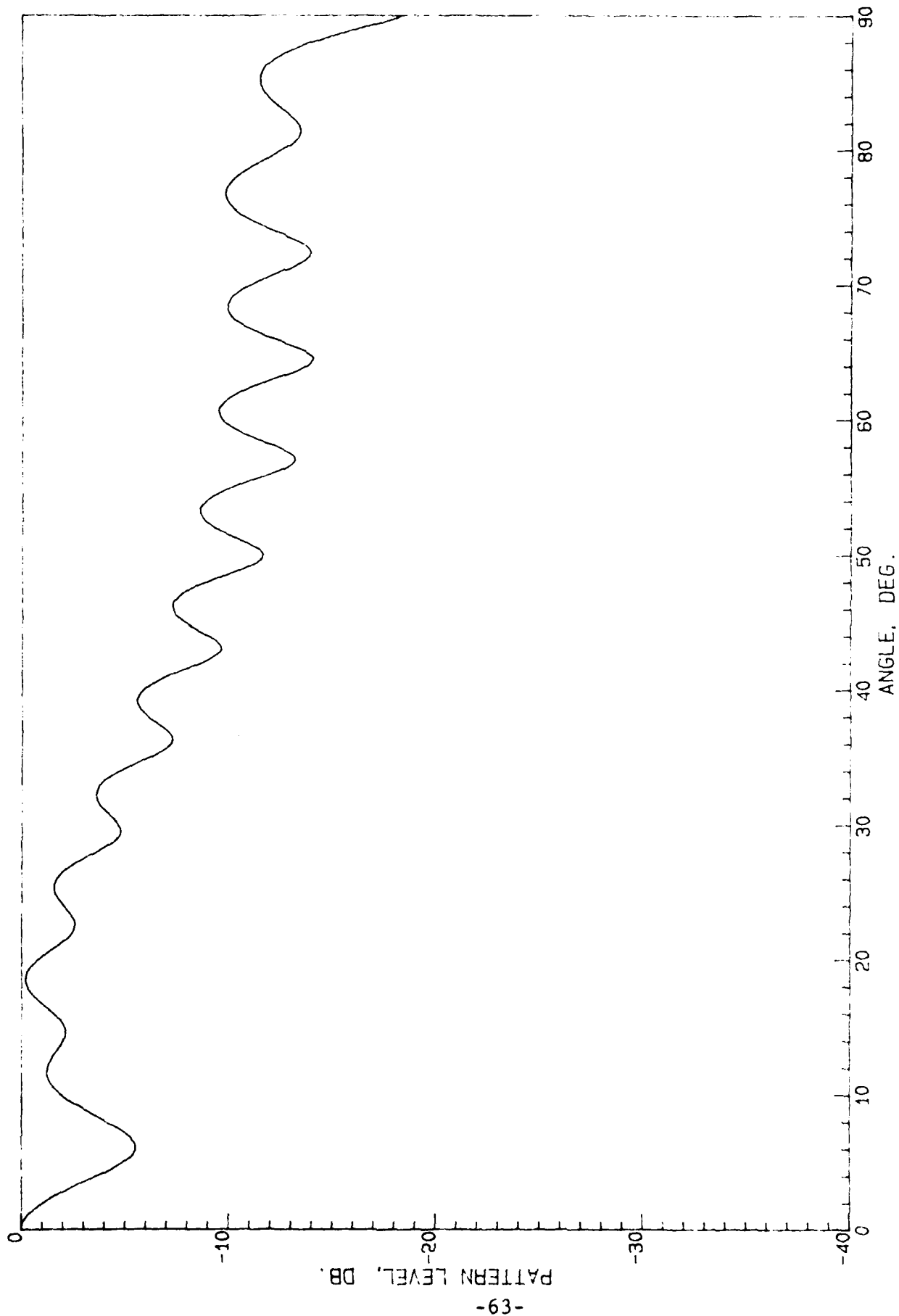
PATTERN OF UNIFORM 15 WV SQUARE APERTURE, BETA=.53, GAMA=.025

Figure 41
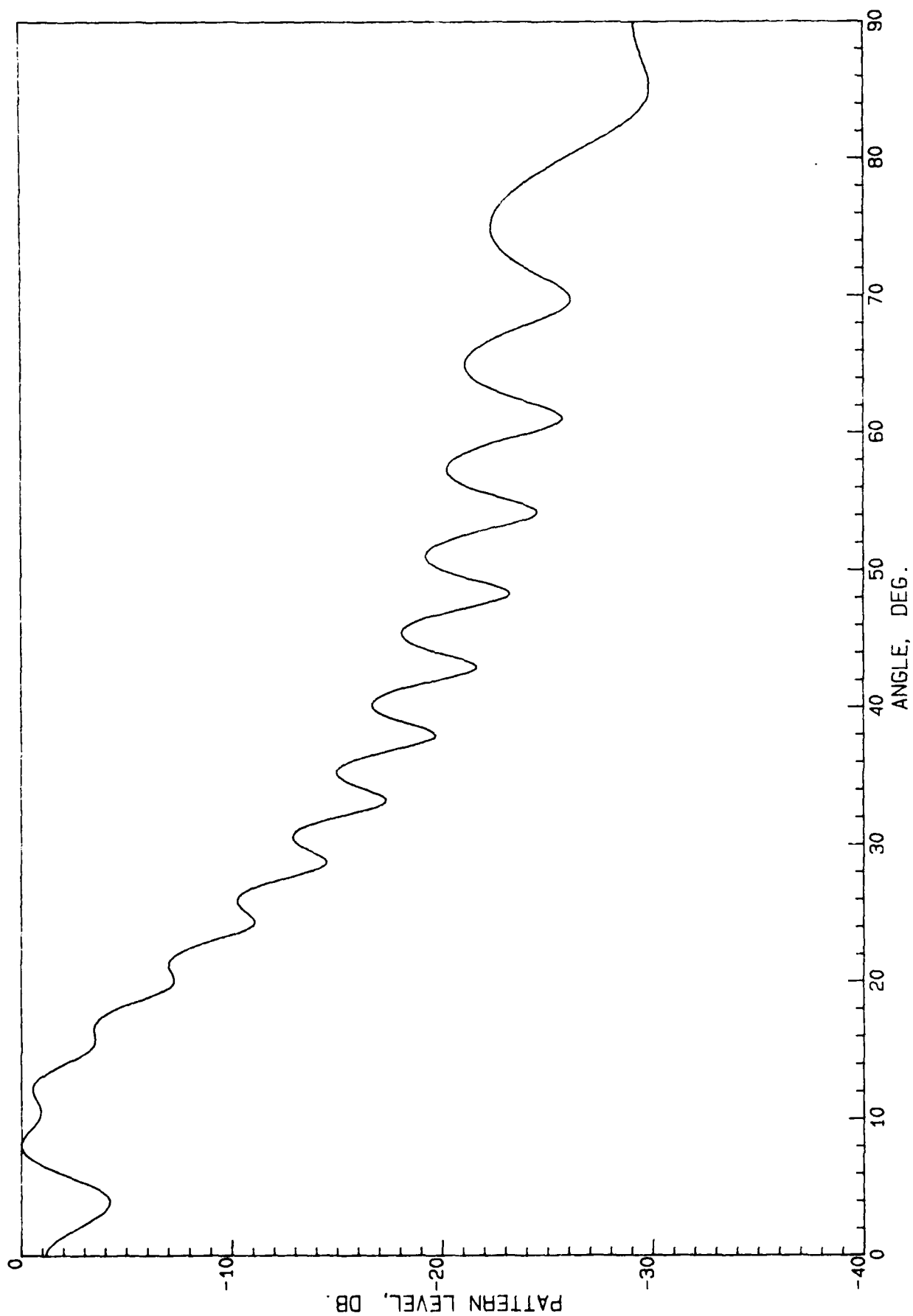
PATTERN OF UNIFORM 15 WV SQUARE APERTURE, BETA=2.36, GAMA=.025

Figure 42
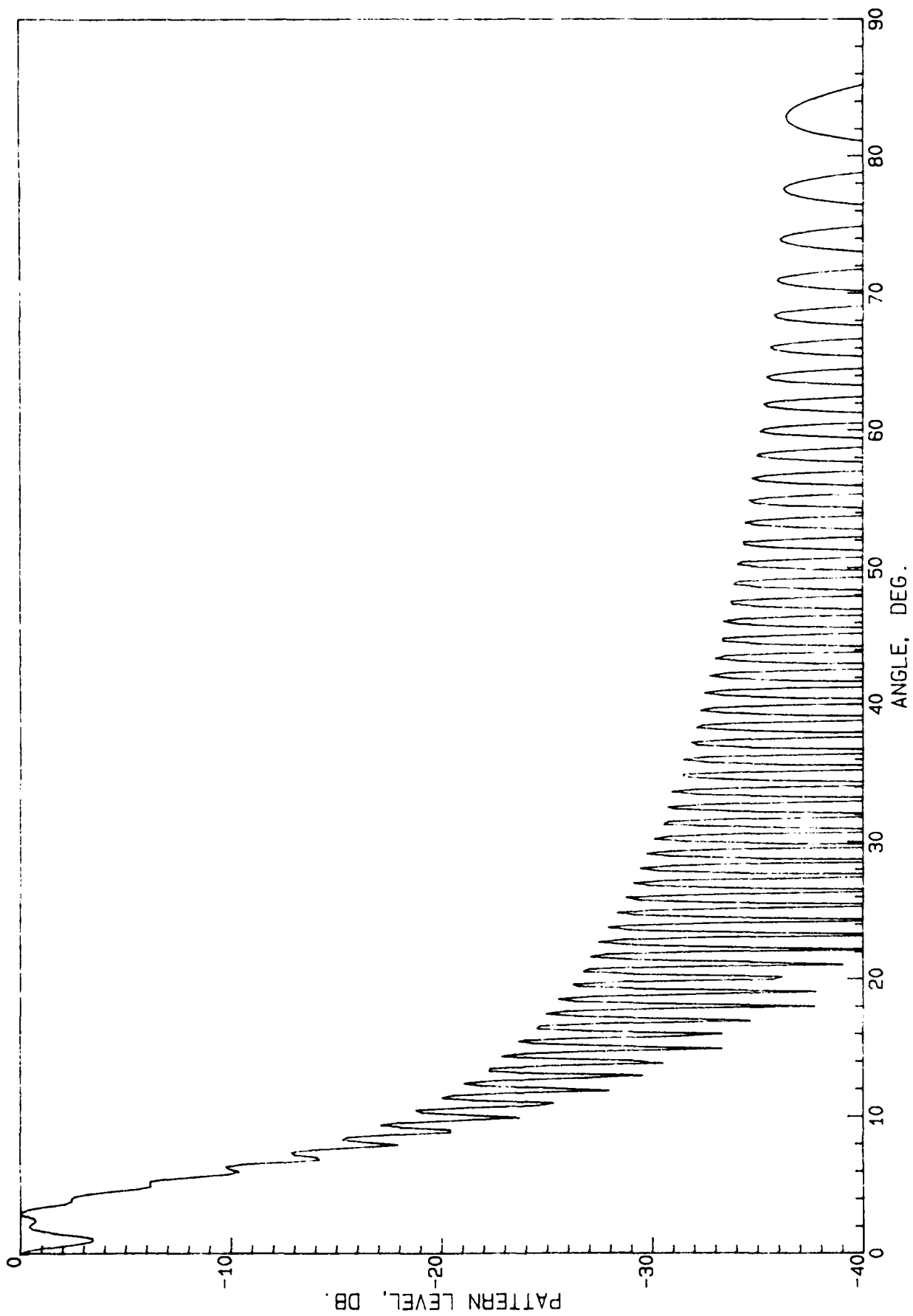
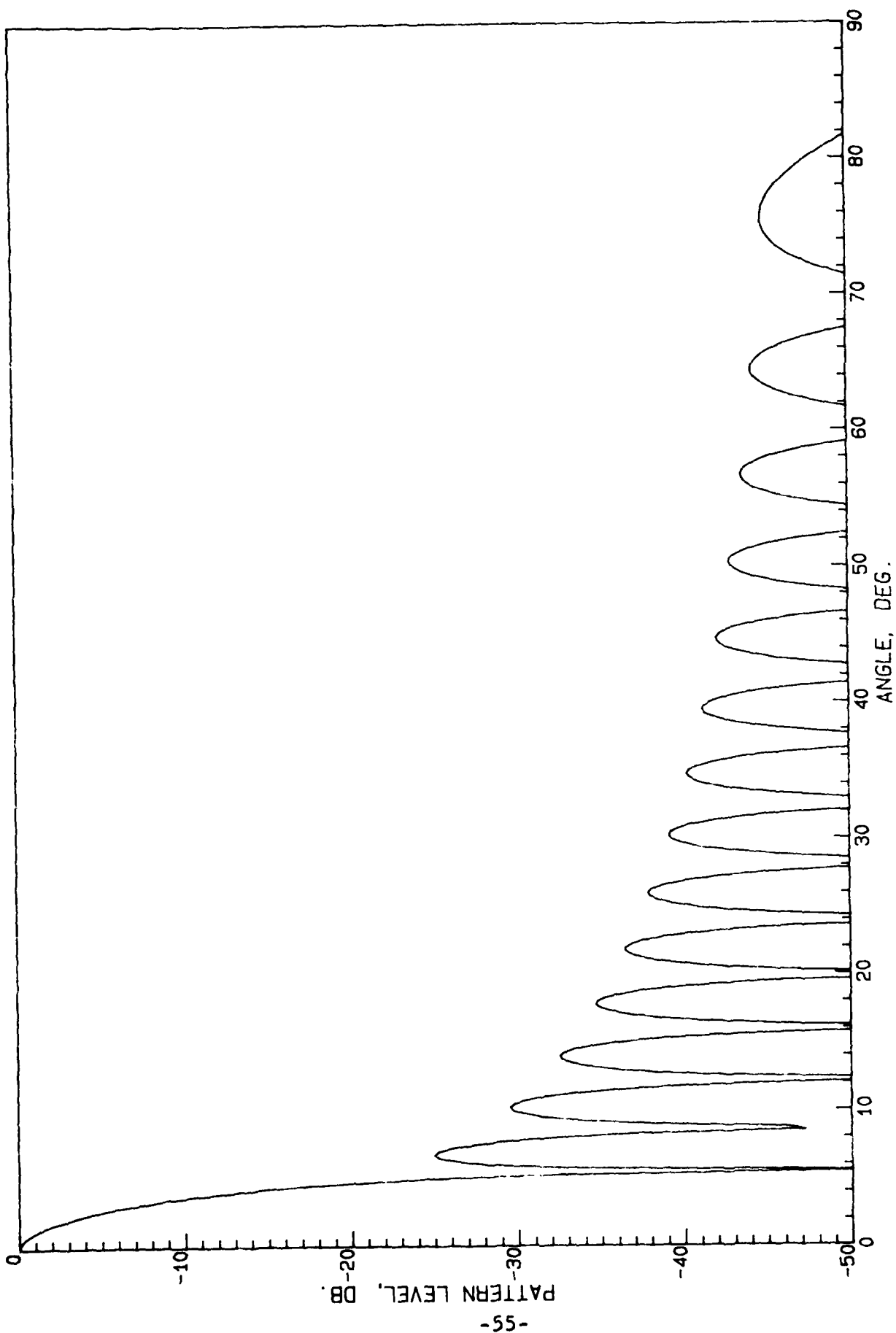PATTERN OF UNIFORM 60 WV SQUARE APERTURE, BETA=.64, GAMA=.025

Figure 43
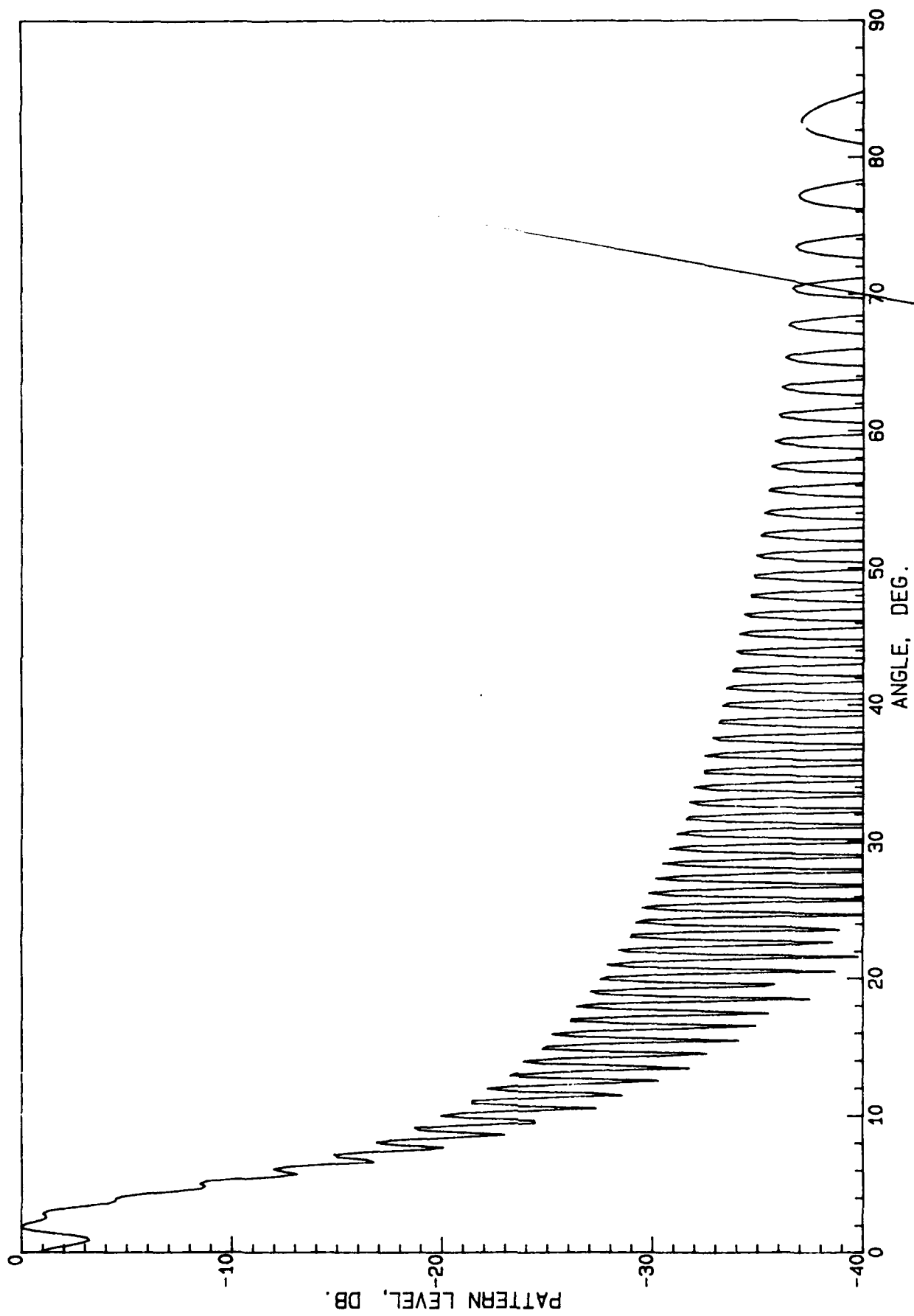
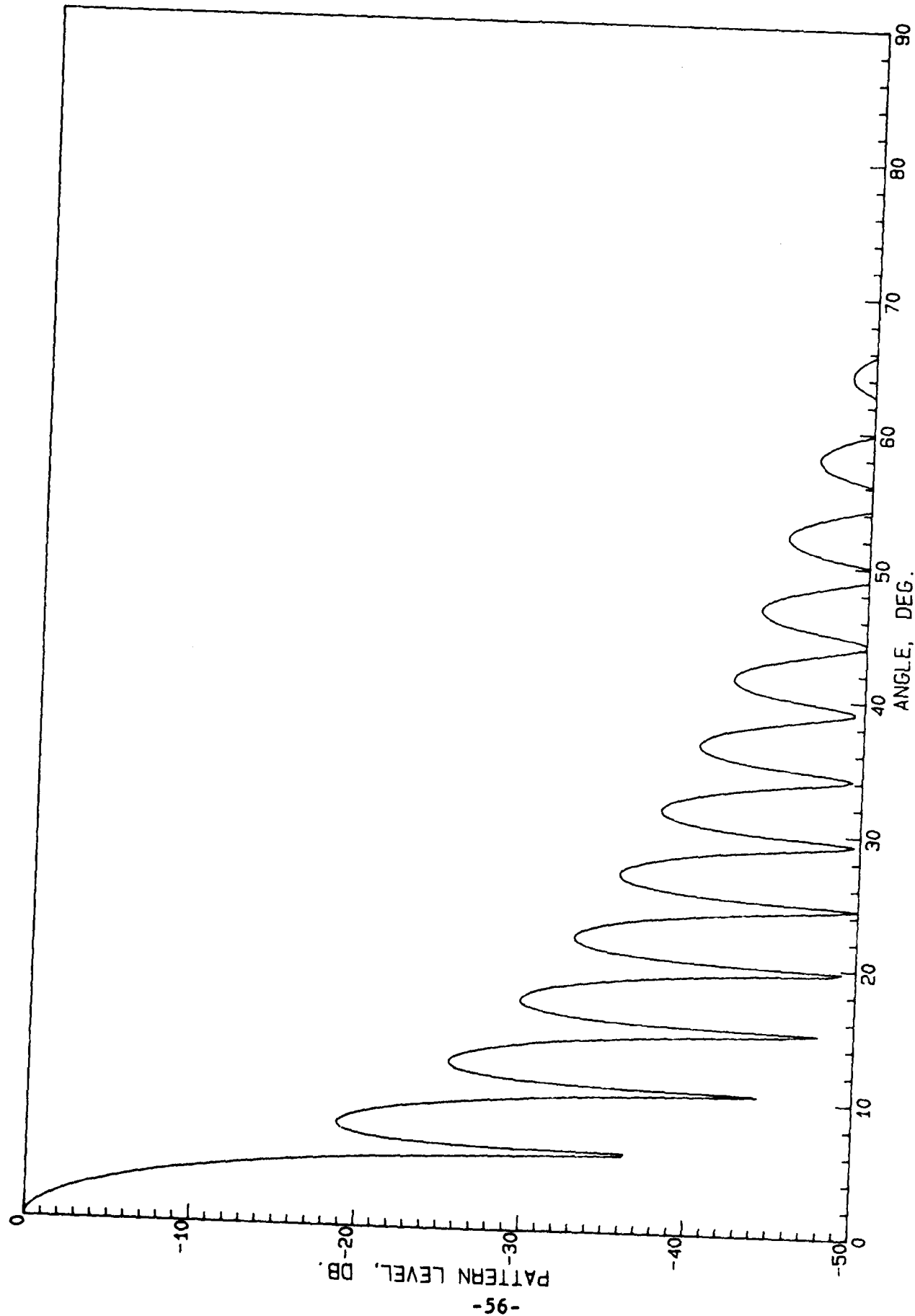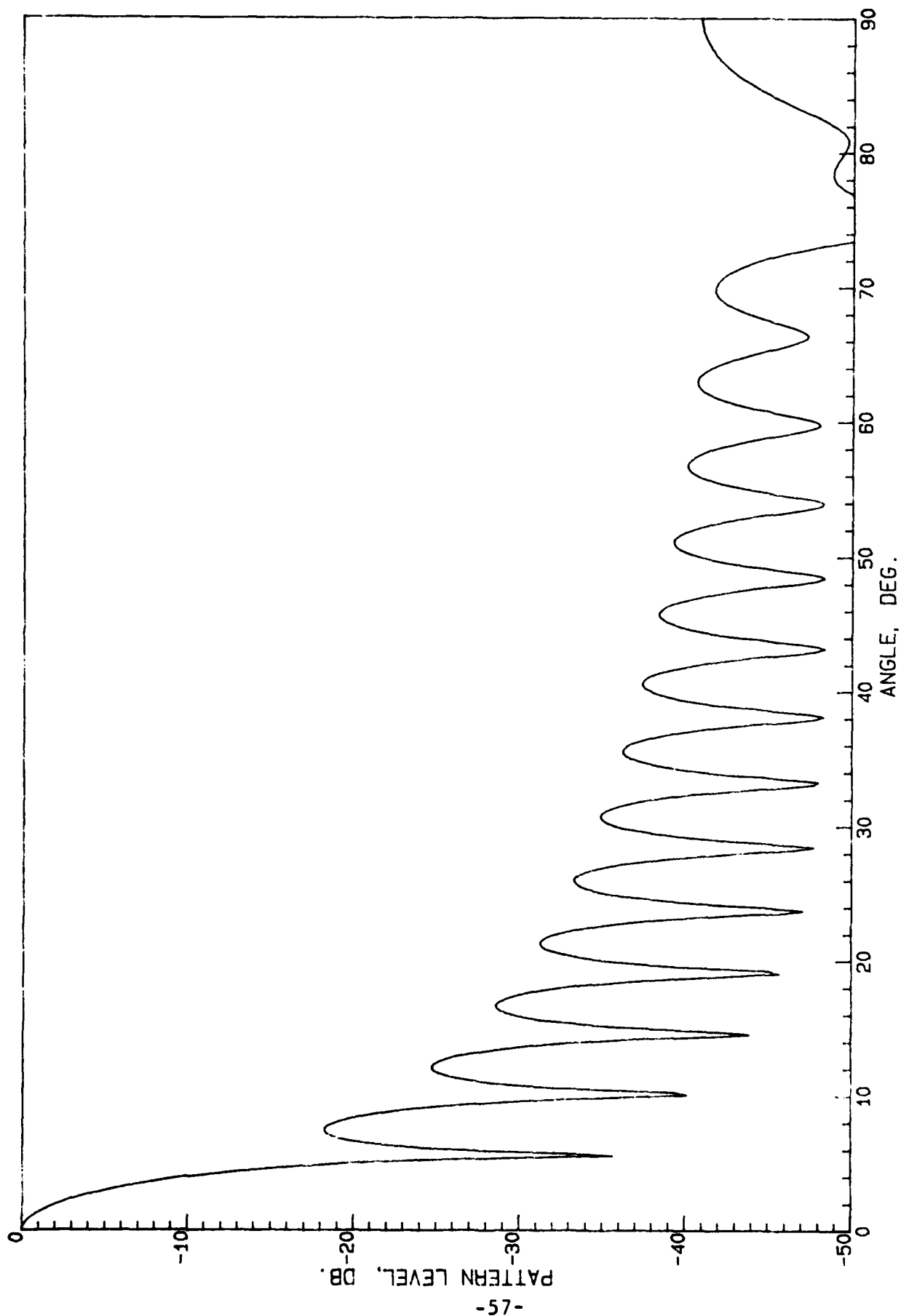PATTERN OF UNIFORM 60 WV SQUARE APERTURE, BETA=1.98, GAMA=.025
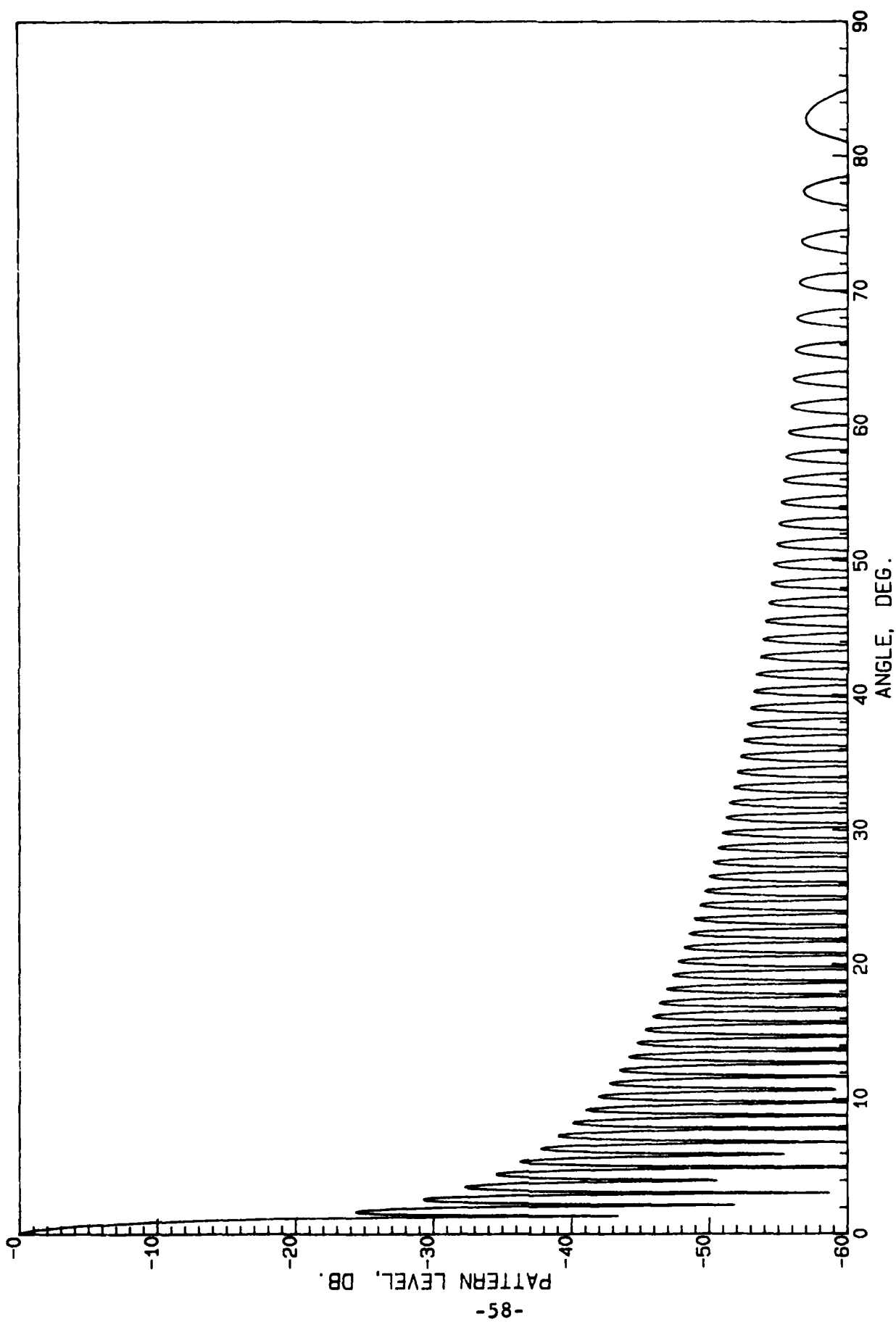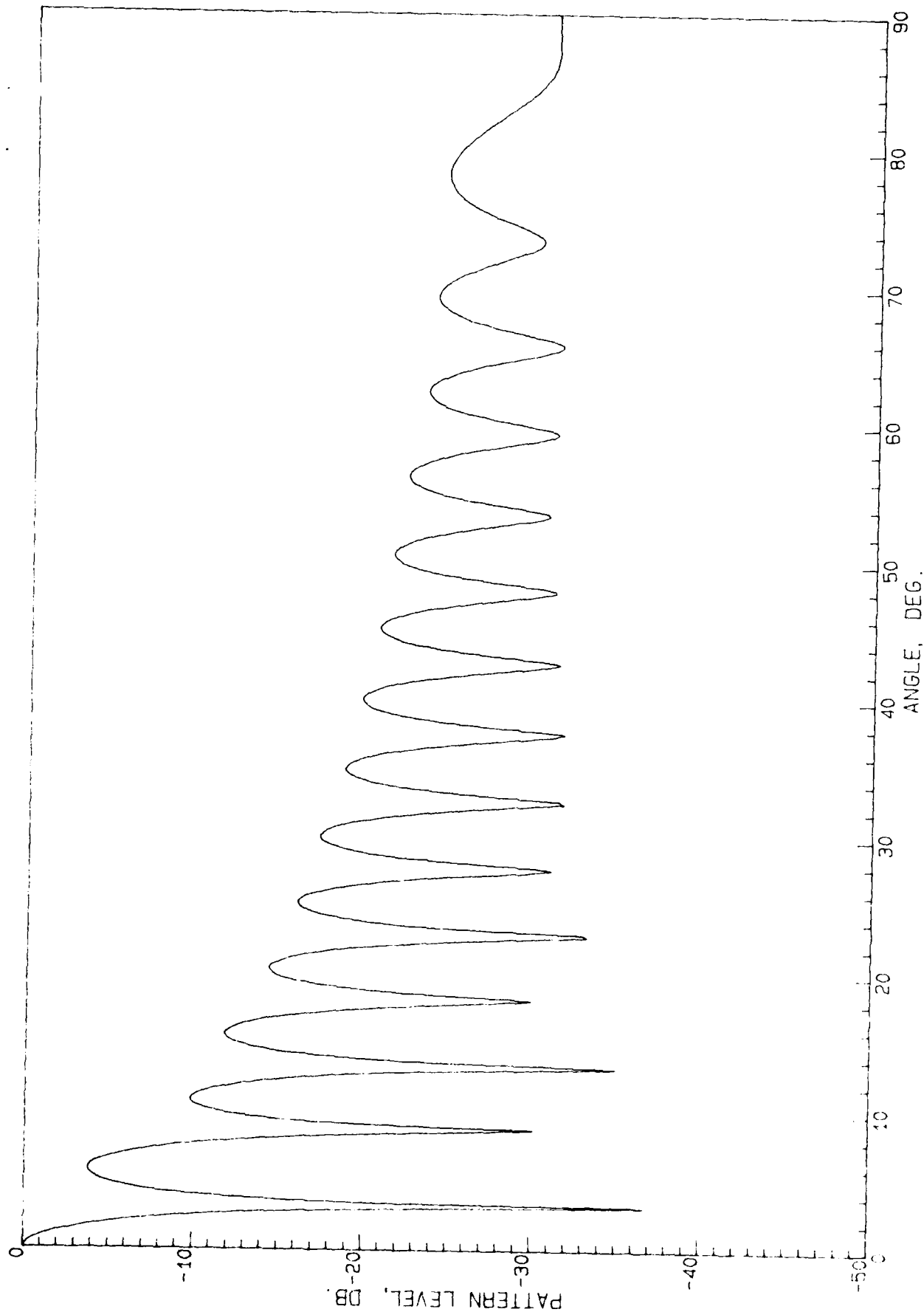
Figure 44
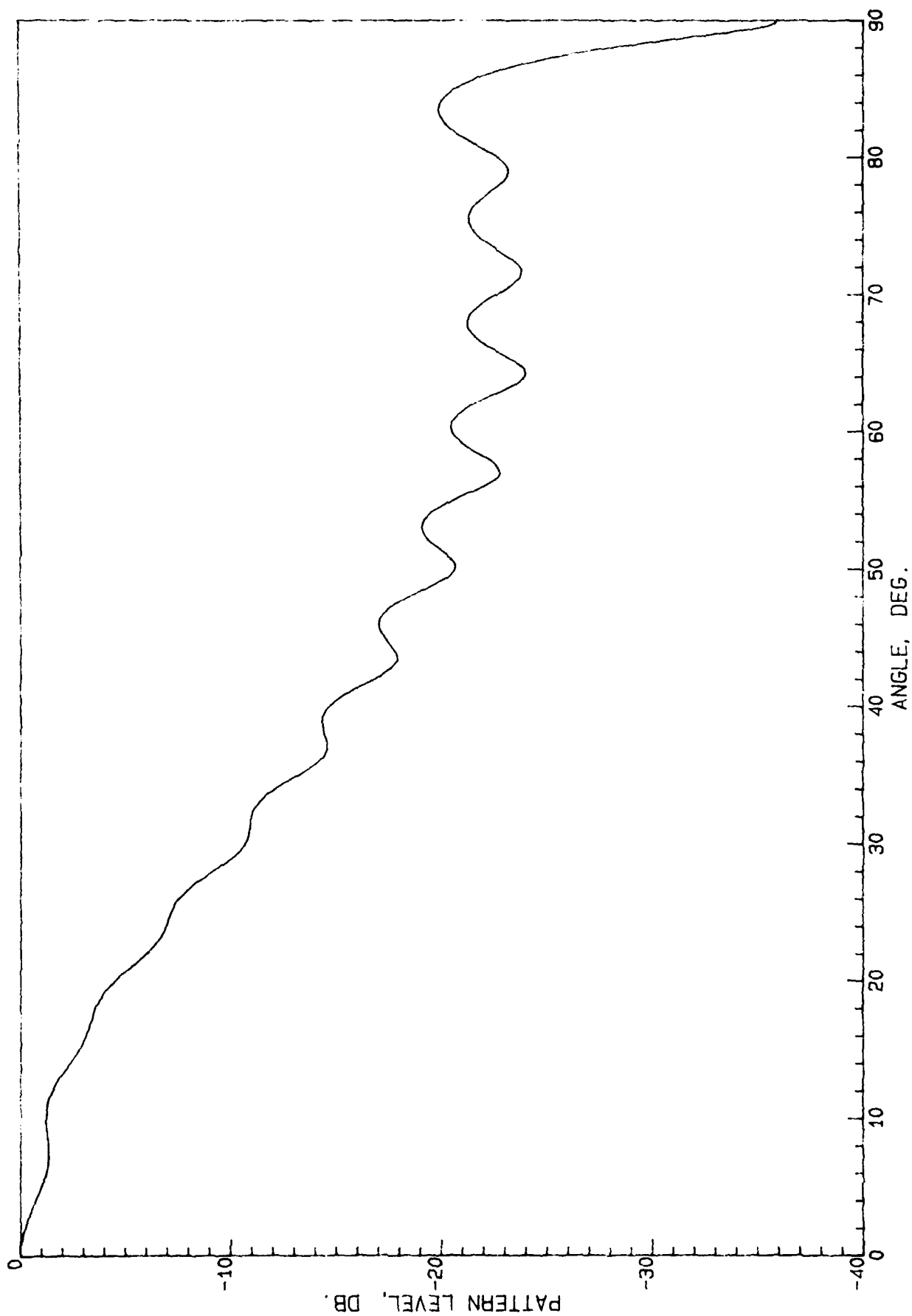
PATTERN OF 25 DB TAYLOR 15 WV SQUARE APERTURE, BETA=.54, GAMA=.025

Figure 45
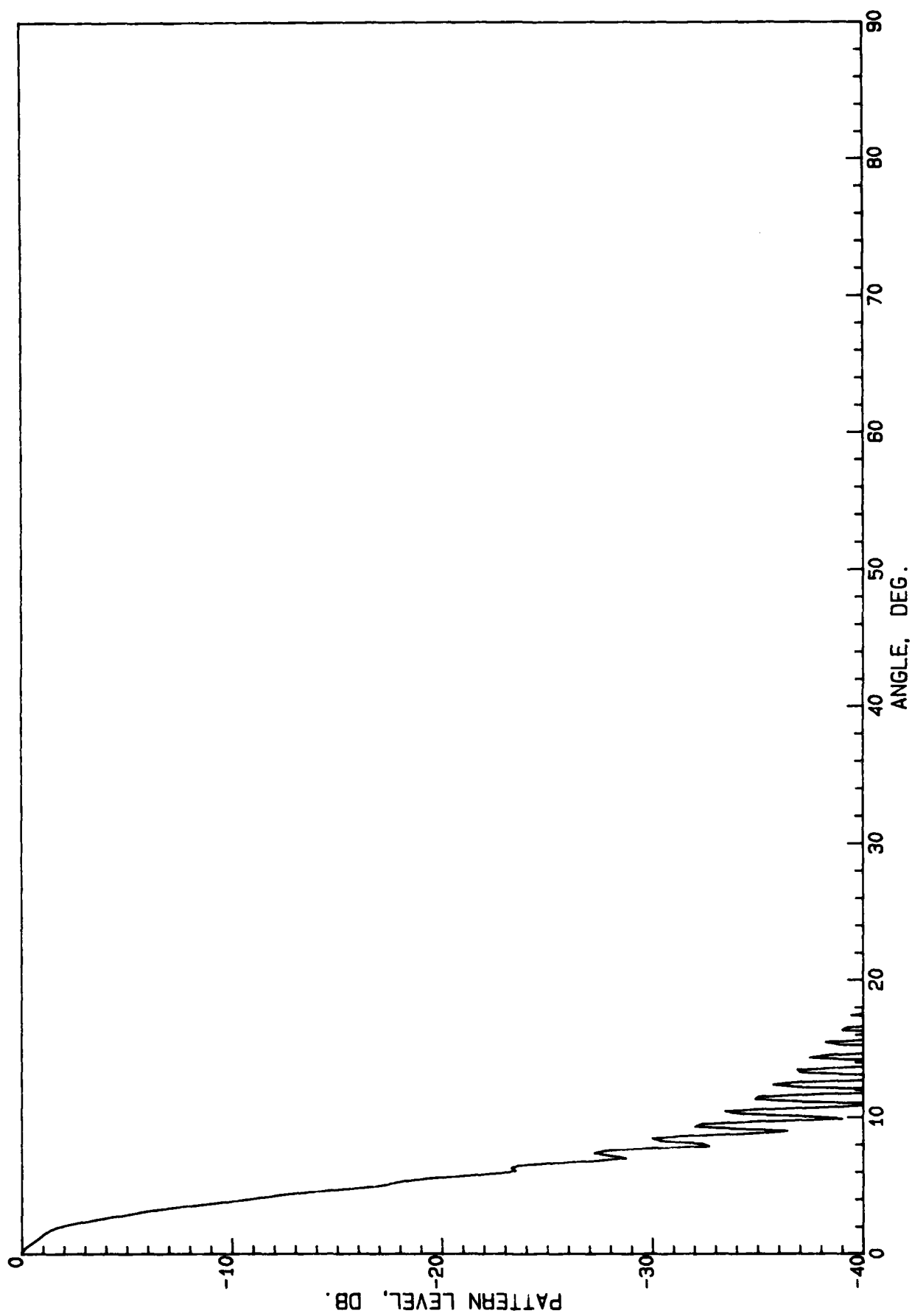
PATTERN OF 25 DB TAYLOR 60 WV SQUARE APERTURE, BETA=.67, GAMA=.025
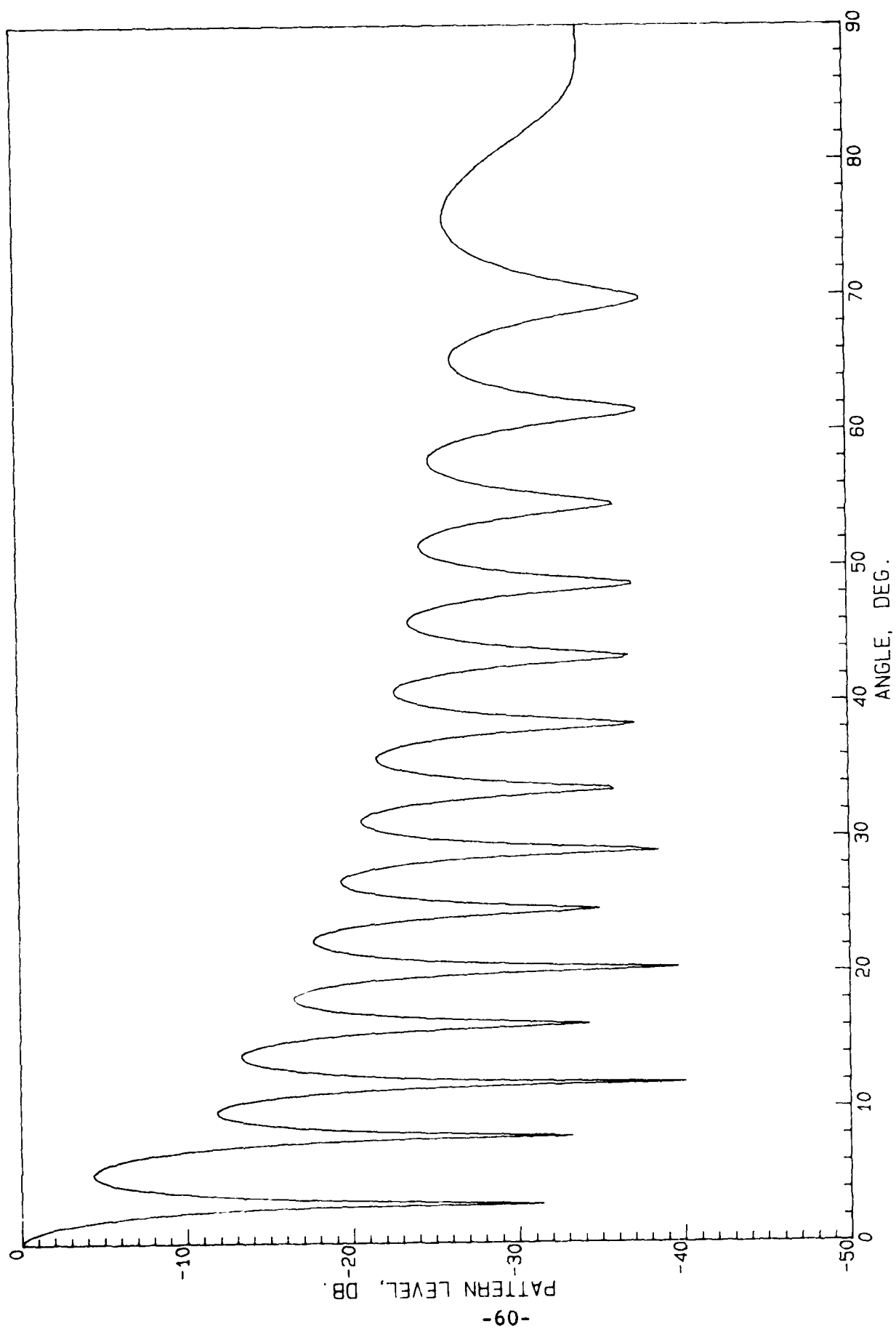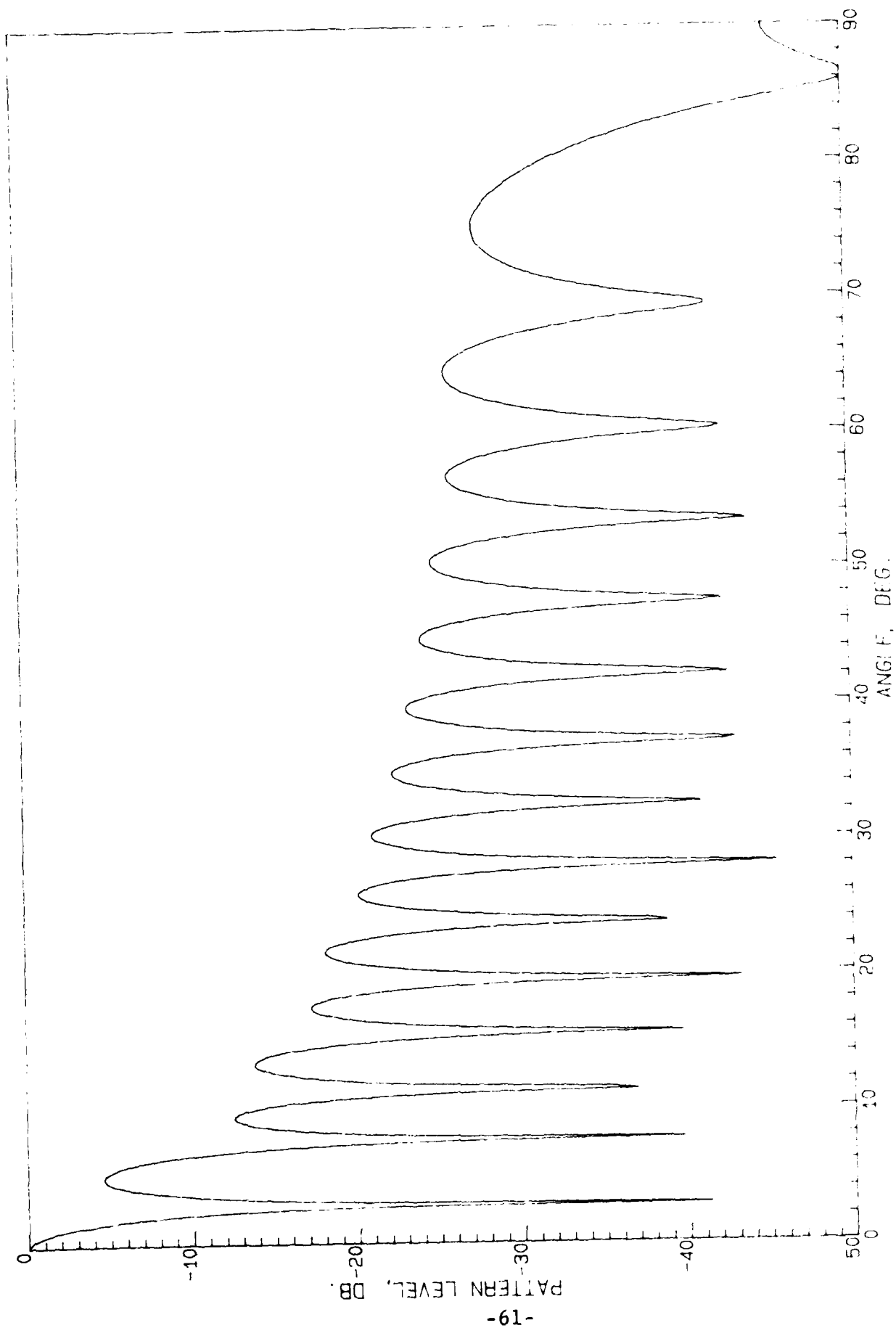
Figure 46

2.3   References

R. Barakat, "Application of the Sampling Theorem to Optical Diffraction Theory", J. Optical Soc. of America, Vol. 54, July 1964, pp. 920-930.

R. B. Barrar & C. H. Wilcox, "On the Fresnel Approximation", Trans. IEEE, Vol. AP-6, January 1958, pp. 43-48.

R.H.T. Bates & J. Elliott, "The Determination of the True Side-Lobe Level of Long Broadside Arrays from Radiation Pattern Measurements Made in the Fresnel Region", Proc. IEE, Vol. 103C, September 1967, pp. 307-312.

R. W. Bickmore, "Fraunhofer Pattern Measurement in the Fresnel Region", Can. J. Physics, Vol. 35, 1957, pp. 1299-1308.

O.M. Bucci et al, "Fast Analysis of Large Antenna - A New Computational Philosophy", Trans. IEEE, Vol. AP-28, May 1980, pp. 306-310.

O.M. Bucci, G. Franceschetti & R. Pierri, "Reflector Antenna Fields - An Exact Aperture-like Approach", Trans. IEEE, Vol. AP-29, July 1981, pp. 580-586.

O.M. Bucci & G. Franceschetti, "Radiation from Reflector Antennas: Exact Aperture and Aperture-like Approaches", Rad. Sci., Vol. 16, Nov-Dec. 1981, p. 1101.

D. K. Cheng, "On the Simulation of Fraunhofer Radiation Patterns in the Fresnel Region", Trans. IRE, Vol. AP-5, October 1957, pp. 399-402.

D.K. Cheng & S.T. Moseley, "On-axis Defocus Characteristics of the Paraboloidal Reflector, " Trans. IRE, Vol. AP-3, October 1955, pp. 214-216.

S. Cornbleet, "The Diffraction Fields of a Non-Uniform Circular Aperture", Proc. URSI Symp. Electromagnetic Theory and Antennas, Part 1, E.C. Jordan, Ed., Pergamon Press, 1962, pp. 157-175.

G. D'Auria & D. Solimini, "Fresnel Diffraction and Focusing
Properties of Apertures Under Partially Coherent Illumination",
Trans. IEEE, Vol. AP-15, May 1967, pp. 480-483.

P. J. Davis & P. Rabinowitz, "Numerical Integration", Blaisdell
Publishing Co., 1967.

Electronic Communications Inc., "Antenna Studies of Focused
Apertures in the Fresnel Region", RADC-TDR-62-330, Vol. II,
June 1, 1962.

M. D. Fahey, T. C. Pierce, W.G. Spaulding, "Phased Array Focused
in Near Field", U.S. Army Missile Command, Report No. RE-TR-72-7,
June 1972.

V. Galindo-Israel & R. Mittra, "A New Series Representation
for the Radiation Integral with Application to Reflector Antennas",
Trans. IEEE, Vol. AP-25, September 1977, pp. 631-641.

V. Galindo-Israel & Y. Rahmat-Samii, "A New Look at Fresnel
Field Computation Using the Jacobi-Bessel Series", Trans. IEEE,
Vol. AP-29, November 1981, pp. 885-898.

W. J. Graham, "Analysis and Synthesis of Axial Field Patterns
of Focused Apertures", Trans. IEEE, Vol. AP-31, July 1983, pp. 665-668.

R. C. Hansen, "Linear Arrays", Chapter 9 in Handbook of Antenna
Design, Vol. 2, A.W. Rudge et al, eds., Peregrinus, London, 1983.

R. C. Hansen, "Minimum Spot Size of Focused Apertures", Proc.
URSI Symp. on EM Theory, Delft, Pergamon Press, 1965, pp. 661-667.

R. C. Hansen, "Microwave Scanning Antennas", Vol. 1, Chapter 1,
Academic Press, 1964.

R. C. Hansen, "Antenna Power Densities in the Fresnel Region",
Proc. IRE, Vol. 47, December 1959, pp. 2119-2120.

R. C. Hansen & L. L. Bailin, "A New Method of Near Field Analysis", Trans. IRE, Vol. AP-7, Dec. 1959, pp. S458-S467.

J. K. Hu, "Fresnel Region Fields of Circular Aperture Antennas", Rad. Sci., Vol. 65D, March-April 1961, pp. 137-147.

M. K. Hu, "Fresnel Region Field Distributions of Circular Aperture Antennas", Trans. IRE, Vol. AP-8, May 1960, pp. 344-346.

IEEE, "Standard Definitions of Terms for Antennas", Trans. IEEE, Vol. AP-17, May 1969, pp. 262-269.

E. Jacobs, "Predicting Power Transfer Between Large Aperture Antennas at Close Separations", Trans. IRE, Vol. EMC-4, October 1962, pp. 23-40.

R. C. Johnson, H. A. Ecker & J. S. Hollis, "Determination of Far-Field Antenna Patterns from Near-Field Measurements", Proc. IEEE, Vol. 61, December 1973, pp. 1668-1694.

E. V. Jull, "An Investigation of Near-Field Radiation Patterns Measured with Large Antennas", Trans. IRE, Vol. AP-10, July 1962, pp. 363-368.

A. F. Kay, "Near-Field Gain of Aperture Antennas", Trans. IRE, Vol. AP-8, November 1960, pp. 586-593.

L. W. Lechtreck, "Fresnel Antenna Patterns", Trans. IRE, Vol. AP-3, July 1955, pp. 138-140.

W. R. Lind, "Fresnel Zone Theory", TR from Moore School, Univ. of Pa., April 25, 1966.

Melpar, "Fresnel Zone Analysis", Rpt. RADC-TDR-64-368, October 1964.

H. Nyquist, "Certain Topics in Telegraph Transmission Theory", Trans. AIEE Vol. 47, 1928, pp. 617-644.

D. P. Petersen & D. Middleton, "Sampling and Reconstruction of Wave-Number-Limited Functions in N-Dimensional Euclidean Spaces", Information and Control, Vol. 5, 1962, pp. 279-323.

C. Polk, "Optical Fresnel-Zone Gain of a Rectangular Aperture", Trans. IRE, Vol. AP-4, January 1956, pp. 65-69.

Y. Rahmat-Samii, R. Mittra, & V. Galindo-Israel, "Computation of Fresnel and Fraunhofer Fields of Planar Apertures and Reflector Antennas by the Jacobi-Bessel Series - A Review", J. of Electromagnetics, April-June 1981, Vol. 1, pp. 155-185.

L. J. Ricardi & R. C. Hansen, "Comparison of Line and Square Source Near Fields", Trans. IEEE, Vol. AP-11, November 1963, p. 711.

J. Ruze, "Circular Aperture Synthesis", Trans. IEEE, Vol. AP-12, November 1964, pp. 691-694.

W. E. Scharfman & G. August, "Focused Antenna Pattern Techniques for Phased-Array Radar", Report for Stanford Research Institute, June 1970.

D. Shanks, "Non-Linear Transformations of Divergent and Slowly Convergent Sequences", J. Math & Physics, Vol. 34, 1955, pp. 1-43.

C. E. Shannon, "Communication in the Presence of Noise", Proc. IRE, Vol. 37, 1949, pp. 10-21.

J. W. Sherman III, "Properties of Focused Apertures in the Fresnel Region", Trans. IRE, Vol. AP-10, July 1962, pp. 399-408.

D. H. Shinn, "Mis-Focusing and the Near-Field of Microwave Aerials", The Marconi Review, Vol. XIX, 1956, pp. 141-149.

T. Soejima, "Fresnel Gain of Aperture Antennas", Harvard Univ., Report No. 13, AFCRL-62-595, May 21, 1962.

A. H. Stroud & D. Secrest, "Gaussian Quadrature Formulas", Prentice-Hall, Inc., 1966.

L. F. Van Buskirk & C. E. Hendrix, "The Zone Plate as a Radio-Frequency Focusing Element", Trans. IEEE, Vol. AP-9, May 1961, pp. 319-320.

P. F. Wacker, "Unified Theory of Near-Field Analysis and Measurement: Nonmathematical Discussion", Trans. IEEE, Vol. AP-30, January 1982, pp. 99-107.

R. S. Wehner, "Limitations of Focused Aperture Antennas", RAND Report RM-262, October 10, 1949.

H. A. Wheeler, "Antenna Beam Patterns Which Retain Shape with Defocusing", Trans. IEEE, Vol. AP-10, September 1962, pp. 573-580.

E. T. Whittaker, "On the Functions Which are Represented by the Expansions of the Interpolatory Theory", Proc. Roy. Soc. Edinburgh, Vol. 35, 1915, pp. 181-194.

G. A. Woonton, "A More Exact Fresnel Field Diffraction Relation", Can Jour. Res., Vol. 28, Sect. A, March 1950, pp. 120-126.

R.F.H. Yang, "Quasi-Fraunhofer Gain of Parabolic Antennas", Proc. IRE, Vol. 43, April 1955, p. 486.

F. Zernike, "Beaugungstheorie des Schneidenvefahrens", Physica, Vol. 1, 1934, p. 689.

3.0   CONCLUSIONS

The following conclusions result from this study.

A.   Axial power density distribution (the axial main
lobe, the first few forelobes and aftlobes) is essen-
tially independent of aperture size in wavelengths.
The forelobe envelope taper, however, decreases more
rapidly with shorter β for larger apertures.

B.   The first forelobe level for uniform excitation
is a strong function of focal distance; for example,
it is roughly -14 db for $\gamma = .025$, roughly -12 db for
$\gamma = .05$, roughly -9 db for $\gamma = .1$, and roughly 6 db
for $\gamma = .2$.   The 25 db Taylor distributions produce
forelobe envelopes with roughly the same shape but at
a higher level and with much smaller oscillations.
For example, the level is roughly -11 db for $\gamma = .025$,
-8 db for $\gamma = .05$, and -5 db for $\gamma = .1$.

C.   Inverse aperture distributions (high at edge, low
in center) can reduce forelobe and aftlobe levels below
those of uniform excitation, but the efficiency is low
(of the order of -12 db) and the transverse sidelobe
level high (of the order of -3 db).   This type of dis-
tribution is not attractive.

D.   The forelobes and aftlobes of the uniform exci-
tation are probably satisfactory for most applications,
and this distribution has the further advantages that
the transverse sidelobes are not high and that the
efficiency is excellent.

E.   The peak power density along the axis does not
occur at the focus because of the $1/R^2$ effect.   For
very close focus (small γ) the axial peak is close to
the focus, but as the focus moves away, the axial peak

moves away much more slowly so that the separation between the two increases. From a systems standpoint, the important parameter is power density versus distance with the latter normalized to $2L^2/\lambda$. The peak power density available above the value at $2L^2/\lambda$ is a function only of this normalized distance $(\beta\gamma)$. Increases of more than 30 db are available for short focal distance and large apertures. These data (Figure 19) allow the systems designer to trade off aperture size, frequency, focal distance, and power density.

F.   The transverse patterns, both through the axial peak, and through the closest forelobe and aftlobe peaks, are well behaved, with rapid falloff for all but modest L/λ. For short distance (small α) the first several sidelobes increased, but again for large uniformly excited apertures this sidelobe degradation was small. The 25 db Taylor distribution had less than a db for apertures 60 wavelengths and larger.

G.   The Gaussian integrators give an acceptable combination of allowable aperture width and running time, although all the calculations were slow. The exact phase integral calculations give lower far out sidelobes than the far field pattern or than the approximate separated phase calculation, for close focal distances. This is due to sidelobe phase interference at the short distances. For all calculations but those of far out sidelobes, the separated phase calculation is adequate, and much faster.

APPENDIX A

FIELD CALCULATION BY SAMPLING INTERPOLATION

The field of an antenna, far or near, can be calculated by starting with field values at some number of discrete points, obtained by FFT or other means, then by using sampling functions to provide all field values in between. Basic theory was developed by Whittaker (1915), Nyquist (1928), Shannon (1949), and others. Extension to multiple dimensions was made by Petersen and Middleton (1962). Application to optics was by Barakat (1964) and to antennas by Ruze (1964) and Bucci and Franschetti (1980, 1981 A & B). Typically, at least one data point per pattern lobe is needed, and the interpolation is performed by a series of interpolation functions; for a linear aperture in the far field these functions are sinc type. In the near field they are basically Fresnel Integral functions. Circular apertures use a $J_1(x)/x$ far field function, while the near field function is basically a Lommel function of two variables.

To evaluate the ability of this technique to produce patterns, a *Taylor one-parameter line source* was used (Hansen, 1983). This allows various sidelobe levels to be evaluated. In addition, expanded sampling is incorporated, where the virtual aperture is increased by a small factor with this larger aperture sampled. The field is given by:

$$F(u) = \sum_{n=-\alpha L/\lambda}^{\alpha L/\lambda} F\left(\frac{n\pi}{2\alpha}\right) \text{ sinc } (2\alpha u - n)\pi$$

where the interpolation function is the sinc $(2\alpha u-n)\pi$, and the F( ) are the Taylor pattern values. As usual, $u = (L/\lambda) \sin\theta$ while α = expanded aperture $/L$, and L is the aperture length. The Taylor values are:

$$F\left(\frac{n\pi}{2\alpha}\right) = \begin{cases} \text{sinc } \pi \sqrt{n^2/4\alpha^2 - B^2} & , \quad n/2\alpha \geq B \\ \\ \text{sinhc } \pi \sqrt{B^2 - n^2/4\alpha^2} & , \quad B \geq n/2\alpha \end{cases}$$

Calculations were made on short (6 and 6.5λ) line sources, as these pose the most difficult test. For a uniform line source, where the sidelobe peaks are uniformly spaced at u = n, one sample per lobe (at the sidelobe peaks) gave an excellent pattern. Of course, the Taylor one-parameter pattern is available in simple closed form, and this was used for comparison. Patterns with lower sidelobes were poorly represented by one sample per lobe. Sidelobes would break up into several lobes, and the sidelobe envelope was irregular. To overcome this limitation, two samples per lobe were used, and the 2 in the interpolation function argument indicates this. Good results were obtained this way; Figures A1 and A2 show a 6 wavelength, 30 db Taylor source with Figure A1 that calculated using interpolation and Figure A2 the exact pattern. There is only a slight discrepancy in the last side-lobe. The fit may be improved through proper choice of α, but this value depends on the source length and sidelobe level. For example, using the 30 db Taylor case, α = 1.05 gives best fit for L = 6λ while α = 1 is best for L = 6.5λ. With a uni-form line source, α = 1.1 gives best fit for L = 6λ while α = 1.05 or 1.2 are best for L = 6.5λ. Thus excellent patterns can be produced using proper interpolation functions. See Appendix C for codes.

Next the computational efficiency of the interpola-tion calculation will be evaluated. Again, consider a linear aperture of length L. The number of pattern sample points, at two per spatial wavelength is 4L/λ; since $\pi u = 2\pi(L/2\lambda) \sin \theta$ the corresponding interval is L/4λ. Thus the pattern must be computed at 4L/λ values of spatial frequency. These values

AZIMUTH ANGLE, DEG.
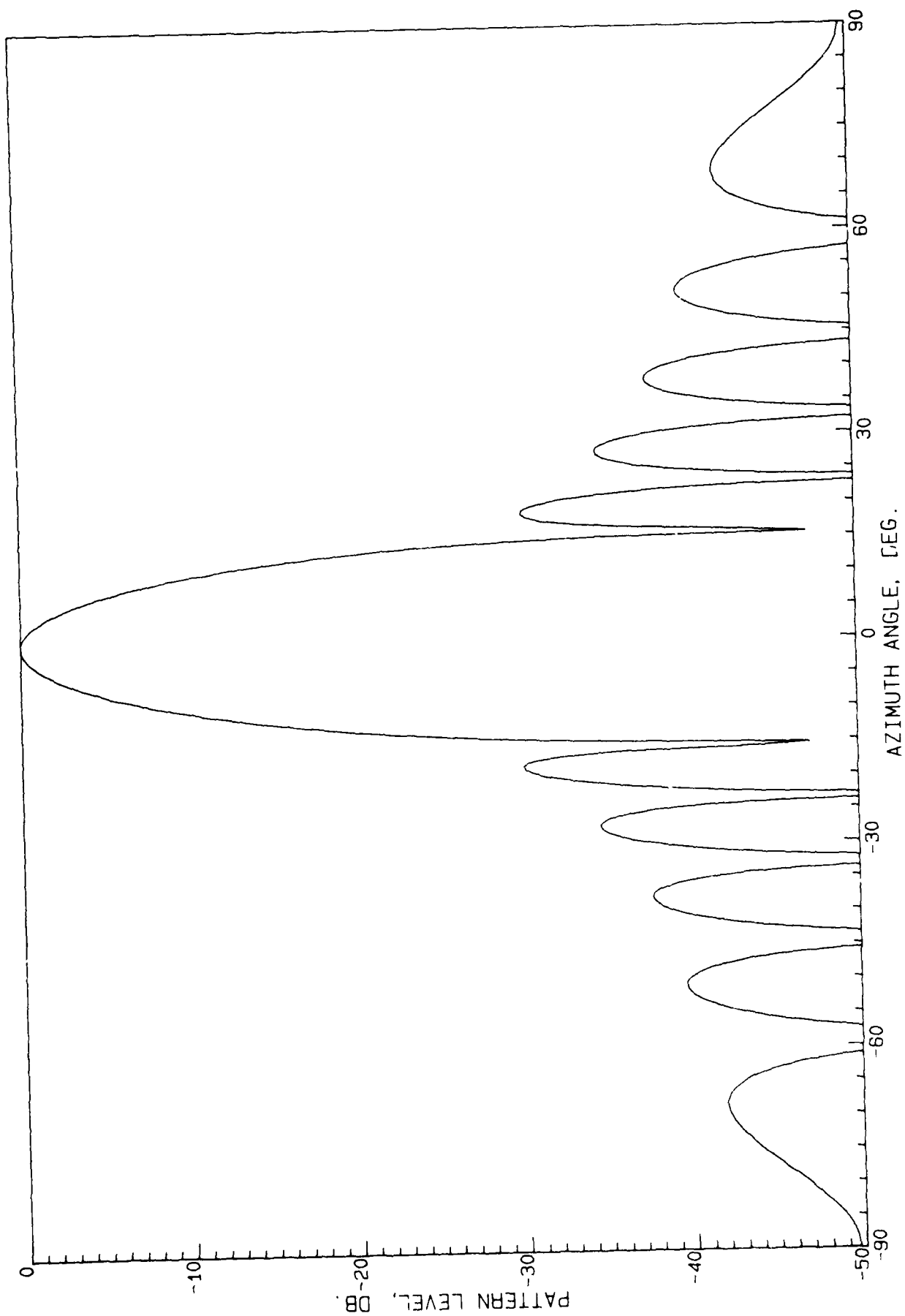
6 WV, 30 DB SLR TAYLOR PATTERN, ALFA=1

Figure A1

PATTERN LEVEL, DB.

AZIMUTH ANGLE, DEG.

PATTERN LEVEL, DB.
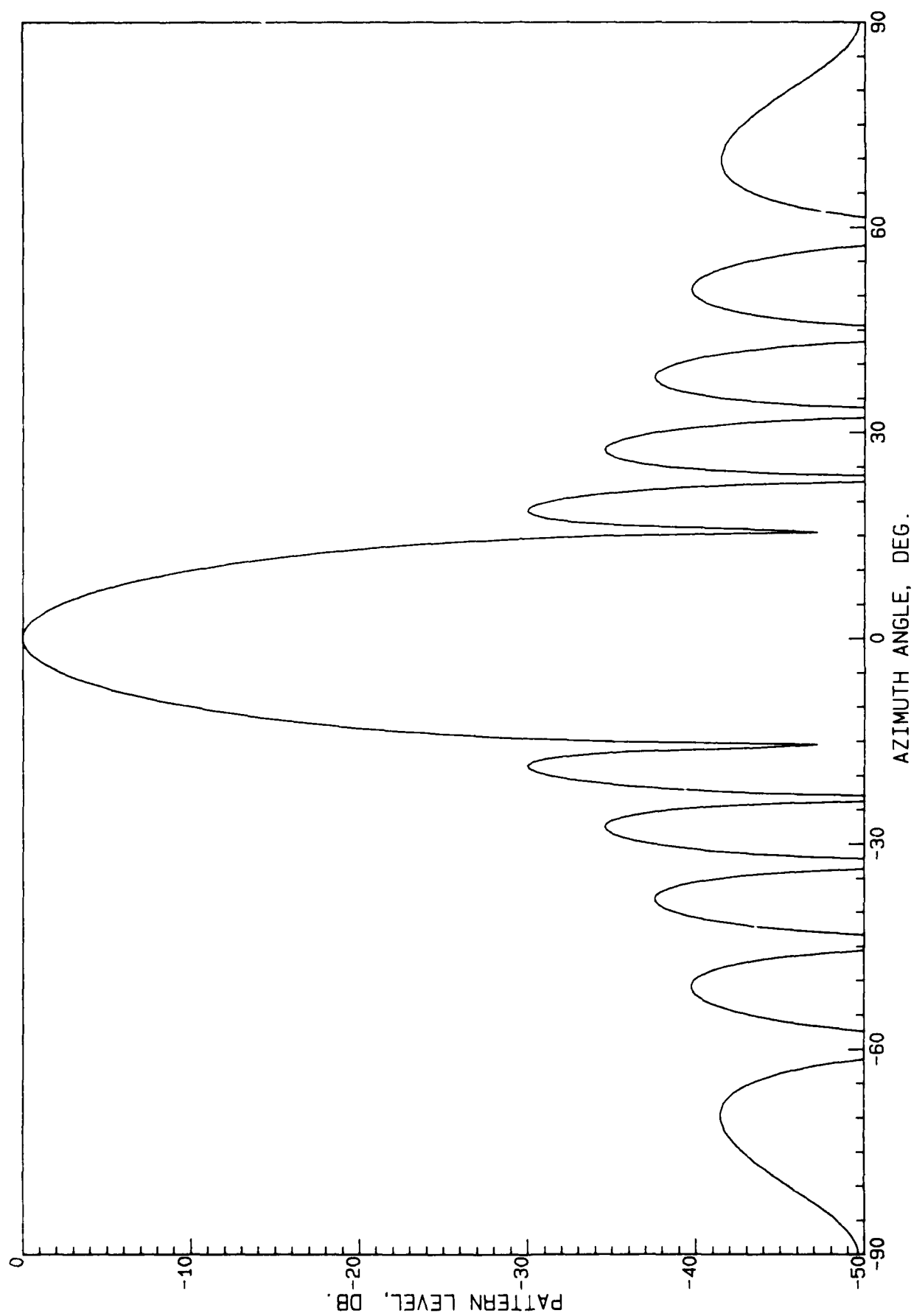
6 WV, 30 DB SLR TAYLOR LINE SOURCE PATTERN

Figure A2

-A4-

are then the coefficients in the sampling sum; each new pattern point to be computed requires a sum of $4L/\lambda$ terms, using these coefficients and the sampling (interpolation) function. A symmetric pattern reduces the coefficient calculations to half. But there are now two sampling functions in each series term. There are then several steps: for each sampling point calculate pattern (this may utilize FFT or may need numerical integration or an equivalent array summation); then for each observation point sum up coefficients times sampling functions. In contrast, the Gaussian integration requires a number of steps roughly equal to D/λ. Each observation point then requires a sum over integrand times constant values, with D/λ terms. Romberg utilizes a simpler sum but the number of terms is roughly 4 times. And finally the replacement of the aperture by an array of $\lambda/4$ spacing requires a sum of $4D/\lambda$, about the same as Romberg. The sampling-interpolation procedure is then attractive only when, a) the coefficients (pattern samples) are easily obtained, and b) the range of pattern values needed is much less than the total range.

APPENDIX B

EVALUATION OF NUMERICAL INTEGRATION METHODS

The interpolation algorithm requires that the field
be known at each of a numer of grid points. When the far
field is of interest, these points can sometimes be calculated
via FFT. However, in the near field it is necessary to use
other techniques. As mentioned elsehwere in this report,
results at wide angles almost always require numerical inte-
gration over the aperture, or something equivalent. The pur-
pose of this section is to compare and evaluate for large
apertures three efficient and widely-used methods. These are
the Romberg with fixed order, the Gaussian with 32 steps, and
aperture summation using quarter-wave spacing.

Romberg integration is adaptive trapezoidal in nature,
where the parameters calculated for each layer of subdivision
are saved for use in the next layer. It is thus highly effi-
cient. In the adaptive form the subdivision continues until
the projected error is less than a specified value. A simpler
version used here is not adaptive in that the order is speci-
fied in advance. The running time closely doubles for each
unit increase in order. This subroutine is faster than the
adaptive version and, with experience, the proper order can
be picked in advance. For large order, however, many values
must be calculated and stored, which makes Romberg inefficient.

Gaussian quadrature is one of the oldest methods and
evaluates the integral at a set cf unevenly spaced points with
weight functions calculated from orthogonal polynomials. See
Davis and Rabinowitz (1967). This procedure is a special case
of the non-linear transformations developed by Shanks (1955).
Tables for values up to 512 steps are by Stroud and Secrest
(1966).

Another method is to replace the integral by a sum where at least two samples per wavelength are used. It will appear later that for satisfactory accuracy at angles near endfire it is necessary to use four samples per wavelength. The resulting sum may incur accumulated roundoff errors for very large linear apertures or for moderately large planar apertures. As the number of terms in the sum becomes large, it may be necessary to utilize double precision.

The comparison test was performed on a Taylor one-parameter line source of varying length. The integral expression and its discrete counterpart are

$$F(u) = \int_0^1 I_0(\pi B \sqrt{1-x^2}) \cos \pi u x \, dx$$

$$F(u) = A_0 + 2 \sum_{n=1}^{\frac{N-1}{2}} A_n \cos 2n\pi u \quad , \quad N \text{ odd}$$

where the A_n are the Taylor amplitude coefficients. The form shown is for quarter-wave spacing in the sum although half-wave spacing was also used. This particular pattern is convenient as it is easily calculated in closed form, see Hansen (1983), so that the numerical results can be compared with the exact space factor. Calculations were made for u = 25 and 50, where $u = (L/\lambda) \sin \theta$. For u = 25, the Romberg results showed high sidelobes in the vicinity of u = 16 for order 5, and an oscillation of 2 db of sidelobe envelope in the same region for order 6. Order 7 gave excellent results with a relative time of 180. The Gaussian with 32 steps gave excellent results for u = 25 with a relative time of 52 but produced high and heavily distorted sidelobes for the u = 50 case at roughly u = 30, with

a relative time of 98. See Figure B1. Similarly, the Romberg for the larger range requires a much higher order and a doubling of its time for each increase of one. However, the Romberg order is simple, and the order is easily increased while doubling the Gaussian numer of steps requires a new program with new coefficients. Thus, although it is faster than the Romberg, it is more difficult to prepare. The array calculations using half-wave spacing gave excellent results out to roughly $u = 10$ with the relative time of 41. With quarter-wave spacing the results were excellent over the entire range with a relative time of 73 for $u = 25$. This time, of course, should increase directly with the aperture length.

Thus, for small apertures the 32-step Gauss is the most efficient and is satisfactory until the aliasing due to sampling appears. A 128-step Gauss allows aperture widths up to 60λ to be calculated.

U = L/WV SIN THETA
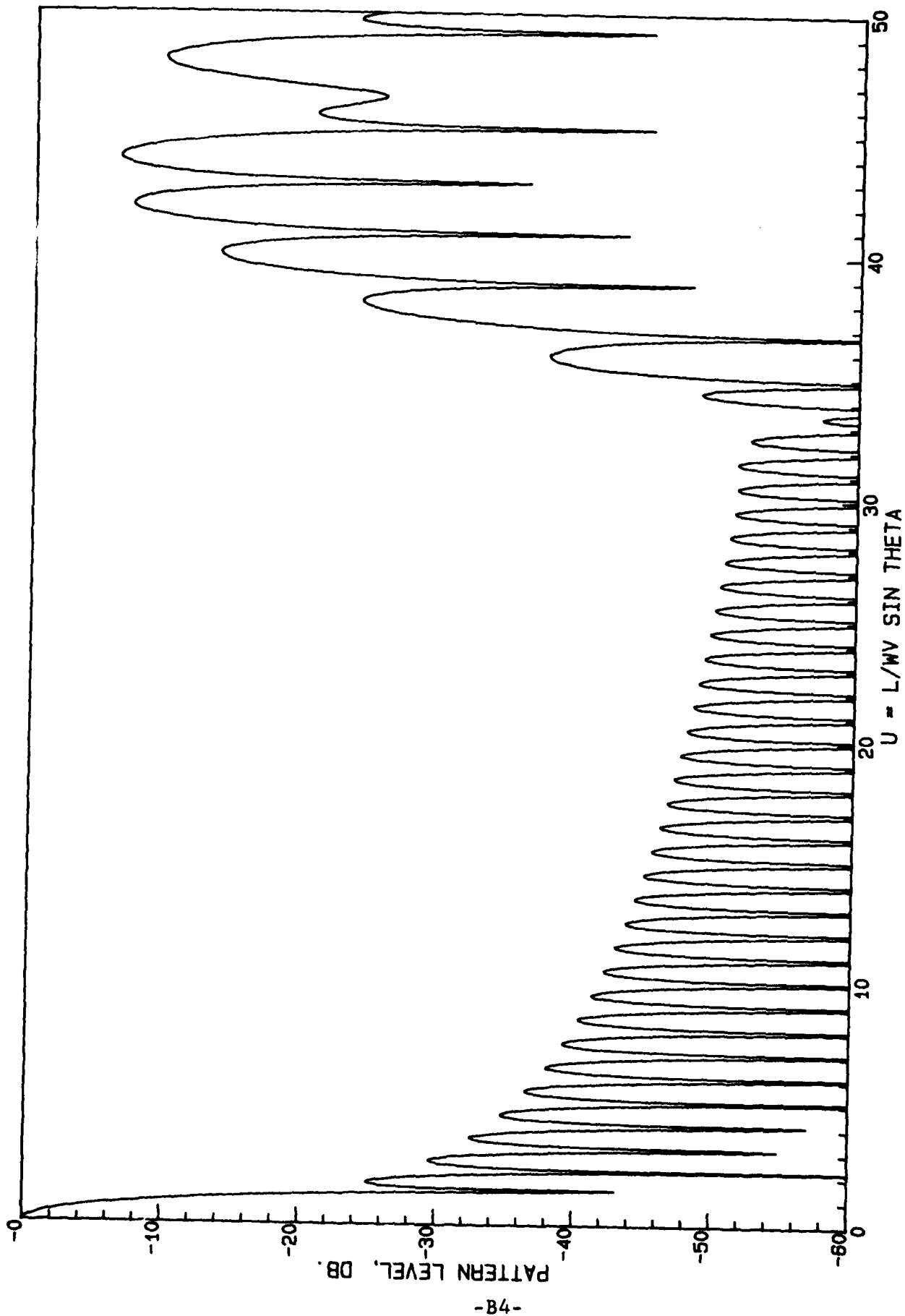
TAYLOR PATTERN BY GAUSSTEST, 32 STEPS, 1001 POINTS

Figure B1

-B4-

APPENDIX C
COMPUTER CODES

```
CCCCCCCCCCCCCCCCCCCCCCCCCCCCCCCCCCCCCCCCCCCCCCCCCCCCCCCCCCCCCCCCC CCC
C                                                                     C
C       FOCSQAX USE TAYBCALC,ROOTW,TAYWFUN,BESI,                      C
C          FOCSQGQ32C,FOCSQFCR,FOCSQGQ32D,FOCSQFCT        FSQ.MC      C
C                                                                     C
C       CALC ON-AXIS FIELD OF SQUARE FOCUSED APERTURE                 C
C       TAYLOR ONE-PARAMETER DISTRIBUTIONS USED IN X AND Y            C
C       USES EXACT PHASE INTEGRAL WITH GAUSSIAN INTEGRATION ALONG X & Y C
C       IDEAL ACTIVE ELEMENT PATTERN USED IN INTEGRATION              C
C                                                                     C
C       FOCAL DISTANCE NORMALIZED TO R0=2*L*L/WV                      C
C       GAMA=R0*WV/2*L*L                                              C
C       RATIO OF DISTANCE TO FOCAL DISTANCE IS BETA=R/R0              C
C       J.WILLIS, P-753, JULY 1983                                    C
C                                                                     C
C       PREPARED BY R.C.HANSEN                                        C
C                                                                     C
CCCCCCCCCCCCCCCCCCCCCCCCCCCCCCCCCCCCCCCCCCCCCCCCCCCCCCCCCCCCCCCCCCCCCCC
C
        DIMENSION E(501)
        DOUBLE PRECISION BGL,BGL2,GL2
        COMPLEX ED,EE
        REAL LWV,KL
        COMMON PB,KL,BGL2,GL2
        COMMON /TAY/ PI,SLR
        PI=3.1415926536
        PR=180/PI
        WRITE (12.900)
900     FORMAT(1X,"PROGRAM FOCSQAX",/)
100     ACCEPT "L/WV,SLR    ",LWV,SLRD
        IF (LWV.EQ.0) GO TO 990
        KL=2*PI*LWV
C       CALC TAYLOR PARAMETERS
        CALL TAYB(SLRD,B)
        PB=PI*B
        CALL BESI(PB,0,E0,IF)
        TYPE "E0=",E0
C       INPUT FOCAL REGION PARAMETERS
        ACCEPT "BETAM, GAMA, NPOINTS    ",BETAM,GAMA,NPT
        DO 160 I=2,NPT
        BETA=(I-1.)*BETAM/(NPT-1.)
        BGL=2.D0*BETA*GAMA*LWV
        BGL2=BGL*BGL
        GL2=(2.D0*GAMA*LWV)**2
C       CALC FIELD AT POINT USING GAUSSIAN INTEGRATION
        CALL GQ32C(0.,1.,ED)
        EE=ED/BETA
        E(I)=20*ALOG10(CABS(EE)/(E0*E0)+1E-6)
        TYPE I,BETA,E(I)
160     CONTINUE
        E(1)=-40
```

```
         EN=E(1)
         DO 170 I=2,NPT
170      IF (E(I).GT.EN) EN=E(I)
         DO 180 I=1,NPT
180      E(I)=E(I)-EN
         TYPE "EN=",EN
         OPEN 1,"PLOTFILE", ERR=980
         WRITE (1,950) (E(L),L=1,NPT)
         CLOSE 1
950      FORMAT (E12.6)
         GO TO 100
980      STOP "FILE OPEN ERROR"
990      WRITE (12,995)
995      FORMAT (1X,"<FF>")
         END
```

```
C       FOCSQFCR; USE FOR FOCSQAX
C       OUTER GAUSSIAN INTEGRAND
        COMPLEX FUNCTION FCR(X)
        DOUBLE PRECISION BGL2,GL2
        COMPLEX GG
        REAL KL
        COMMON PB,KL,BGL2,GL2
        COMMON /FUN/ XX
        XX=X
        CALL GQ32D(0.,1.,GG)
        CALL BESI(PB*SQRT(1-X*X),0,BI,IF)
        FCR=BI*GG
        RETURN
        END




C       FOCSQFCT; USE FOR FOCSQAX
C       INNER GAUSSIAN INTEGRAND
        COMPLEX FUNCTION FCT(Y)
        DOUBLE PRECISION F,BGL2,GL2
        COMPLEX EXP
        REAL KL
        COMMON PB,KL,BGL2,GL2
        COMMON /FUN/ X
        F=.25D0*(X*X+Y*Y)
        EXP=CEXP(CMPLX(0.,SNGL(KL*(DSQRT(BGL2+F)-DSQRT(GL2+F)))))
        CALL BESI(PB*SQRT(1-Y*Y),0,BI,IF)
        AEP=1./(1.+SNGL(F/BGL2))**.25
        FCT=BI*EXP*AEP
        RETURN
        END




RLDR FOCSQAX TAYBCALC ROOTW BESI TAYWFUN FOCSQGQ32C^
 FOCSQFCR FOCSQGQ32D FOCSQFCT @FLIB@
FOCSQAX
```

```
C       FOCSQGQ32C; USE FOR FOCSQAX
        SUBROUTINE GQ32C(XL,XU,Y)
C       32 POINT GAUSSIAN QUADRATURE INTEGRATION ROUTINE
        COMPLEX FCR,Y
        A=.5*(XU+XL)
        B=XU-XL
        C=.49863193*B
        Y=.35093050E-2*(FCR(A+C)+FCR(A-C))
        C=.49280575*B
        Y=Y+.81371974E-2*(FCR(A+C)+FCR(A-C))
        C=.48238112*B
        Y=Y+.12696032E-1*(FCR(A+C)+FCR(A-C))
        C=.46745303*B
        Y=Y+.17136931E-1*(FCR(A+C)+FCR(A-C))
        C=.44816057*B
        Y=Y+.21417949E-1*(FCR(A+C)+FCR(A-C))
        C=.42468380*B
        Y=Y+.25499029E-1*(FCR(A+C)+FCR(A-C))
        C=.39724189*B
        Y=Y+.29342046E-1*(FCR(A+C)+FCR(A-C))
        C=.36609105*B
        Y=Y+.32911111E-1*(FCR(A+C)+FCR(A-C))
        C=.33152213*B
        Y=Y+.36172897E-1*(FCR(A+C)+FCR(A-C))
        C=.29385787*B
        Y=Y+.39096947E-1*(FCR(A+C)+FCR(A-C))
        C=.25344995*B
        Y=Y+.41655962E-1*(FCR(A+C)+FCR(A-C))
        C=.21067563*B
        Y=Y+.43826046E-1*(FCR(A+C)+FCR(A-C))
        C=.16593430*B
        Y=Y+.45586939E-1*(FCR(A+C)+FCR(A-C))
        C=.11964368*B
        Y=Y+.46922199E-1*(FCR(A+C)+FCR(A-C))
        C=.072235980*B
        Y=Y+.47819360E-1*(FCR(A+C)+FCR(A-C))
        C=.024153832*B
        Y=B*(Y+.48270044E-1*(FCR(A+C)+FCR(A-C)))
        RETURN
        END
```

```
C       FOCSQGQ32D; USE FOR FOCSQAX
        SUBROUTINE GQ32D(XL,XU,Y)
C       32 POINT GAUSSIAN QUADRATURE INTEGRATION ROUTINE
        COMPLEX FCT,Y
        A=.5*(XU+XL)
        B=XU-XL
        C=.49863193*B
        Y=.35093050E-2*(FCT(A+C)+FCT(A-C))
        C=.49280575*B
        Y=Y+.81371974E-2*(FCT(A+C)+FCT(A-C))
        C=.48238112*B
        Y=Y+.12696032E-1*(FCT(A+C)+FCT(A-C))
        C=.46745303*B
        Y=Y+.17136931E-1*(FCT(A+C)+FCT(A-C))
        C=.44816057*B
        Y=Y+.21417949E-1*(FCT(A+C)+FCT(A-C))
        C=.42468380*B
        Y=Y+.25499029E-1*(FCT(A+C)+FCT(A-C))
        C=.39724189*B
        Y=Y+.29342046E-1*(FCT(A+C)+FCT(A-C))
        C=.36609105*B
        Y=Y+.32911111E-1*(FCT(A+C)+FCT(A-C))
        C=.33152213*B
        Y=Y+.36172897E-1*(FCT(A+C)+FCT(A-C))
        C=.29385787*B
        Y=Y+.39096947E-1*(FCT(A+C)+FCT(A-C))
        C=.25344995*B
        Y=Y+.41655962E-1*(FCT(A+C)+FCT(A-C))
        C=.21067563*B
        Y=Y+.43826046E-1*(FCT(A+C)+FCT(A-C))
        C=.16593430*B
        Y=Y+.45586939E-1*(FCT(A+C)+FCT(A-C))
        C=.11964368*B
        Y=Y+.46922199E-1*(FCT(A+C)+FCT(A-C))
        C=.072235980*B
        Y=Y+.47819360E-1*(FCT(A+C)+FCT(A-C))
        C=.024153832*B
        Y=B*(Y+.48270044E-1*(FCT(A+C)+FCT(A-C)))
        RETURN
        END
```

```
CCCCCCCCCCCCCCCCCCCCCCCCCCCCCCCCCCCCCCCCCCCCCCCCCCCCCCCCCCCCCCCCCCCCCC
C                                                                    C
C       FOCANTPAT; USE TAYBCALC,ROOTW,TAYWFUN,BESI,                  C
C          FOCANTFCR,FOCANTFCT,FOCGQ32C,FOCGQ32D        FOC.MC       C
C                                                                    C
C       CALC NEAR FIELD PATTERNS OF SQUARE FOCUSED APERTURE          C
C       TAYLOR ONE-PARAMETER DISTRIBUTIONS USED IN X AND Y           C
C       USES EXACT PHASE INTEGRAL WITH GAUSSIAN INTEGRATION ALONG X & Y   C
C       IDEAL ACTIVE ELEMENT PATTERN USED IN INTEGRATION             C
C                                                                    C
C       FOCAL DISTANCE NORMALIZED TO R0=2*L*L/WV                     C
C       GAMA=R0*WV/2*L*L                                             C
C       RATIO OF DISTANCE TO FOCAL DISTANCE IS BETA=R/R0             C
C       J.WILLIS, P-753, JULY 1983                                   C
C                                                                    C
C       PREPARED BY R.C.HANSEN                                       C
C                                                                    C
CCCCCCCCCCCCCCCCCCCCCCCCCCCCCCCCCCCCCCCCCCCCCCCCCCCCCCCCCCCCCCCCCCCCCC
C
        DIMENSION E(501)
        DOUBLE PRECISION BGL,BGL2,GL2
        COMPLEX ED,EE
        REAL LWV,KL
        COMMON PB,KL,BGL,BGL2,GL2,U,V
        COMMON /TAY/ PI,SLR
        PI=3.1415926536
        PR=180/PI
        WRITE (12,900)
900     FORMAT(1X,"PROGRAM FOCANTPAT",/)
100     ACCEPT "L/WV,SLR    ",LWV,SLRD
        IF (LWV.EQ.0) GO TO 990
        IF (LWV.GT.20.) STOP "L/WV MUST BE <= 20"
        KL=2*PI*LWV
C       CALC TAYLOR PARAMETERS
        CALL TAYB(SLRD,B)
        PB=PI*B
        CALL BESI(PB,0,E0,IF)
        TYPE "E0=",E0
C       INPUT FOCAL REGION PARAMETERS
        ACCEPT "BETA, GAMA    ",BETA,GAMA
        BGL=2.D0*BETA*GAMA*LWV
        BGL2=BGL*BGL
        GL2=(2.D0*GAMA*LWV)**2
        WRITE (12,910) BETA,GAMA
910     FORMAT (1X,"BETA=",F7.2,"    GAMMA=",F7.2,/)
C       INPUT PATTERN DATA
150     ACCEPT "PHI, NPOINTS    ",PH,NPT
        SP=SIN(PH/PR)
        CP=COS(PH/PR)
        DO 160 I=1,NPT
        TH=90.*(I-1.)/(NPT-1.)
        ST=SIN(TH/PR)
        CT=COS(TH/PR)
        U=ST*CP
```

```
        V=ST*SP
C       CALC PATTERN AT POINT USING GAUSSIAN INTEGRATION
        CALL GQ32C(-1.,1.,ED)
        E(I)=20*ALOG10(.25*CABS(ED)/(E0*E0)+1E-6)
        TYPE I,TH,E(I)
160     CONTINUE
        EN=E(1)
        DO 170 I=2,NPT
170     IF (E(I).GT.EN) EN=E(I)
        DO 180 I=1,NPT
180     E(I)=E(I)-EN
        TYPE "EN=",EN
        OPEN 1,"PLOTFILE", ERR=980
        WRITE (1,950) (E(L),L=1,NPT)
        CLOSE 1
950     FORMAT (E12.6)
        GO TO 100
980     STOP "FILE OPEN ERROR"
990     WRITE (12,995)
995     FORMAT (1X,"<FF>")
        END
```

RLDR FOCANTPAT TAYBCALC ROOTW TAYWFUN BESI FOCANTFCR^
 FOCANTFCT FOCGQ32C FOCGQ32D @FLIB@
FOCANTPAT

```
C       FOCANTFCR; USE FOR FOCANTPAT
C       OUTER GAUSSIAN INTEGRAND
        COMPLEX FUNCTION FCR(X)
        DOUBLE PRECISION BGL,BGL2,GL2
        COMPLEX GG
        REAL KL
        COMMON PB,KL,BGL,BGL2,GL2,U,V
        COMMON /FUN/ XX
        XX=X
        CALL GQ32C(-1.,1.,GG)
        CALL BESI(PB*SQRT(1-X*X),0,BI,IF)
        FCR=BI*GG
        RETURN
        END
```

```
C       FOCANTFCT; USE FOR FOCANTPAT
C       INNER GAUSSIAN INTEGRAND
        COMPLEX FUNCTION FCT(Y)
        DOUBLE PRECISION BGL,BGL2,GL2,F1,F2,RD
        COMPLEX EXP
        REAL KL
        COMMON PB,KL,BGL,BGL2,GL2,U,V
        COMMON /FUN/ X
        F1=DBLE(X*U+Y*V)
        F2=.25D0*(X*X+Y*Y)
        RD=DSQRT(BGL2-BGL*F1+F2)
        EXP=CEXP(CMPLX(0.,SNGL(KL*(RD-DSQRT(GL2+F2)))))
        CALL BESI(PB*SQRT(1-Y*Y),0,BI,IF)
        AEP=SQRT(SNGL(BGL*SQRT(1.-U*U-V*V)/RD))
        FCT=BI*EXP*AEP
        RETURN
        END
```

MICROCOPY RESOLUTION TEST CHART
NATIONAL BUREAU OF STANDARDS-1963-A

```
CCCCCCCCCCCCCCCCCCCCCCCCCCCCCCCCCCCCCCCCCCCCCCCCCCCCCCCCCCCCCCCCCCCCCCC
 · C                                                                       C
   C        FOCANTPAT1; USE TAYBCALC,ROOTW,TAYWFUN,BESI,FOCANT1FCR,         C
   C          FOCANT1FCT,GAUSS32C,GAUSS128DC              PC1.MC            C
   C                                                                        C
   C     CALC NEAR FIELD PATTERNS OF SQUARE FOCUSED APERTURE                C
   C     TAYLOR ONE-PARAMETER DISTRIBUTIONS USED IN X AND Y                 C
   C     PHASE INTEGRAL SPLIT INTO X & Y FACTORS; GAUSSIAN INTEGRATION       C
   C     IDEAL ACTIVE ELEMENT PATTERN USED IN INTEGRATION                   C
   C                                                                        C
   C     FOCAL DISTANCE NORMALIZED TO R0=2*L*L/WV                           C
   C     GAMA=R0*WV/2*L*L                                                    C
   C     RATIO OF DISTANCE TO FOCAL DISTANCE IS BETA=R/R0                    C
   C     J.WILLIS, P-753, JULY 1983                                         C
   C                                                                        C
   C     PREPARED BY R.C.HANSEN                                             C
   C                                                                        C
CCCCCCCCCCCCCCCCCCCCCCCCCCCCCCCCCCCCCCCCCCCCCCCCCCCCCCCCCCCCCCCCCCCCCCCCC
   C
         DIMENSION E(1001)
         DOUBLE PRECISION COMPLEX EUU,EVV
         DOUBLE PRECISION BGL,BGL2,GL2
         COMPLEX EE,EU,EV
         REAL LWV,KL
         COMMON PB,KL,BGL,BGL2,GL2,W
         COMMON /TAY/ PI,SLR
         PI=3.1415926536
         PR=180/PI
         WRITE (12,900)
   900   FORMAT(1X,"PROGRAM FOCANTPAT1",/)
   100   ACCEPT "L/WV,SLR    ",LWV,SLRD
         IF (LWV.EQ.0) GO TO 990
         KL=2*PI*LWV
   C     CALC TAYLOR PARAMETERS
         CALL TAYB(SLRD,B)
         PB=PI*B
         CALL BESI(PB,0,E0,IF)
         TYPE "E0=",E0
   C     INPUT FOCAL REGION PARAMETERS
         ACCEPT "BETA, GAMA    ",BETA,GAMA
         BGL=2.D0*BETA*GAMA*LWV
         BGL2=BGL*BGL
         GL2=(2.D0*GAMA*LWV)**2
         WRITE (12,910) BETA,GAMA
   910   FORMAT (1X,"BETA=",F7.2,"    GAMMA=",F7.2,/)
   C     INPUT PATTERN DATA
   150   ACCEPT "PHI, NPOINTS    ",PH,NPT
         SP=SIN(PH/PR)
         CP=COS(PH/PR)
         DO 160 I=1,NPT
         TH=90.*(I-1.)/(NPT-1.)
         ST=SIN(TH/PR)
         CT=COS(TH/PR)
         U=ST*CP
```

```fortran
      V=ST*SP
C     CALC PATTERN AT POINT USING GAUSSIAN INTEGRATION
      W=U
      IF (LWV.GT.15.) GO TO 120
      CALL GQ32C(-1.,1.,EU)
      W=V
      CALL GQ32C(-1.,1.,EV)
      EE=EU*EV
      GO TO 125
120   CALL GQ128(-1.D0,1.D0,EUU)
      W=V
      CALL GQ128(-1.D0,1.D0,EVV)
      EE=DCXCX(EUU*EVV)
125   E(I)=20*ALOG10(.25*CABS(EE)/(E0*E0)+1E-6)
      TYPE I,TH,E(I)
160   CONTINUE
      EN=E(1)
      DO 170 I=2,NPT
170   IF (E(I).GT.EN) EN=E(I)
      DO 180 I=1,NPT
180   E(I)=E(I)-EN
      TYPE "EN=",EN
      OPEN 1,"PLOTFILE", ERR=980
      WRITE (1,950) (E(L),L=1,NPT)
      CLOSE 1
950   FORMAT (E12.6)
      GO TO 100
980   STOP "FILE OPEN ERROR"
990   WRITE (12,995)
995   FORMAT (1X,"<FF>")
      END
```

```
C       FOCANT1FCR; USE FOR FOCANTPAT1
C       GAUSSIAN INTEGRAND
        DOUBLE PRECISION COMPLEX FUNCTION FCR(X)
        DOUBLE PRECISION COMPLEX EXP
        DOUBLE PRECISION BGL,BGL2,GL2,F
        REAL KL
        COMMON PB,KL,BGL,BGL2,GL2,W
        F=.25D0*X*X
        EXP=DCEXP(DCMPLX(0.D0,KL*(DSQRT(BGL2-BGL*W*X+F)-DSQRT(GL2+F))))
        CALL BESI(PB*SQRT(1-X*X),0,BI,IF)
        AEP=1./(1.+SNGL(F/BGL2))**.25
        FCR=BI*EXP*AEP
        RETURN
        END




C       FOCANTFCT; USE FOR FOCANTPAT
C       INNER GAUSSIAN INTEGRAND
        COMPLEX FUNCTION FCT(Y)
        DOUBLE PRECISION BGL,BGL2,GL2,F1,F2,RD
        COMPLEX EXP
        REAL KL
        COMMON PB,KL,BGL,BGL2,GL2,U,V
        COMMON /FUN/ X
        F1=DBLE(X*U+Y*V)
        F2=.25D0*(X*X+Y*Y)
        RD=DSQRT(BGL2-BGL*F1+F2)
        EXP=CEXP(CMPLX(0.,SNGL(KL*(RD-DSQRT(GL2+F2)))))
        CALL BESI(PB*SQRT(1-Y*Y),0,BI,IF)
        AEP=SQRT(SNGL(BGL*SQRT(1.-U*U-V*V)/RD))
        FCT=BI*EXP*AEP
        RETURN
        END




RLDR FOCANTPAT1 TAYBCALC ROOTW BESI TAYWFUN^
 FOCANT1FCR FOCANT1FCT GAUSS32C GAUSS128DC @FLIB@
FOCANTPAT1
```

```fortran
C        GAUSS128DC; GAUSSIAN QUADRATURE 128 STEPS, DOUBLE PRECISION COMPLEX
         SUBROUTINE GQ128(XL,XU,Y)
         DOUBLE PRECISION COMPLEX FCR,Y
         DOUBLE PRECISION XL,XU,A,B,C
         A=.5D0*(XU+XL)
         B=XU-XL
         C=.499991244397356D0*B
         Y=.224690480146045D-3*(FCR(A+C)+FCR(A-C))
         C=.499538729988868D0*B
         Y=Y+.52290633967017D-3*(FCR(A+C)+FCR(A-C))
         C=.49886662431275D0*B
         Y=Y+.82125150933451D-3*(FCR(A+C)+FCR(A-C))
         C=.49789637926749D0*B
         Y=Y+.11191442154813D-2*(FCR(A+C)+FCR(A-C))
         C=.49662855645010D0*B
         Y=Y+.14163757357289D-2*(FCR(A+C)+FCR(A-C))
         C=.49506390924586D0*B
         Y=Y+.17127630204551D-2*(FCR(A+C)+FCR(A-C))
         C=.49320337136229D0*B
         Y=Y+.20081274918693D-2*(FCR(A+C)+FCR(A-C))
         C=.49104805421785D0*B
         Y=Y+.23022921283515D-2*(FCR(A+C)+FCR(A-C))
         C=.48859924573295D0*B
         Y=Y+.25950809163381D-2*(FCR(A+C)+FCR(A-C))
         C=.48585840937356D0*B
         Y=Y+.28863187714328D-2*(FCR(A+C)+FCR(A-C))
         C=.48282718321598D0*B
         Y=Y+.31758315808536D-2*(FCR(A+C)+FCR(A-C))
         C=.47950737892684D0*B
         Y=Y+.34634462834494D-2*(FCR(A+C)+FCR(A-C))
         C=.47590098067063D0*B
         Y=Y+.37489909628273D-2*(FCR(A+C)+FCR(A-C))
         C=.47201014391511D0*B
         Y=Y+.40322949452430D-2*(FCR(A+C)+FCR(A-C))
         C=.46783719413895D0*B
         Y=Y+.43131888993083D-2*(FCR(A+C)+FCR(A-C))
         C=.46338462543947D0*B
         Y=Y+.45915049358304D-2*(FCR(A+C)+FCR(A-C))
         C=.45865509904048D0*B
         Y=Y+.48670767075034D-2*(FCR(A+C)+FCR(A-C))
         C=.45365144170087D0*B
         Y=Y+.51397395079161D-2*(FCR(A+C)+FCR(A-C))
         C=.44837664402457D0*B
         Y=Y+.54093303697515D-2*(FCR(A+C)+FCR(A-C))
         C=.44283385867269D0*B
         Y=Y+.56756881620402D-2*(FCR(A+C)+FCR(A-C))
         C=.43702639847901D0*B
         Y=Y+.59386536863701D-2*(FCR(A+C)+FCR(A-C))
         C=.43095773446977D0*B
         Y=Y+.61980697719754D-2*(FCR(A+C)+FCR(A-C))
         C=.42463149378898D0*B
         Y=Y+.64537813696336D-2*(FCR(A+C)+FCR(A-C))
         C=.41805145753045D0*B
         Y=Y+.67056356443081D-2*(FCR(A+C)+FCR(A-C))
```

```
C=.41122155847782D0*B
Y=Y+.69534820664755D-2*(FCR(A+C)+FCR(A-C))
C=.40414587875395D0*B
Y=Y+.71971725020834D-2*(FCR(A+C)+FCR(A-C))
C=.39682864738108D0*B
Y=Y+.74365613010731D-2*(FCR(A+C)+FCR(A-C))
C=.38927423775320D0*B
Y=Y+.76715053844326D-2*(FCR(A+C)+FCR(A-C))
C=.38148716502204D0*B
Y=Y+.79018643296996D-2*(FCR(A+C)+FCR(A-C))
C=.37347208339853D0*B
Y=Y+.81275004548926D-2*(FCR(A+C)+FCR(A-C))
C=.36523378337095D0*B
Y=Y+.83482789007996D-2*(FCR(A+C)+FCR(A-C))
C=.35677718884179D0*B
Y=Y+.85640677115557D-2*(FCR(A+C)+FCR(A-C))
C=.34810735418475D0*B
Y=Y+.87747379135588D-2*(FCR(A+C)+FCR(A-C))
C=.33922946122385D0*B
Y=Y+.89801635925043D-2*(FCR(A+C)+FCR(A-C))
C=.33014881613632D0*B
Y=Y+.91802219886657D-2*(FCR(A+C)+FCR(A-C))
C=.32087084628115D0*B
Y=Y+.93747934702723D-2*(FCR(A+C)+FCR(A-C))
C=.31140109695529D0*B
Y=Y+.95637618049754D-2*(FCR(A+C)+FCR(A-C))
C=.30174522807927D0*B
Y=Y+.97470140293533D-2*(FCR(A+C)+FCR(A-C))
C=.29190901081438D0*B
Y=Y+.99244406164154D-2*(FCR(A+C)+FCR(A-C))
C=.28189832411330D0*B
Y=Y+.100959355521065D-1*(FCR(A+C)+FCR(A-C))
C=.27171915120640D0*B
Y=Y+.10261396243480D-1*(FCR(A+C)+FCR(A-C))
C=.26137757602558D0*B
Y=Y+.10420723890375D-1*(FCR(A+C)+FCR(A-C))
C=.25087977956807D0*B
Y=Y+.10573823234110D-1*(FCR(A+C)+FCR(A-C))
C=.24023203620208D0*B
Y=Y+.10720602769604D-1*(FCR(A+C)+FCR(A-C))
C=.22944070991677D0*B
Y=Y+.10860974769026D-1*(FCR(A+C)+FCR(A-C))
C=.21851225051855D0*B
Y=Y+.10994855334230D-1*(FCR(A+C)+FCR(A-C))
C=.20745318977613D0*B
Y=Y+.11122164446900D-1*(FCR(A+C)+FCR(A-C))
C=.19627013751663D0*B
Y=Y+.11242826016372D-1*(FCR(A+C)+FCR(A-C))
C=.18496977767492D0*B
Y=Y+.11356767925118D-1*(FCR(A+C)+FCR(A-C))
C=.17355886429881D0*B
Y=Y+.11463922071843D-1*(FCR(A+C)+FCR(A-C))
C=.16204421751220D0*B
Y=Y+.11564224412193D-1*(FCR(A+C)+FCR(A-C))
C=.15043271943883D0*B
```

```
Y=Y+.11657614997031D-1*(FCR(A+C)+FCR(A-C))
C=.13873131008895D0*B
Y=Y+.11744038008269D-1*(FCR(A+C)+FCR(A-C))
C=.12694698321134D0*B
Y=Y+.11823441792224D-1*(FCR(A+C)+FCR(A-C))
C=.11508678211332D0*B
Y=Y+.11895778890501D-1*(FCR(A+C)+FCR(A-C))
C=.10315779545103D0*B
Y=Y+.11961006068352D-1*(FCR(A+C)+FCR(A-C))
C=.91167152992668D-1*B
Y=Y+.12019084340512D-1*(FCR(A+C)+FCR(A-C))
C=.79122021357112D-1*B
Y=Y+.12069978994509D-1*(FCR(A+C)+FCR(A-C))
C=.67029599730594D-1*B
Y=Y+.12113659611407D-1*(FCR(A+C)+FCR(A-C))
C=.54897115563822D-1*B
Y=Y+.12150100083986D-1*(FCR(A+C)+FCR(A-C))
C=.42731820252257D-1*B
Y=Y+.12179278632345D-1*(FCR(A+C)+FCR(A-C))
C=.30540984802069D-1*B
Y=Y+.12201177816925D-1*(FCR(A+C)+FCR(A-C))
C=.18331895484366D-1*B
Y=Y+.12215784548925D-1*(FCR(A+C)+FCR(A-C))
C=.61118494803079D-2*B
Y=B*(Y+.12223090098131D-1*(FCR(A+C)+FCR(A-C)))
RETURN
END
```

```
C        PATINTERP2; USE ROOTW, TAYLORWFUN            USE PLOTRECT
C        SINC INTERPOLATION OF TAYLOR ONE-PARAMETER LINE SOURCE PATTERN
C        WITH EXPANDED SAMPLING, ALFA >= 1
C        J. WILLIS, P-753,  JULY 1983
         DIMENSION A(100),E(600)
         REAL LWV
         COMMON PI,SLR
         PI=3.1415926536
         PR=180/PI
         WRITE (12,900)
900      FORMAT (1X,"PROGRAM PATINTERP2;  SINC INTERPOLATION OF PATTERN",/)
100      ACCEPT "L/WV,SLR.NPTS,ALFA    ",LWV,SLRD,NP,ALFA
         IF (LWV.EQ.0.) GO TO 990
         IF (SLRD.LT.13.26144) STOP "SLR TOO SMALL"
         WRITE (12,920) LWV,NP,ALFA
920      FORMAT (1X,"L/WV=",F8.2,"    N POINTS=",I4,"    ALPA=",F6.2,/)
C        USE WEGSTEIN ROOTER TO CALC B VALUE
         SLR=10.**(.05*SLRD)
         BS=.4603+.0479*(SLRD-13.26)
         CALL ROOTW(B,F0,BS,1E-6,200,IFL)
         IF (IFL.EQ.0) GO TO 105
         TYPE "ERROR FLAG    ",IFL
105      TYPE BS,F0,"   B=",B
         WRITE (12,925) SLRD,B
925      FORMAT (1X,"SLR=",F5.2," DB,     B=",F9.6,/)
C        NMAX IS MAXIMUM INDEX IN SUMMATION
         NMAX=2*INT(.5*(2*ALFA*LWV+1))-1
C        NSAMP IS NUMBER OF SAMPLES EACH SIDE
         NSAMP=NMAX+1
         TYPE "NMAX=",NMAX,"    NSAMPLES=",NSAMP
C        CALC PATTERN POINTS
         B2=B*B
         E0=SINH(PI*B)/(PI*B)
         IF (B.LT..001) E0=1
         TYPE "E NORM=",E0
         DO 110 I=1,NSAMP
         A3=.5*I/ALFA
         A32=A3*A3
         IF (A32.GE.B2) GO TO 115
         ARG=PI*SQRT(B2-A32)
         IF (ARG.LT..00001) GO TO 116
         A(I)=SINH(ARG)/ARG
         GO TO 110
115      ARG=PI*SQRT(A32-B2)
         IF (ARG.LT..001) GO TO 118
         A(I)=SIN(ARG)/ARG
         GO TO 110
116      A(I)=1
         GO TO 110
118      A(I)=1
110      CONTINUE
         A0=1
         TYPE "A(I)=",(A(L),L=1,NSAMP)
C        CALC PATTERN AT NP ANGLES
```

```fortran
      DO 120 I=1,NP
      TH=90.*(2*I-NP-1.)/(NP-1.)
      THR=TH/PR
      U=LWV*SIN(THR)
      SUM=0
      DO 130 J=1.NSAMP
      A1=PI*(2*U*ALFA-J)
      IF (ABS(A1).LT..001) GO TO 125
      SNC1=SIN(A1)/A1
      GO TO 126
125   SNC1=1
126   A2=PI*(2*U*ALFA+J)
      IF (ABS(A2).LT..001) GO TO 127
      SNC2=SIN(A2)/A2
      GO TO 130
127   SNC2=1
130   SUM=SUM+A(J)*(SNC1+SNC2)
      SNC=SIN(2*PI*U*ALFA)/(2*PI*U*ALFA)
      IF (ABS(U).LT..001) SNC=1
      SUM=SUM/E0+A0*SNC
      SUMDB=20*ALOG10(ABS(SUM)+1.E-6)
      TYPE U,SUMDB
120   E(I)=SUMDB
C     SCALE PATTERN TO ZERO DB
      EN=E(1)
      DO 135 I=2,NP
135   IF (E(I).GT.EN) EN=E(I)
      DO 140 I=1,NP
140   E(I)=E(I)-EN
C     WRITE PLOT FILE
      OPEN 1."PLOTFILE",ERR=980
      WRITE (1,950) (E(L),L=1,NP)
      CLOSE 1
950   FORMAT (E12.6)
      WRITE (12,910)
910   FORMAT (1X,/,/,/)
      GO TO 100
980   STOP "FILE OPEN ERROR"
990   WRITE (12,995)
995   FORMAT (1X,"<FF>")
      END
```

```
C       ROMBTEST; USE ROMBER,TAYBCALC,ROOTW,TAYWFUN,BESI,ROMBTSTFCT
C       COMPARE ROMBERG, 32 POINT GAUSS, AND ARRAY CALC
C       USE CLOSED FORM PATTERN AS REFERENCE
C       USE TAYLOR ONE-PARAMETER DISRIBUTION
C       LARGE U RANGE GIVES TIME AND ACCURACY CHECK
C       SEE ALSO GAUSSTEST AND ARRAYTEST
C       PREPARED BY R. C. HANSEN, OCT. 1983
        DIMENSION E(1001),ITIME(3)
        COMMON /TAY/ PI,SLR
        COMMON /R/ PB,PU
        PI=3.1415926536
100     ACCEPT "SLR,M,UMAX,NPOINTS     ", SLRD,M,UMAX,NPT
        CALL TAYB(SLRD,B)
        PB=PI*B
        E0=SINH(PB)/PB
        IF (PB.LT..001) E0=1
        CALL TIME(ITIME,IER)
        TYPE (ITIME(L),L=1,3)
        DO 120 I=1,NPT
        PU=PI*(I-1)*UMAX/(NPT-1.)
        CALL ROMBER(0.,1.,M,F)
        E(I)=20*ALOG10(ABS(F)/E0+1E-6)
120     TYPE I, E(I)
        CALL TIME(ITIME,IER)
        TYPE (ITIME(L),L=1,3)
C       SCALE BY LARGEST VALUE
        EN=E(1)
        DO 130 I=2,NPT
130     IF(E(I).GT.EN)EN=E(I)
        DO 140 I=1,NPT
140     E(I)=E(I)-EN
        OPEN 1,"PLOTFILE", ERR=980
        WRITE (1,950) (E(L),L=1,NPT)
        CLOSE 1
950     FORMAT (E12.6)
        GO TO 100
980     STOP "FILE OPEN ERROR"
        END




C       ROMBTSTFCT; USE FOR ROMBTEST
        FUNCTION FCT(X)
        COMMON /R/ PB,PU
        CALL BESI(PB*SQRT(1-X*X),0,BI,IF)
        FCT=BI*COS(PU*X)
        RETURN
        END
```